Multi-antenna underwater acoustic localization system

Pan He

Doctor of Philosophy

University of York
Electronic Engineering

May 2023

Abstract

This work develops and investigates localization and beamforming techniques with multiple antennas for multiple access schemes in underwater acoustic (UWA) communication systems. To enhance the accuracy of node localization, a non-coherent ambiguity function (AF) approach has been developed based on matched field processing (MFP) for localization of a single-antenna UWA communication receiver to one or more transmit antennas. Firstly, we demonstrate that a non-coherent AF allows significant improvement in the localization performance compared to the coherent AF previously used for this purpose, especially at the high frequencies typically used in communication systems. Secondly, we propose a two-step (coarse-to-fine) localization technique. The second step provides a refined spatial sampling of the AF in the vicinity of its maximum found on the coarse space grid covering an area of interest (in range and depth), computed at the first step. This technique allows high localization accuracy and reduction in complexity and memory storage, compared to single step localization. Thirdly, we propose a joint refinement of the AF around several maxima to reduce outliers. Fourthly, the combination of different beamforming techniques with two-step localization in a UWA communication system with orthogonal frequency-division multiplexing (OFDM) has been investigated. For an approximate minimum mean square error (MMSE) transmit antenna precoder with subcarrier-by-subcarrier regularization and with diagonal loading, it is demonstrated that with a suitable assumed signal-to-noise ratio (SNR), the MMSE precoder can achieve a significant improvement in the detection performance compared to a previously proposed zero-forcing precoder. Numerical experiments for multiple communication scenarios and acoustic environments are run for validation of these proposed techniques.

Table of contents

List of tables

List of figures

Acknowledgements

I would like to express my great thanks to my supervisor, Dr. Yuriy V. Zakharov, for all his advice, support, inspiration and encouragement during my Ph.D. study.

I would also like to thank my supervisor, Dr. Benjamin Henson for all his help, advice and encouragement during my Ph.D. study.

I am very grateful to Prof. Paul Mitchell, who is my thesis advisor. Paul provided a lot of ideas and helped me a lot during my Ph.D. study.

I would also like to thank all my colleagues at the Department of Electronic Engineering and all the members of the Underwater Acoustics Research Group for their advice and ideas at the seminars.

This thesis is dedicated to my parents who always understand me, support and encourage me, and give me confidence during my Ph.D. study in York.

Declaration

I declare that this thesis is a presentation of original work and I am the sole author. This work has not previously been presented for an award at this, or any other university. All sources are acknowledged as references.

Publications

Publications directly associated with thesis work

- P. He, L. Shen, B. Henson, and Y. V. Zakharov, "Coarse-to-fine localization of underwater acoustic communication receivers," *Sensors*, vol. 22, no. 18, p. 6968, 2022

Pan He
May 2023

Acronyms

AF Ambiguity Function

AOA Angle Of Arrival

AUVs Autonomous Underwater Vehicles

BEM Basis Expansion Model

BER Bit Error Rate

BPSK Binary Phase-Shift Keying

CDF Cumulative Distribution Function

CIRs Channel Impulse Responses

CP Cyclic Prefix

CSI Channel State Information

FER Frame Error Rate

FFT Fast Fourier Transform

FPGA Field Programmable Gate Array

FS Frequency Shift

GPS Global Positioning System

IFFT Inverse Fast Fourier Transform

ISI Inter-Symbol Interference

LBL Long Baseline

LS Least Square

MACs Multiple and Accumulate Operations

MFP Matched Field Processing

MISO Multiple Input Single Output

MIMO Multiple Input Multiple Output

MMSE Minimum Mean Square Error

OFDM Orthogonal Frequency Division Multiplexing

ROVs Remotely Operated Vehicles

SBL Short Baseline

SDMA Spatial Division Multiple Access

SISO Single Input Single Output

SIMO Single Input Multiple Output

SNR Signal to Noise Ratio

SSP Sound Speed Profile

UASNs Underwater Acoustic Sensor Networks

USBL Ultra-Short Baseline

UWA Underwater Acoustic

UOWC Underwater Optical Wireless Communication

ZF Zero-Forcing

Chapter 1

Introduction

1.1 Underwater communication

In comparison to the terrestrial realm, the underwater environment comprises a significant proportion of the planet. It contains abundant natural resources, such as valuable minerals and offshore oil fields, which are highly sought-after and require efficient exploration strategies to be developed [8]. Underwater communication has been an attractive topic to researchers for several decades, and it is the process of transmitting information between underwater devices or between an underwater device and a surface station. However, communication underwater is a challenging field due to the physical properties of water, and due to the complex and dynamic nature of the underwater environment.

A common approach to providing real-time communication in underwater applications involves the deployment of wired communication systems. However, the practicality of such systems has been challenged by various factors, including their high cost, complex deployment procedures, and limited flexibility [8, 9]. To overcome the limitations of traditional wired communication systems, there has been a growing need for the development of underwater wire-free communication systems. These wire-free systems have the potential to provide more cost-effective and flexible solutions for a wide range of underwater applications related to ocean exploration and industrial activities such as environmental monitoring, maritime archaeology, disaster prevention, tactical surveillance, offshore exploration, climate change monitoring and oceanography research [8, 10, 11].

For underwater wire-free communications, the feasibility of using different physical waves has been investigated. Typically, three distinct categories of physical waves are suitable for transmission in an underwater wire-free context: radio, optical, and acoustic.

Radio waves can offer high data rates due to their high bandwidth, however, they cannot propagate very far through water, even at low frequencies which limits their use to short range

underwater transmission [11]. Radio waves are also limited by high absorption and rapid attenuation, which require high transmission power [11–13]. Therefore, radio waves have limited practical utility for underwater applications and are typically restricted to specialized systems and specific use cases.

In underwater optical wireless communication (UOWC) systems, optical waves can achieve high data rates with low power consumption. The UOWC systems can also support low latency and simpler computational complexities in short-range transmission [11]. However, these systems are subject to distance limitations and are affected by water absorption and scattering. Consequently, only a limited number of applications have been developed utilizing UOWC technology.

Compared to the aforementioned electromagnetic waves, acoustic waves have garnered significant attention due to their low attenuation in water, particularly in thermally stable and deep water environments [14]. Acoustic systems have been identified as a promising solution for underwater communications, particularly in situations where tethering poses physical limitations on mobile systems [15, 16].

In an acoustic system, the available frequency range is from 100 Hz to 100 kHz and higher [17]. However, the utilization of acoustic waves for communication in shallow water can be adversely affected by temperature gradients, surface ambient noise, as well as multipath propagation resulting from reflection and refraction. Compared with radio and optical waves, the significantly slower speed of acoustic propagation in water (approximately 1500 m/s) poses an additional limitation for efficient communications and networking. However, despite these limitations, acoustic waves remain the favoured technologies for underwater communication in current research and applications [14]. It is acknowledged that acoustic waves are considered the most practical physical medium for underwater communications in longer ranges and diverse water environments [18]. Therefore, underwater acoustic (UWA) communication systems are widely recognized as the predominant form of wireless communication in underwater environments and continue to be the focus of extensive research in the field.

1.2 Underwater acoustic communication

In recent years, UWA communication has attracted significant interest due to a wide range of environmental, commercial and military applications [19–24]. Typical applications are search and rescue [25], environmental and biological monitoring [26], sea floor mapping [27] and oil and gas exploration [28]. In fact, UWA communication systems can provide greater mobility and accessibility for underwater vehicles, such as autonomous underwater vehicles

(AUVs) and remotely operated vehicles (ROVs), allowing for more efficient and effective exploration and data collection.

In UWA communication, acoustic waves can be transmitted over several tens of kilometers [29–35]. The propagation distance is mainly determined by the physical characteristics of the underwater channel, including absorption, scattering, multipath propagation, and so on. These phenomena can result in attenuation, delay, and distortion of the acoustic signal, which can limit the bandwidth of the channel. The constrained available bandwidth poses a challenge for transmitting a large amount of data in UWA communication systems.

UWA communication faces significant challenges due to the unique properties of the underwater environment. The fundamental physics of sound propagation in water (including the limited bandwidth, significant signal attenuation, and multipath propagation caused by scattering and reflection) are major obstacles to reliable communication underwater. In addition, underwater communication is further complicated by the Doppler effect induced by the motion of the transmitter and receiver, ocean noise from numerous mechanisms, including natural and human-made sources, and uncertainties arising from the lack of a priori knowledge of the underwater environment. These challenges require the development of advanced signal processing, modulation techniques, and communication protocols to improve the reliability and performance of UWA communication systems. Therefore, it is necessary to explore the unique properties of the underwater environment.

1.3 Characteristics of UWA channels

UWA channels are significantly different to radio channels. They are dynamic and dispersive resulting from the complex and dynamic sea environment [36]. There is no such thing as a fixed UWA communication due to the dynamic UWA environment. It means that one designed acoustic communication system that works well in a shallow water environment may not suitable to a deep water environment at all. Furthermore, there are some key factors, influencing the UWA channels including the special noise environment, multipath effect and the Doppler effect [37]. UWA channels are frequency-selective due to the unavoidable multipath interference [18] and the time-varying effect together with the frequency-selectivity leads to the doubly-selective fading channel [33]. Therefore, UWA channels can be regarded as frequency-selective fading channels.

In a time-varying linear channel, a received signal, $y(t)$, can be represented by [38]

$$y(t) = \int_{-\infty}^{\infty} h(t,\tau)s(t-\tau)d\tau, \quad t \in [0, T_{sig}], \tag{1.1}$$

assuming there is no noise, where $h(t,\tau)$ indicates the channel impulse response, $s(t)$ is the transmitted signal, and T_{sig} represents signal duration.

When designing an UWA channel for stable and reliable communication systems, it is crucial to consider the physical characteristics of the underwater environment. Therefore, to design a better acoustic channel for UWA communication systems, the following factors are especially important, they are ambient noise, transmission loss, multipath propagation and the Doppler effect.

1.3.1 Ambient noise

Ambient noise is widespread and a kind of unwanted background sound. Underwater environments are typically characterized by various sources of ambient noise, such as the noise generated by the sea surface, noise due to biological activity, ocean currents, and anthropogenic activities. It may appear at a specific place of the ocean at a particular time in the deep sea [37, 39] and considered separately to transient sounds and all forms of self-noise including the current flow noise produced by the transducer [39]. Ambient noise can be represented using a Gaussian model including the white noise [5]. The ambient noise can significantly impact the performance of underwater communication systems by reducing the signal-to-noise ratio (SNR). Therefore, it is essential to understand and model the characteristics of the ambient noise in the target underwater environment when designing an effective and reliable UWA communication system.

1.3.2 Transmission loss

Acoustic waves in underwater environments experience attenuation or transmission loss when they propagate through the water medium. Transmission loss depends on various factors, including frequency, distance, and environmental conditions such as temperature, salinity, and water absorption. In UWA communication, the total loss experienced by the acoustic signal can be decomposed into two main components: spreading loss and absorption loss [39]. In UWA communication, transmission loss is considered in terms of the distance between the transmitter and receiver [40]. The overall transmission loss, A, can be described as [37],

$$A(l,f) = \left(\frac{l}{l_r}\right)^k a(f)^{l-l_r}, \tag{1.2}$$

where l is the propagation distance between the transmitter and receiver, f represents the signal frequency, l_r is a reference distance, k indicates the spreading loss, its value is chosen between 1 to 2, which is used for cylindrical and spherical spreading, respectively, a is the

absorption coefficient. Eq. (1.2) can be rewritten in the form of dB,

$$10\log\frac{A(l,f)}{A_0} = k \times 10\log(l) + l \times 10\log a(f), \tag{1.3}$$

where two items on the right side of the equation represent separately spreading loss and absorption loss.

The absorption coefficient $a(f)$ results from an empirical formula, the Thorp formula given [40, 41] by

$$10\log a(f) = \frac{0.11f^2}{1+f^2} + \frac{44f^2}{4100+f^2} + 2.75 \times 10^{-4} f^2 + 0.003, \tag{1.4}$$

where $a(f)$ is in dB/km, f represents frequency in kHz.

The bandwidth limitation results from the physical property of acoustic propagation [40], mainly influenced by the attenuation characteristic of sea water [36]. Signal-to-noise ratio (SNR) is an important characteristic defined by the transmission loss and ambient noise. The SNR in a narrow band can be defined as [5],

$$\mathrm{SNR}(l,f) = \frac{S_l(f)}{A(l,f)N(f)}, \tag{1.5}$$

where $S_l(f)$ indicates the power spectral density of transmitted signals, $N(f)$ is the power spectral density of the ambient noise. The AN product $A(l,f)N(f)$ is the frequency-dependent term in SNR when given the specific distance.

The relationship between the narrow-band SNR, distance and frequency is illustrated in Fig 1.1. The available bandwidth for UWA communication systems is influenced by the transmission distance. At shorter distances, the available bandwidth is larger, whereas at longer distances, the available bandwidth becomes more limited. For example, at a distance of 10 km, the available bandwidth is around 8.5 kHz (frequency range is from 2 kHz to 10.5 kHz); while at a distance of 100 km, the available bandwidth is only about 1 kHz. This decrease in available bandwidth with increasing distance is primarily due to the attenuation of the acoustic signal. This attenuation is caused by spreading loss and absorption loss in the underwater environment.

The available bandwidth is also affected by the SNR or the reciprocal of the ambient noise ($\frac{1}{\mathrm{AN}}$). A worse SNR or higher ambient noise level results in a narrower available bandwidth. For example, a lower $\frac{1}{\mathrm{AN}}$ value of -130 dB at a distance of 100 km corresponds to a narrower available bandwidth of about 1 kHz, compared to a higher $\frac{1}{\mathrm{AN}}$ value of -102 dB at a distance of 10 km, which corresponds to a wider available bandwidth of about 8.5 kHz.

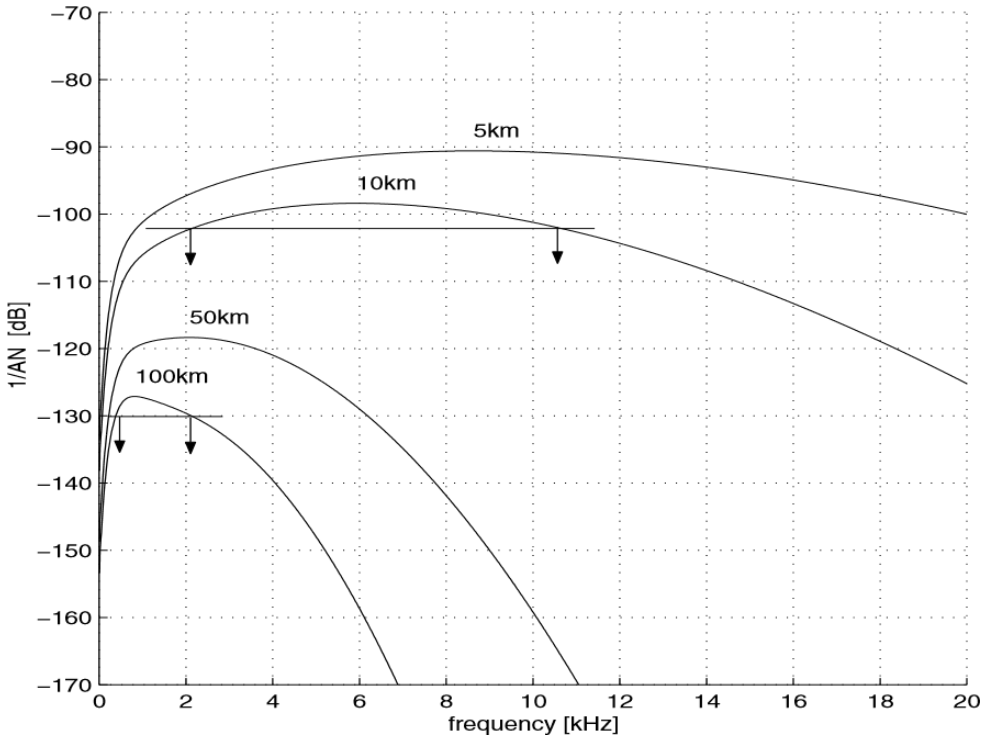

Fig. 1.1 SNR in an acoustic channel depends on the frequency and distance through the factor $\frac{1}{A(l,f)N(f)}$. Copied from [5].

Furthermore, the deployment of transducers (antennas) also can affect the bandwidth of the UWA communication systems [37, 40]. The transducers used for transmitting and receiving acoustic signals may have limitations in their bandwidth, which can further restrict the available bandwidth for communication purposes. Therefore, there is a demand for bandwidth-efficient modulation methods that can effectively utilize the limited available bandwidth in UWA communication systems. These modulation methods need to be carefully designed and optimized to achieve reliable and efficient communication performance, considering the available bandwidth, transmission distance and ambient noise in the underwater environment.

1.3.3 Multipath propagation

Multipath propagation is a phenomenon that occurs in UWA communication systems due to the complex sea environment. The sea environment includes various elements such as the surface, bottom (which can be hard or soft), and objects, which can cause physical reflection and refraction of acoustic waves, leading to the formation of multiple paths or rays that can reach the receiver (hydrophone) at different times and angles [37]. The sound speed in water,

influenced by factors such as temperature, salinity, and pressure, also varies with depth and location, further contributing to multipath phenomena [14, 37].

As a result, when an acoustic wave is transmitted from a transducer in an UWA communication system, it can take multiple paths due to reflections, refractions, and variations in sound speed, and arrive at the receiver with different propagation delays. These propagation delays can be estimated and quantified, as they are generally stable in time-varying UWA channels [18]. However, multipath propagation can also result in excessively long multipath delays, which can cause time dispersion of the acoustic wave and result in severe intersymbol interference (ISI) in the received signal [14].

To mitigate the effects of multipath propagation in UWA communication systems, techniques such as orthogonal frequency division multiplexing (OFDM) with longer guard symbols can be applied [42]. OFDM is a modulation technique that allocates the transmission data across multiple subchannels in the frequency domain, allowing for effective mitigation of frequency-selective fading channels caused by multipath propagation. By using longer guard symbols, which are designed to protect against the ISI caused by multipath delays, the effects of multipath propagation can be reduced, improving the overall communication performance in underwater environments.

Mitigating the multipath effect is a crucial aspect of UWA communication system design, because it helps to minimize the impact of time dispersion, ISI, and other signal distortions caused by multipath propagation, ultimately leading to more reliable and efficient communication performance in underwater environments.

1.3.4 Doppler effect

The Doppler effect is a phenomenon that occurs due to the relative motion between a transmitter and a receiver, resulting in a shift in the frequency of the transmitted signal as observed by the receiver. The Doppler effect exists due to the motion of the transmitter and/or receiver [43]. However, in UWA communication systems, the additional variation and complexity of the Doppler effect can be caused by such factors as the sea surface motion and/or internal waves.

In UWA communication, the Doppler spread effect is particularly significant due to the propagation medium with a low propagation speed of sound (normally assuming 1500 m/s) in water compared to radio frequency channels. The normalized carrier frequency offset, which represents the Doppler shift, can be extremely large in UWA communication due to the motion-induced Doppler effect [44, 45]. This can result in significant frequency shifts in the received signal, leading to potential signal distortions and degradation of communication performance.

Therefore, it is essential to consider the Doppler effect when designing UWA communication systems. Techniques such as robust modulation and channel estimation methods that can handle the effects of Doppler spread are commonly applied in UWA communication to mitigate the impact of Doppler-induced frequency shifts.

1.4 Multiple antenna transmission

Information theory states that the channel capacity of a communication system increases proportionally to the minimum number of antennas at the transmitter and receiver [46]. Therefore, it is necessary to explore the various implications of antenna deployment in underwater communication systems.

In UWA sensor networks, it is feasible to deploy multiple antennas at the base station (a single gateway node), but not practical to install multiple antennas at many sensor nodes, which should be of low cost, low complexity, and low power consumption. For the downlink transmission, this means that multiple transmit antennas are practical, whereas multiple receive antennas are not practical.

Based on the number of antennas utilized at the transmitter and receiver, the same antenna techniques used in terrestrial wireless communication systems, including single-input single-output (SISO), single-input multiple-output (SIMO), multiple-input single-output (MISO), and multiple-input multiple-output (MIMO), can also be applied to underwater communication systems. Each antenna technique has its advantages and limitations, and careful consideration of the appropriate antenna technique is crucial for optimizing the performance of wireless UWA communication systems.

In SISO systems, only one antenna is used at the transmitter and one antenna at the receiver. SISO UWA communication systems have been widely used in practice due to their relatively lower cost and simpler deployment compared to other antenna techniques [47, 48]. SISO UWA communication systems with multi-carrier modulation techniques like OFDM are feasible [49]. SISO UWA communication systems can still provide basic communication capabilities in certain scenarios, but their limitations in terms of potential distortion, low data rates, and error rates may restrict their use in more complex underwater communication environments. To enhance the performance of UWA communication systems, it is necessary to extend research to multi-antenna systems.

In SIMO systems, there is only one antenna at the transmitter, while multiple antennas are used at the receiver. SIMO systems exploit receiver diversity, where the multiple antennas at the receiver are used to receive the same signal from different spatial paths, effectively mitigating the effects of multipath propagation [50, 51]. Indeed, SIMO-OFDM communi-

cation systems over UWA channels have been shown to improve bandwidth efficiency [52]. However, due to the high attenuation of acoustic waves in water, the SIMO technique may have limited range and performance in UWA communication systems.

Compared to the SISO and SIMO systems, MIMO is a more complex system, allowing an increased capacity of the whole system. The development of MIMO systems in terrestrial wireless communications has achieved higher data rates [8]. In UWA communication, MIMO techniques have been researched in [36, 44, 45, 53–55] for increasing data rates but MIMO UWA systems bring about space-time interference and time-varying phase distortion [45]. In addition, the extra space interference among concurrent transmission streams degrades the detection performance significantly [44].

In MISO systems, multiple antennas are deployed at the transmitter and one antenna at the receiver. It is impractical to use spatial division multiple access (SDMA) when deploying a small number of antennas at the base station and large number of antennas in the receivers [56]. MISO systems are combined with SDMA to maximize data rates faced with power constraints and quality of service requirements [42]. MIMO and MISO techniques show good performance in improving data rates in wireless communication systems. However, it is not practical when the MIMO systems apply SDMA with the deployment of a small number of antenna and a larger group of users. MISO systems with SDMA present a more realistic implementation because a single antenna at each user are multiplexed spatially and independently [56]. Multi-antenna and OFDM techniques have been employed to increase data rates in the broadband communication systems. It has been shown that MISO-OFDM systems can significantly reduce the transmission power [57]. In this thesis, the multi-antenna technique, a MISO system combined with OFDM technique is investigated and an advanced receiver localization technique is proposed to improve the accuracy performance.

1.5 Underwater Localization

One of important applications in multi-antenna UWA communication systems is underwater localization. Underwater localization is a difficult problem. In fact, the localization technologies for terrestrial communications cannot be applied directly to the underwater localization problem. The well-known land localization technique, the Global Positioning System (GPS) would experience significant attenuation underwater due to the use of radio waves.

Research and development into non-acoustic and acoustic technologies for positioning and tracking underwater assets are on going [58]. In recent years, non-acoustic localization techniques, such as inertial navigation methods have been adopted in some underwater

communication systems to improve localization accuracy and reliability [59–61]. Inertial navigation makes use of accelerometers and gyroscopes to measure the motion and orientation of a platform, such as an underwater vehicle or a diver, and uses this information to estimate the position and velocity of the platform relative to a reference point. However, inertial navigation systems are subject to inherent errors and biases, which can accumulate over time and lead to drift in the estimated navigation data. This drift can result in a degradation of the localization accuracy over time, especially for long-duration underwater missions. In addition, the limited transmission range and coverage challenge the development of the non-acoustic localization techniques.

In comparison to the non-acoustic localization techniques, acoustic localization techniques offer several benefits, including long range, wide coverage, robustness to environmental variability, complementarity with other localization techniques, and cost-effectiveness [59, 62, 63]. These advantages make acoustic localization as a popular choice for many underwater communication and navigation applications.

There are three types of commercially available systems applying localization techniques using acoustic waves, including long baseline (LBL) systems, short baseline (SBL) systems and ultra-short-baseline (USBL) systems [64]. These systems measure the distance between the baseline stations and determine target position by trilateration.

In LBL systems, the method is that an underwater vehicle takes triangulation measurements based on estimating the round-trip delay to transponders which are deployed at the bottom of the sea [59, 65]. It can lead to a good localization accuracy but its limitation is the substantial time consuming calibration [59]. In SBL systems, the core method is to measure the time difference of arrivals to locate, for example, a ship equipped with receivers on the surface. In USBL systems, the surface buoys are set as the reference points and other functions are similar to the LBL systems [59]. A small array of hydrophones is used to assess the acoustic signals from the undersea emitters in order to calculate the angle of arrival (AOA). More aspects are considered including combining the AOA information with a range estimation. This method can provide static positioning accuracy and precision comparing to other methods and significantly reduces the time and cost of the offshore project [66]. Thus, it can achieve much better localization performance. These are the three types of UWA communication systems for localization through the acoustic waves and they need improving to provide better performance.

Acoustic localization techniques have pushed the development of UWA communication. Acoustic localization techniques are important for further exploration in terms of data analysis, tracking and detection [13]. Such technologies have been used in underwater acoustic sensor networks (UASNs) to improve its performance including medium access and

network protocols [13]. One deterministic factor of localization estimation is ranging, which is to directly estimate the distance between the transmitter and the receiver.

The work in this thesis mainly contributes to the localization problem of the underwater nodes, within a multi-antenna UWA communication system, thus enhancing the performance of the whole system.

1.6 Discussion of Li Liao's work [1]

This work can be considered as a continuation of what has been done in the thesis by Li Liao [1]. For localization, he uses the coherent processing. Here, we will propose a new non-coherent metric, which results in much more accurate localization. He considers only the coarse localization approach. This approach requires huge computation for a large number of points on the grid. We propose more advanced approaches, coarse-to-fine localization techniques, which only need a small number of points on the grid, thereby greatly reducing the computational complexity and further improving the localization accuracy.

For beamforming techniques, although he did precoding, his work was focused only on two fixed positions of the receivers between grid points in the space, and he didn't explore what the detection performance would be for different random receiver positions. Testing beamforming techniques with different random receiver positions provides a more comprehensive understanding of the detection performance in real-world conditions. We also investigate different transmit beamforming techniques, not only the zero-forcing (ZF) precoder considered in [1].

Overall, the techniques proposed in this thesis can significantly improve both the accuracy of localization and the detection performance of transmit beamforming techniques, as well as reducing the computational complexity.

1.7 Motivation and Contributions

1.7.1 Motivation

Underwater localization techniques and transmit beamforming (MISO systems) are essential for UWA communication. Developing such techniques will improve our ability to navigate and track underwater sensor targets, and increase efficiency for underwater applications in research and rescue [25], environment and biological monitoring [26], sea floor mapping [27], mining exploration [67] and oil and gas exploration [28]. In recent years, many localization and transmit beamforming techniques underwater have been developed, but they are still

limited in performance, including relatively low data rates, high complexity, low accuracy and detection performance, which demand further research.

The pre-computation of channel state information (CSI) in an area of interest can reduce that complexity. Based on the grid pre-computation algorithm, the system can achieve better localization accuracy with lower complexity. The estimated localization information can be sent back to the transmitter through the feedback link. To avoid interference from other users, the transmit beamforming can be designed through the feedback and achieve higher detection performance. In such a way, the transmitter can transmit data to users simultaneously without interference to increase data rates.

The non-coherent ambiguity function (AF) effectively achieves additional complexity reduction by employing a smaller number of grid points in comparison to the coherent AF. In addition, the work [68] shows that simulation results using the BELLHOP cannot be matched to the experimental results when using the coherent AF, but have a good match when the non-coherent AF applied.

Multi-antenna communication techniques can provide spatial diversity and improve UWA communication reliability and capacity. However, an accurate receiver localization in UWA communication is still a significant problem. In this situation, the localization accuracy directly affects the designing of the transmit beamforming and further influences the detection performance. In other words, this puts forward requirements for higher precision localization.

The aim of this thesis is to develop and investigate multi-antenna communication techniques, more specifically, developing advanced underwater localization techniques and investigating transmit beamforming techniques for such systems.

1.7.2 Contributions

The contributions of this thesis are summarized as follows.

- We demonstrate that a non-coherent ambiguity function (AF) allows significant improvement in the localization performance compared to the coherent AF previously used for this purpose, especially at high frequencies.
- A two-step (coarse and fine step) technique is proposed. The first step is to find the AF maximum by comparing the estimated channel frequency response with the pre-computed frequency responses in the grid map; the second step provides a refined spatial sampling of the AF in the vicinity of its maximum found on the coarse space grid covering an area of interest (in range and depth), computed at the first step. This

technique allows high localization accuracy and a reduction in complexity and memory storage, compared to single-step localization.

- A joint refinement of the AF in the vicinities of several maxima is proposed to reduce outliers in the position measurement.
- The combination of the zero-forcing (ZF) transmit beamforming with the two-step localization is demonstrated and investigated. This allows significant improvement in the detection performance compared to the existing localization in a particular scenario.
- A precoder, called approximate MMSE precoder with subcarrier-by-subcarrier regularization by the diagonal loading, is demonstrated and investigated. This precoder allows high detection performance and is shown to be feasible for a more general scenario.
- For validation of the proposed techniques, we run numerical experiments in different UWA environments, with different parameters for spatial sampling, number of transmit antennas and different accuracy for estimates of the acoustic channel response, plus different precoders.

1.8 Thesis outline

This thesis is organized into five chapters. It explores the techniques of localization and transmit beamforming in UWA communication systems.

Following the introduction and literature review described in Chapter 1, Chapter 2 presents the structure of matched field processing (MFP) localization using the non-coherent ambiguity function (AF), which extends the work in [69], where receiver localization based on the grid computation with coherent AF is described. The non-coherent AF provides a significant improvement in the localization performance compared to the coherent AF previously used for this purpose. Because the non-coherent AF focuses on comparing magnitudes of channel impulse responses thus avoiding the phase information, the complexity is reduced. In addition, better localization performance can be achieved especially at high frequencies.

In Chapter 3, a two-step (coarse and fine step) localization technique is proposed. The first step is to find the AF maximum by comparing the estimated channel frequency response with the pre-computed frequency responses in the grid map; the second step provides a refined spatial sampling of the AF in the vicinity of its maximum found on the coarse space grid covering an area of interest. This technique provides higher localization accuracy and a reduction in complexity and memory storage, compared to single step localization.

In Chapter 4, we demonstrate and investigate two different linear precoders for transmit beamforming with the combination of the two-step localization technique. The first precoder is a zero-forcing (ZF) precoder. It allows significant improvement in the detection performance, compared to the existing localization. The second precoder is an approximate minimum mean square error (MMSE) precoder. This precoder is combined with subcarrier-by-subcarrier regularization using diagonal loading. The MMSE precoder with an assumed SNR allows better detection performance than the ZF precoder, especially in the mismatched environments.

Finally, in Chapter 5, we conclude the thesis and present ideas for future work.

Chapter 2

Coarse Localization

2.1 Introduction

In recent years, UWA communication in sensor networks has gained increasing attention due to its potential for various commercial and military applications [70–76]. Underwater localization for acoustic sensors is a crucial task in many underwater applications, as the collected data from sensors is often associated with their precise location. However, underwater localization presents unique challenges because of the limitations of using radio-based techniques, such as the global positioning system (GPS), which cannot operate underwater due to the high attenuation of radio waves in water [77–79].

Matched Field Processing (MFP) is an effective and widely investigated technique for underwater localization in acoustic sensor networks [80, 68, 81, 82]. MFP is a signal processing technique that uses the principles of wave propagation and signal coherence to estimate the position of a sensor by matching the received signals with modelled or measured signals. MFP relies on an acoustic model to calculate a replica field, which represents the expected acoustic field that would be received at each hydrophone in the array for a given source position [83, 84]. This replica field is then compared to the field measured by the hydrophones to estimate the source position.

In MFP, the similarity between the measured field at the hydrophones and the replica field is typically quantified using an ambiguity function (AF). The AF is computed on a grid of points in space (range and depth), covering the area of interest, and it represents the degree of match between the measured field and the replica field at each grid point.

The AF is a measure of the similarity or coherence between the measured and replica fields, and it can be computed using various techniques, such as cross-correlation, or other similarity measures. The AF can be calculated over a range of possible source positions, covering the region of interest where the source is likely to be located. The grid of points in

an area of interest where the AF is computed represents the possible source positions that are being considered for localization. This grid can be defined based on the expected range and depth range of the source, and the grid step depends on the spatial resolution requirements of the localization task.

The peak of the AF represents the best match or highest coherence between the measured and replica fields, and it indicates the estimated source location [81, 85]. The source position corresponding to the peak of the AF is considered as the localization estimate or the most likely source location.

In MFP, AF processing can be categorized into two types: coherent AF processing and non-coherent AF processing. Coherent AF processing takes into account the phase relationship between the transmitted signal and the received signal. It provides a measure of the time-delay and Doppler frequency shift of a target in a coherent manner, meaning that it considers the phase information of the received signals. This coherent processing is most often effective at low frequencies, typically up to 1 kHz, where the underwater sound waves propagate well and exhibit coherent behaviour [68, 82].

However, the MFP with a coherent AF at high frequencies (where UWA communication systems typically operate) can distort phase information in the received signals, resulting in poor localization estimates or outliers. To mitigate this distortion, non-coherent processing can be used in MFP for UWA communication systems operating at high frequencies. Using numerical and real experiments, it is shown in [68] that with a non-coherent AF, the localization accuracy at high frequencies (8 - 16 kHz) significantly improves.

Theoretically, the performance of the coherent AF should be better than the non-coherent AF. The peak of the coherent AF or non-coherent AF can be found through their sampling over the area of interest. In fact, the sampling interval for the coherent AF must be inversely proportional to the carrier frequency and that of the non-coherent AF is inversely proportional to the frequency bandwidth. Obviously, the coherent AF can always provide better localization than the non-coherent AF when using a proper sampling rate. For example, if the carrier frequency is 3 kHz and the frequency bandwidth is 1 kHz, the sampling interval of the coherent AF is 3 times smaller, which means increasing the number of grid points by $3^2 = 9$ times. In practice, in UWA communication systems the carrier frequencies and this ratio are even higher, so that the coherent AF localization cannot be implemented due to the high demand of the memory and high complexity. With the non-coherent AF, the number of the grid points is significantly lower, thus, making the localization more feasible.

The work in [69] addresses the problem of localization in an underwater communication network with multiple transmit antennas at the base station and single-antenna receivers at the network nodes. The purpose of localization in this work is to reduce the amount of data

needed to represent the channel state information (CSI) that is sent from the nodes back to the base station for transmit antenna precoding. In [69], the coherent AF is used for the MFP localization, and therefore, a large number of transmit antennas and dense spatial sampling are required, resulting in high complexity and high memory storage requirements. Therefore, it is necessary to explore other methods to improve the localization accuracy in MFP based localization.

2.2 MFP coarse localization

UWA localization based on the coherent AF is described in this section, as proposed in [69]. Then, the non-coherent AF is introduced and the corresponding localization method is considered. These two methods are compared through a number of numerical experiments with the consideration of localization accuracy, complexity and storage requirement. The localization methods with the resolution corresponding to the grid step will be considered to be the coarse localization as opposed to the fine localization methods proposed in Chapter 3, which provide a resolution better than the grid step (fine grid points are inserted between the coarse grid points).

To make a further consideration of trade-offs between localization accuracy, complexity and storage requirement in UWA communication systems, based on the work in [69], localization with coherent AF and non-coherent AF is investigated in the following subsections.

2.2.1 Coarse localization based on coherent AF

In this subsection, we present a communication scenario and MFP coarse localization technique exploiting a coherent AF, as described in [69].

Consider an UWA environment, where a geographical area of interest is defined as illustrated in Fig. 2.1. We assume that the UWA environment is perfectly known, in particular, that the sound speed profile (SSP) is available. The area of interest is covered by grid points, each at a specific sea depth and range from the transmit antenna. Using an acoustic model and the UWA environment parameters, the channel response between the transmit antenna and every grid point is computed and stored in memory. We will call the result of this computation a grid map for the transmit antenna. Such computations are repeated for every transmit antenna and the corresponding grid maps represent a dictionary. This dictionary is available at the receiver, which is located within the area of interest. Using the signal transmitted from each transmit antenna, the receiver estimates the channel responses and

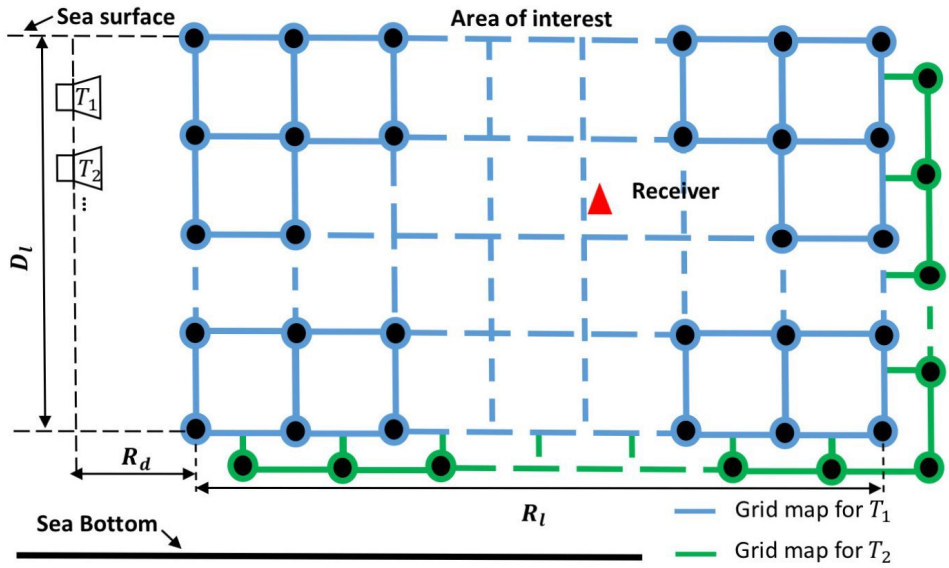

Fig. 2.1 An example of two grid maps for a geographical area; every grid map corresponds to a specific transmit antenna.

compares them with the channel responses of the corresponding grid maps. The best match is assumed to indicate the grid point closest to the true receiver location.

In [69], it is assumed that by using a feedback communication channel, the node sends the grid point index to the base station, where the dictionary channel responses are used for optimization of transmit antenna beamforming. However, this information can also be used for other applications, e.g. attributing the information from sensors to geographical locations. Here, we only consider the localization problem.

For comparison of channel estimates with entries in the dictionary, different metrics can be used. For communication systems, it is typical to describe the channel as a linear filter with an impulse response or corresponding frequency response. Let $\mathbf{g}_m$ be a $K \times 1$ vector representing the channel frequency response, corresponding to the mth grid point. Elements of the vector are K samples of the frequency response (K subcarrier amplitudes) within the frequency bandwidth of the communication system. Let $\hat{\mathbf{h}}$ be a $K \times 1$ estimate of the channel frequency response at the receiver. For comparison of these two vectors, the following metric can be used [69]:

$$c_m = \frac{|\mathbf{g}_m^H \hat{\mathbf{h}}|^2}{\|\mathbf{g}_m\|_2^2 \|\hat{\mathbf{h}}\|_2^2}, \quad m = 1, ..., M, \tag{2.1}$$

where M is the number of grid points in the grid map. The set of values c_m over m represents a coherent AF. The best match between the channel response estimate and channel responses

in the grid map is given by

$$m_{\mathrm{o}} = \arg \max_{m=1,\ldots,M} c_m. \tag{2.2}$$

The grid point index m_{o} defines the receiver location estimate.

With the knowledge of the specific acoustic environment including the SSP, acoustic parameters of the sea bottom, the depth of transmit antennas, and the position of the grid point, a ray tracing acoustic simulator is used to compute $\mathbf{g}_m$. Elements of the vector $\mathbf{g}_m$ are then given by

$$g_m(f_k) = \sum_{i=0}^{L_m-1} A_{m,i} e^{-j2\pi f_k \tau_{m,i}}, \tag{2.3}$$

where f_k, $k = 0,\ldots,K-1$, are subcarrier frequencies at which the channel frequency responses are computed, L_m represents the number of rays, $A_{m,i}$ is the complex-valued amplitude and $\tau_{m,i}$ is the delay of the ith ray on the mth grid point. For our simulation below, the ray information is generated by the BELLHOP3D ray tracing program [86].

However, there is an unknown propagation delay τ between the channel response estimate and channel responses in the grid map. In the frequency domain, at a frequency f, this delay is represented as a factor $e^{-j2\pi f\tau}$. With the unknown delay τ, the measure for comparison of channel frequency responses is given by

$$c_m = \frac{\max_{\tau\in[\tau_{\min},\tau_{\max}]} |\mathbf{g}_m^H \mathbf{\Lambda}_\tau \hat{\mathbf{h}}|^2}{\|\mathbf{g}_m\|_2^2 \|\hat{\mathbf{h}}\|_2^2}, \tag{2.4}$$

where

$$\mathbf{\Lambda}_\tau = \begin{bmatrix} e^{-j2\pi f_0\tau} & & 0 \\ & \ddots & \\ 0 & & e^{-j2\pi f_{K-1}\tau} \end{bmatrix},$$

$\mathbf{\Lambda}_\tau$ is a $K \times K$ diagonal matrix. The parameters $\tau_{\min}$ and $\tau_{\max}$ define the delay uncertainty interval. The metric (2.4) describes a coherent AF $\{c_m\}$, which provides an improved location estimate m_{o} compared to the AF in (2.1).

Computation in (2.4) can be efficiently done using the fast Fourier transform (FFT),

$$c_m = \frac{\max_{i=1,\ldots,pK} |q(i)|^2}{\|\mathbf{g}_m\|_2^2 \|\hat{\mathbf{h}}\|_2^2}, \tag{2.5}$$

where $q(i)$ are elements of the vector $\mathbf{q} = \mathbf{F}\boldsymbol{\eta}$ and $\boldsymbol{\eta}$ is obtained by zero-padding the vector $\mathbf{g}_m^H \odot \hat{\mathbf{h}}$. $\mathbf{F}$ is a $pK \times pK$ discrete Fourier transform (DFT) matrix and p is an integer, $p \geq 1$. Using $p > 1$ allows improvement in the delay resolution.

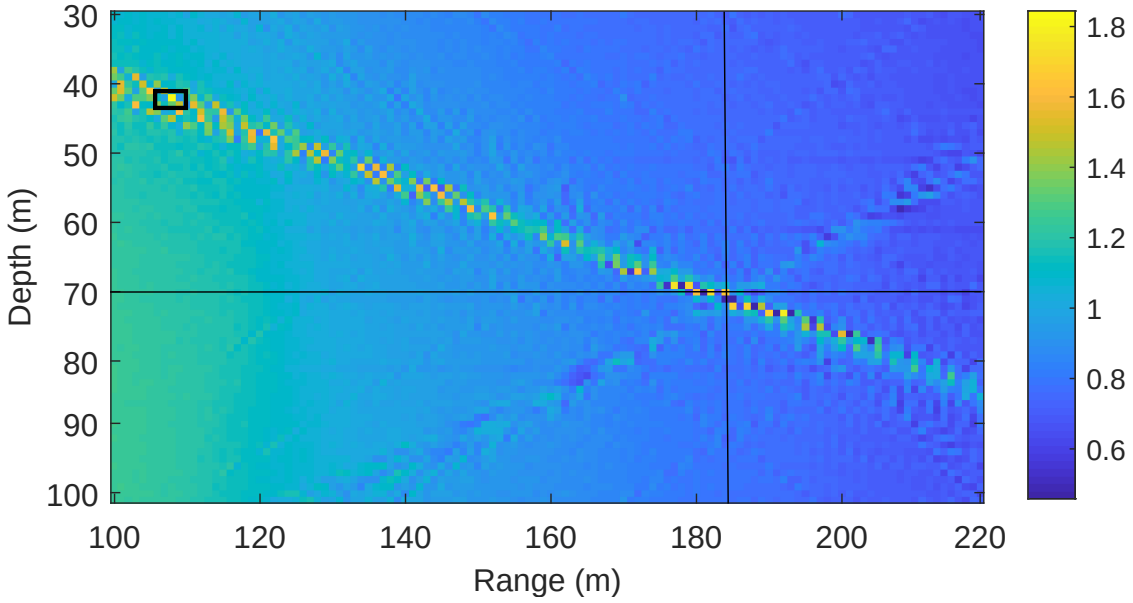

Fig. 2.2 An example of the coherent AF in (2.6) for parameters of the acoustic environment in Table 2.1. The crossing point of the horizontal and vertical black lines indicates the true receiver position. The black square indicates the position estimate (the AF maximum). Here we use the acoustic environment with the uniform SSP as shown in Fig. 2.3.

Note that the AF for a particular transmit antenna can have multiple maximums close in magnitude. Since the channel estimates are corrupted by noise, a wrong (local) AF maximum can be chosen for the localization, resulting in outliers. The probability that AFs computed for different antennas have the same positions of maximums is low, which can be exploited to reduce the outliers.

Therefore, with multiple transmit antennas, the localization performance could be further improved by using the AF

$$c_m = \sum_{t=1}^{N_\mathrm{T}} \frac{\max_{\tau\in[\tau_{\min},\tau_{\max}]} |\mathbf{g}_{t,m}^H \mathbf{\Lambda}_\tau \hat{\mathbf{h}}_t|^2}{\|\mathbf{g}_{t,m}\|_2^2 \|\hat{\mathbf{h}}_t\|_2^2}, \tag{2.6}$$

where N_T is the number of transmit antennas, $\mathbf{g}_{t,m}$ is the channel frequency response vector at the mth grid point on the tth grid map and $\hat{\mathbf{h}}_t$ is the estimate of the channel frequency response between the tth transmit antenna and receiver antenna.

Table 2.1 Simulation parameters used in an example of receiver localization.

Variable name	Value	Description
B	1024 Hz	Frequency bandwidth
C_{d}	1 m	Coarse grid step in depth
C_{r}	1 m	Coarse grid step in range
D_{T}	$50, 60, 70, 80$ m	Depth of transmit antennas
D_l	70 m	Depth for area of interest
f_c	3072 Hz	Carrier frequency
K	1024	Number of subcarriers
N_{T}	4	Number of transmit antennas
R_l	120 m	Range for area of interest
δ	1 Hz	Subcarrier spacing
τ	$[-0.5\ \mathrm{s}, 0.5\ \mathrm{s}]$	Delay uncertainty interval

Fig. 2.2 shows the coherent AF defined in (2.6) for an acoustic environment described in Table 2.1. Specifically, the SSP is uniform (sound speed is consistent, assuming $1500\mathrm{m/s}$) as shown in Fig. 2.3, the number of transmit antennas $N_{\mathrm{T}} = 4$, the area of interest in range is from 100 m to 220 m and in depth from 30 m to 100 m, the grid steps in both range and depth are 1 m. It can be seen in Fig. 2.2 that the true position of the receiver is at the range of 184.5 m and in 70 m depth. However, the maximum of the AF is found at a depth of 41 m and a range of 108 m. It can be seen that the location estimate is very poor, the estimate is about 82 m away from the true location. This happens because the spatial sampling interval is too large to provide accurate representation of the AF, i.e., the AF samples miss the AF maximum. To overcome this problem, we need to reduce the spatial sampling interval, so that we do not miss the AF maximum. However, this results in a higher number of grid points M, and thus the memory required for saving the dictionary increases and the complexity of the AF computation in (2.6) also increases.

This limitation of the coherent AF in terms of dense spatial sampling, computation complexity, and potential false localization motivates the need for alternative approaches, such as the non-coherent AF method proposed in subsection 2.2.2 and coarse-to-fine localization approaches in the following chapters, which can provide more efficient localization results with reduced computational requirements.

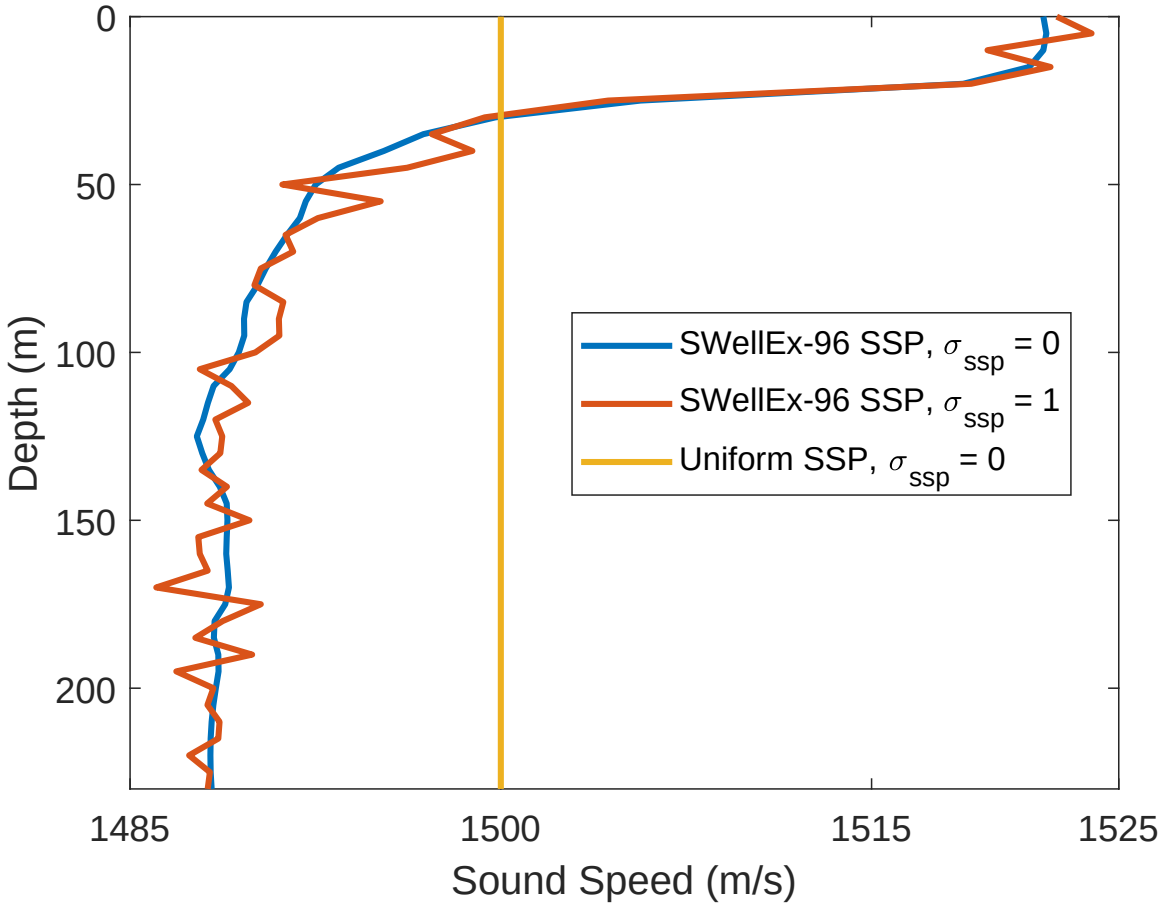

Fig. 2.3 Sound speed profiles (SSPs): uniform, SWellEx-96 [6] and the mismatched SWellEx-96 when the variance sound speed $\sigma^2_{\text{ssp}} = 1\ (m^2/s^2)$. (Note: there is no change for the SSP when $\sigma^2_{\text{ssp}} = 0$, the mismatched SSP with a non-zero σ^2_{ssp} is discussed in subsection 3.4.3)

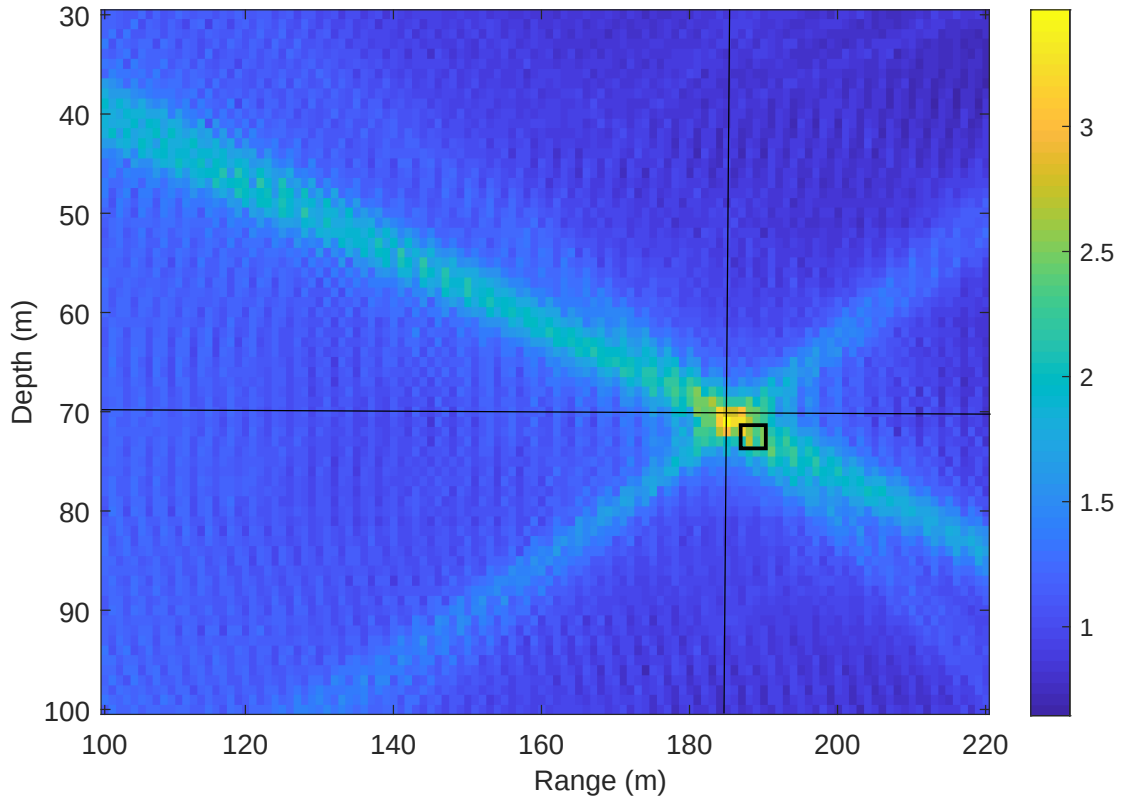

Fig. 2.4 An example of the non-coherent AF in (2.7) with specific parameters of the acoustic environment as described in Table 2.1. The true receiver position is indicated by the crossing point of horizontal and vertical black lines, while the position estimate (the AF maximum) is denoted by a black square. The acoustic environment is assumed to have a uniform SSP as shown in Fig. 2.3.

2.2.2 Coarse localization with non-coherent AF

In this subsection, a non-coherent AF is introduced as an alternative to the coherent AF for UWA MFP localization, and its effectiveness is demonstrated in comparison to the coherent AF.

The coherent AF method requires dense spatial sampling, which results in a high computation complexity and large memory storage for saving the dictionary. In practical scenarios, even with relatively low carrier frequencies and small grid steps for the AF, false localization (outliers) can occur when the receiver is located between the grid points. This is illustrated in the example of coherent AF shown in Fig. 2.2, where even with such a low carrier frequency as $f_c = 3072$ Hz and small grid steps of $C_{\mathrm{d}} = C_{\mathrm{r}} = 1$ m, false localization can happen when the receiver is located between grid points.

In order to keep the memory and complexity low, a better localization performance can be achieved with the method of the non-coherent AF, which is defined as

$$c_m = \sum_{t=1}^{N_\mathrm{T}} \frac{\max_{\tau\in[\tau_{\min},\tau_{\max}]} \left|\tilde{\mathbf{g}}_{t,m}^H \mathbf{\Lambda}_\tau \tilde{\mathbf{h}}_t\right|^2}{\left|\left|\tilde{\mathbf{g}}_{t,m}\right|\right|_2^2 \left|\left|\tilde{\mathbf{h}}_t\right|\right|_2^2}, \tag{2.7}$$

where $\tilde{\mathbf{g}}_{t,m} = \tilde{\mathbf{F}}\mathrm{abs}(\tilde{\mathbf{F}}^H \mathbf{g}_{t,m})$, $\tilde{\mathbf{h}}_t = \tilde{\mathbf{F}}\mathrm{abs}(\tilde{\mathbf{F}}^H \mathbf{h}_t)$, $\tilde{\mathbf{F}}$ is the $K \times K$ DFT matrix and the vector function $\mathrm{abs}(\mathbf{g})$ is defined as

$$\mathrm{abs}(\mathbf{g}) = \begin{bmatrix} |g_1| \\ \vdots \\ |g_K| \end{bmatrix},$$

where g_k, $k = 1,\ldots,K$, are elements of the vector $\mathbf{g}$.

Obviously, the non-coherent AF is based on comparing the magnitudes of the channel impulse responses (CIRs) without considering the phase information.

Fig. 2.4 shows an example of receiver localization using the non-coherent AF in (2.7) for the parameters of acoustic environment in Table 2.1. When comparing Fig. 2.4 and Fig. 2.2, it can be seen that the non-coherent AF is significantly smoother (i.e., accepting higher grid steps for the AF approximation) than the coherent AF and the maximum of the non-coherent AF provides an accurate estimate of the receiver location.

Therefore, the non-coherent AF without relying on phase information can provide reasonable localization accuracy with lower computational complexity and memory storage requirements. This method can be more efficient and robust in certain localization applications, especially in scenarios where dense spatial sampling is challenging or not feasible.

2.2.3 Coarse localization with multiple antenna transmission

In this subsection, we present results of numerical experiments that aim to compare the localization accuracy of the coarse MFP approach using the coherent and non-coherent AFs, in scenarios where multiple transmit antennas are employed. We apply the MISO multiple antenna scheme to the coarse MFP localization for improving data rate. We expect the localization performance of both coherent and non-coherent approaches to improve with the number of transmit antennas, but in different levels.

Table 2.2 Parameters for coarse receiver localization.

Variable name	Value	Description
C_{d}	1 m	Coarse grid step in depth
C_{r}	1 m	Coarse grid step in range
D_{T}	$50, 60, 70, 80$ m	Depth of transmit antennas
D_l	200 m	Depth for area of interest
K	1024	Number of subcarriers
N_{T}	1, 2, 4	Number of transmit antennas
R_l	500 m	Range for area of interest
S_c	201×501	Size of the coarse grid map
δ	1 Hz	Subcarrier spacing
τ	$[-0.5 \text{ s}, 0.5 \text{ s}]$	Delay uncertainty interval

In the experiments, to measure the localization performance, the cumulative distribution function (CDF) is computed for the position error

$$\varepsilon = \sqrt{(\hat{x}-x)^2 + (\hat{y}-y)^2}, \tag{2.8}$$

where $\hat{x}$ and $\hat{y}$ are estimates of the true range x and depth y, respectively. The CDF is obtained in 100 simulation trials. In each simulation trial, the receiver position is uniformly random within the area of interest. The main simulation parameters are given in Table 2.2.

In these numerical experiments, we compare the coarse localization performance using the coherent AF and non-coherent AF metrics. We analyse the CDF of the localization error ε for both metrics, considering low and high carrier frequencies f_c, and varying the number of transmit antennas N_{T}. The SSP is assumed to be uniformly distributed, as shown in Fig. 2.3.

The results, as shown in Fig. 2.5, Fig. 2.6, Fig. 2.7 and Fig. 2.8, demonstrate that the localization performance provided by the non-coherent AF is significantly better than that provided by the coherent AF. As the number of transmit antennas N_{T} increases, the performance improves for both metrics.

At the low carrier frequency $f_c = 3072$ Hz, when using the non-coherent AF with $N_{\mathrm{T}} = 2$, all receivers are localized within an error of $\varepsilon \leq 2$ m, whereas, for the coherent AF even with $N_{\mathrm{T}} = 4$, in more than 40% of cases, the error is higher than 2 m. Thus, the use of the non-coherent AF significantly reduced the number of outliers, as was previously demonstrated in Fig. 2.4.

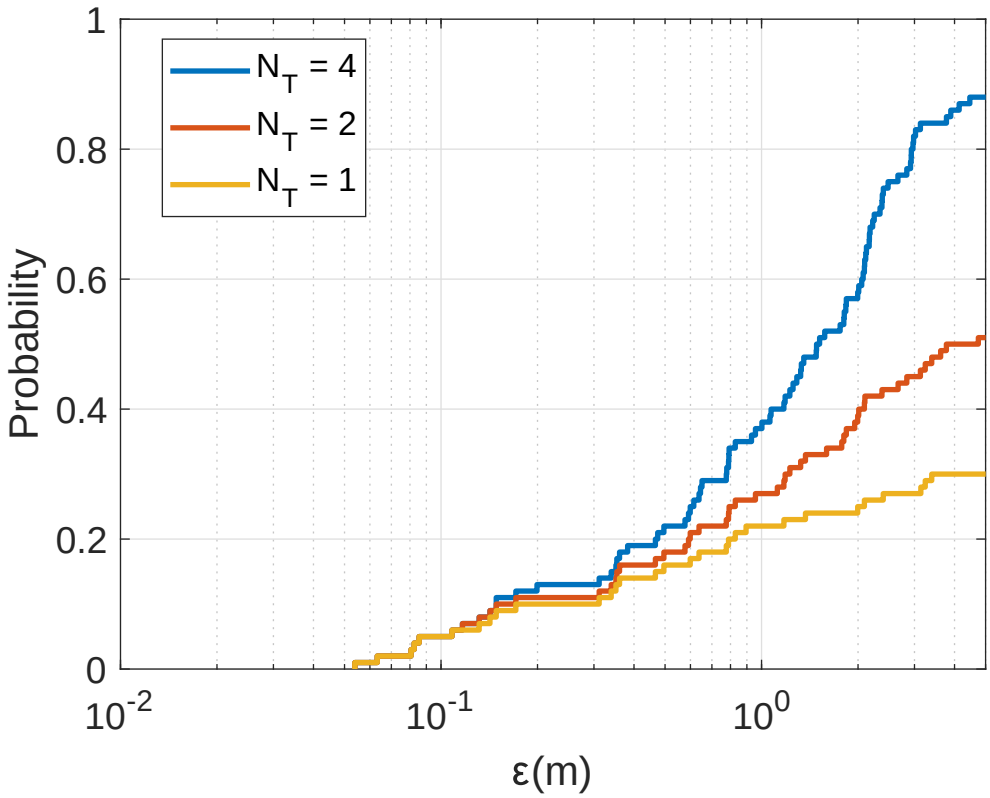

Fig. 2.5 CDF of the localization error ε for the coarse localization using the coherent AF at low carrier frequency $f_c = 3072$ Hz against the number of transmit antennas N_{T}.

Furthermore, the results show that the increase of carrier frequency f_c results in a significant degradation of localization performance with the coherent AF, whereas the non-coherent AF maintains consistent performance. This indicates that the non-coherent AF is more robust to changes in carrier frequency compared to the coherent AF, which may suffer from performance degradation at higher carrier frequencies.

Therefore, these findings suggest that the non-coherent AF is more accurate and robust for coarse MFP localization compared to the coherent AF, especially when the carrier frequency is high or the number of transmit antennas is limited.

2.3 Conclusions

This chapter has focused on the investigation of an underwater coarse MFP localization technique. The considered techniques are designed for a single-antenna UWA communication

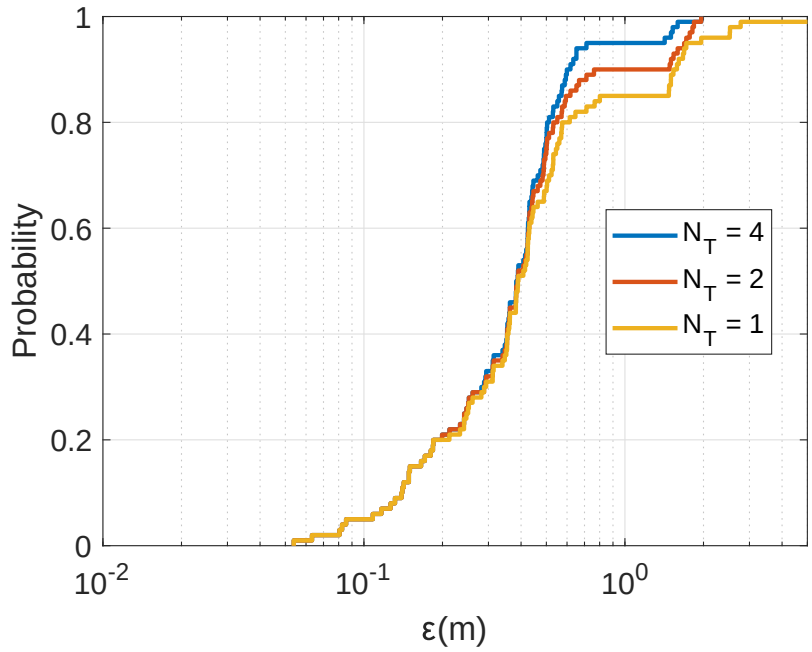

Fig. 2.6 CDF of the localization error ε for the coarse localization using the non-coherent AF at low carrier frequency $f_c = 3072$ against the number of transmit antennas N_{T}.

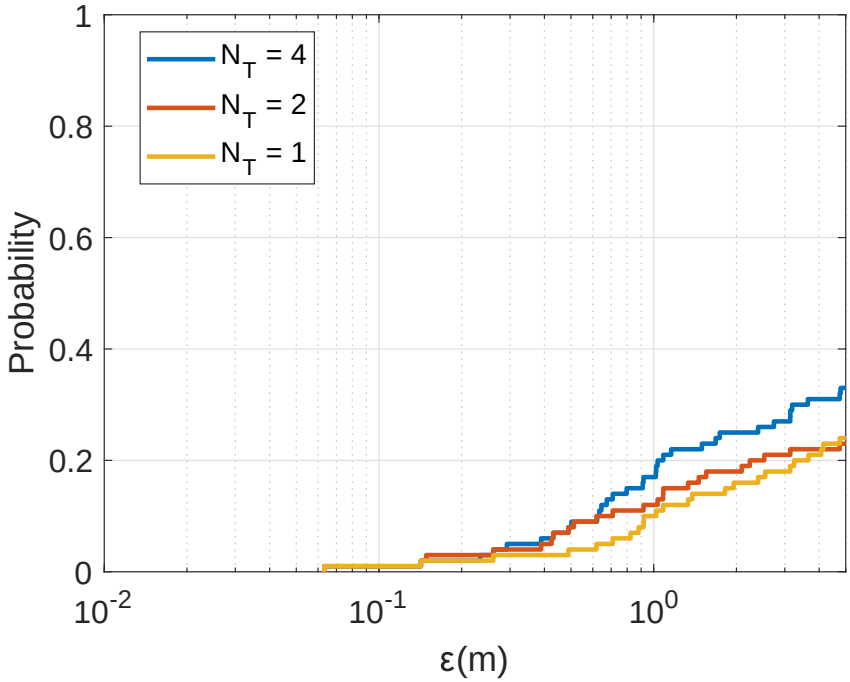

Fig. 2.7 CDF of the localization error ε for the coarse localization using the coherent AF at relatively high carrier frequency $f_c = 15360$ Hz against the number of transmit antennas N_{T}.

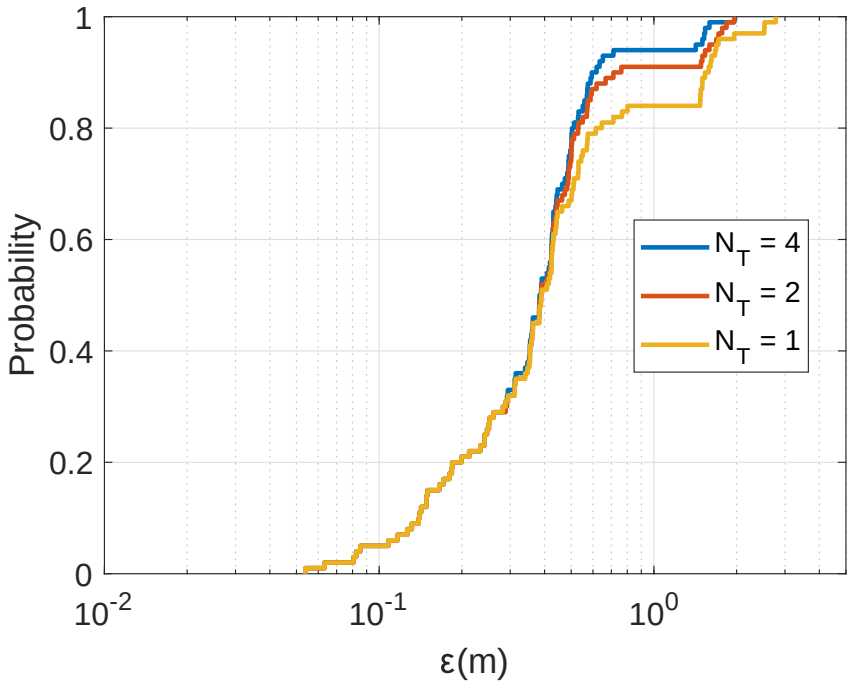

Fig. 2.8 CDF of the localization error ε for the coarse localization using the non-coherent AF at relatively high carrier frequency $f_c = 15360$ Hz against the number of transmit antennas N_{T}.

receiver. A non-coherent AF method has been proposed to improve the localization accuracy when compared to the method based on using the coherent AF, especially at high frequencies.

While the non-coherent AF has been shown to reduce the number of grid points compared to the coherent method, it may still be computationally intensive for real-time implementation in UWA communication receivers with limited computation resources. To address this, further reduction in computation can be achieved by employing pre-localization techniques, such as using known methods to estimate the receiver's depth. This can significantly reduce the grid size and, as demonstrated in the later chapters, can also result in higher localization accuracy.

The several maximum search and multiple refinement techniques proposed in the following chapter can also contribute to achieving a very high localization accuracy. These techniques can compensate for potentially low spatial resolution at the coarse grid level when using the non-coherent AF, by refining the localization results at a finer scale. This can further improve the accuracy of the localization process and enhance the performance of the proposed technique.

Chapter 3

Coarse-to-fine localization

3.1 Introduction

Localization accuracy is a crucial factor in underwater wireless sensor networks (UWSNs) [87, 88]. Accurate localization of sensor nodes enables an autonomous underwater vehicle (AUV) to determine its positions accurately, allowing for efficient data collection. A high localization accuracy allows the AUV to decrease its communication distance to sensor nodes, reducing the energy required for communication and increasing the data delivery ratio, particularly in high signal-to-noise ratio (SNR) communication environments [89]. On the other hand, low localization accuracy may result in the AUV failing to discover sensor nodes, leading to incomplete data collection and reduced system performance.

The communication range in UWSNs refers to the maximum distance over which sensor nodes can exchange data [90, 91]. Accurate localization allows for better estimation of the distance between nodes, which in turn enables optimized communication range planning. Inaccurate localization may result in unreliable communication links, leading to higher packet loss rates, increased retransmissions, and reduced communication range, which can significantly degrade the overall system performance.

Data delivery ratio indicates the proportion of successfully delivered data packets to the intended destination [92, 93]. Accurate localization enables efficient routing and forwarding of data packets based on accurate location information, resulting in higher data delivery ratios. Inaccurate localization may result in incorrect routing decisions, leading to packet losses, increased overhead, and reduced data delivery ratio.

Energy consumption is a critical factor in UWSNs due to the limited energy resources of underwater sensor nodes [94]. Accurate localization can optimize energy-efficient routing and communication protocols. In addition, it enables effective sleep scheduling and duty cycling of sensor nodes [73]. Inaccurate localization may result in inefficient energy usage, leading

to higher energy consumption, shorter network lifetime, and increased energy replenishment requirements.

Therefore, localization accuracy is a crucial factor in UWSNs, and there is a growing demand for more accurate localization techniques to overcome the challenges of the underwater environment and enable reliable and precise underwater monitoring and sensing applications.

In the coarse localization techniques from Chapter 2, the estimated channel frequency response is compared with pre-computed frequency responses in a grid map [69]. The grid map covers a large area of interest in terms of range and depth. The maximum value of the AF (either coherent or non-coherent) corresponds to the most likely target location, but low spatial resolution and outliers may limit localization performance. The accuracy of the estimated source location cannot be lower than the grid step; the outliers also influence the receiver localization, resulting in a totally wrong position.

To solve these problems and further improve localisation accuracy, a two-step (coarse-to-fine) technique for underwater localization is proposed and investigated in this chapter. This localization technique involves a coarse step and a fine step, aimed at achieving high accuracy while reducing complexity and memory storage requirements.

In the coarse-search step, by comparing the estimated channel response with the pre-computed frequency responses, the technique aims to find the maximum of the AF, which corresponds to the most likely source location. This step provides an initial estimate of the source location.

In the fine-search step, after obtaining the maximum of the AF in the coarse step, a refined spatial sampling of the AF is performed in the vicinity of the maximum. This means that the localization search is focused at an area around the estimated source location obtained at the coarse step, which reduces the search space and computational complexity. The refined spatial sampling allows for a more accurate estimation of the source location by obtaining a higher resolution of the AF in the vicinity of the maximum. The coarse step helps to reduce the complexity, as it narrows down the search space to a smaller region of interest, while the fine step improves the final localization resolution.

The two-step technique offers several advantages over a single step localization approach. It allows for high localization accuracy by refining the estimation in the fine step while reducing the computational complexity and memory storage requirements compared to exhaustive searching over the entire area of interest. By leveraging the pre-computed frequency responses in the grid map, the technique can efficiently estimate the source location with reduced computational overhead. Overall, the proposed two-step technique can be a promising approach for underwater localization, providing accurate results with reduced complexity and memory storage requirements.

3.2 Refinement

The receiver location can be estimated on the grid map using the coarse localization scheme. However, the accuracy of the coarse estimation is limited by the coarse grid steps; additionally, outliers are more likely when the receiver is not located on a grid point, which will be discussed in subsection 3.2.1. Therefore, a fine estimation of the receiver location is required to reduce the error between the estimated and true receiver positions. For the refinement, the estimated position resulting from the coarse estimation is regarded as a center point, and a small-size (refined) grid map around the center point is generated with a finer resolution.

The localization performance can be improved by the refinement of the grid map in the vicinity of the coarse estimate. Fig. 3.1 demonstrates how the refinement works. The sign △ represents the true receiver position. The sign ■ denotes the maximum of the AF on the coarse grid. Assuming that this is not an outlier, these two positions will be close to each other as shown in Fig. 3.1. For the refinement, additional grid points are computed with a finer resolution. In Fig. 3.1, the refined steps (in the following text, these will also be called refinement steps) for both range and depth are half the size of the coarse grid steps. In Fig. 3.1a, the refinement area size is chosen as $2C_\mathrm{r} \times 2C_\mathrm{d}$, where C_r and C_d are coarse grid steps in range and depth, respectively. The choice of the refinement area can impact the localization accuracy. In some cases, as will be shown in Section 3.4, a larger refinement area can improve the localization performance, such as the larger refinement area shown in Fig. 3.1b, where the refinement area size is $4C_\mathrm{r} \times 4C_\mathrm{d}$. The error of the coarse localization is the distance between the signs △ and ■, whereas the error of the fine localization is the distance between the sign △ and the closest refined grid point, which is smaller than the coarse error due to the use of a small refined step.

The refined grid map can be computed by using the ray tracing model, similar to how the coarse grid map is computed. However, a computationally more efficient approach is based on bilinear interpolation between coarse grid points.

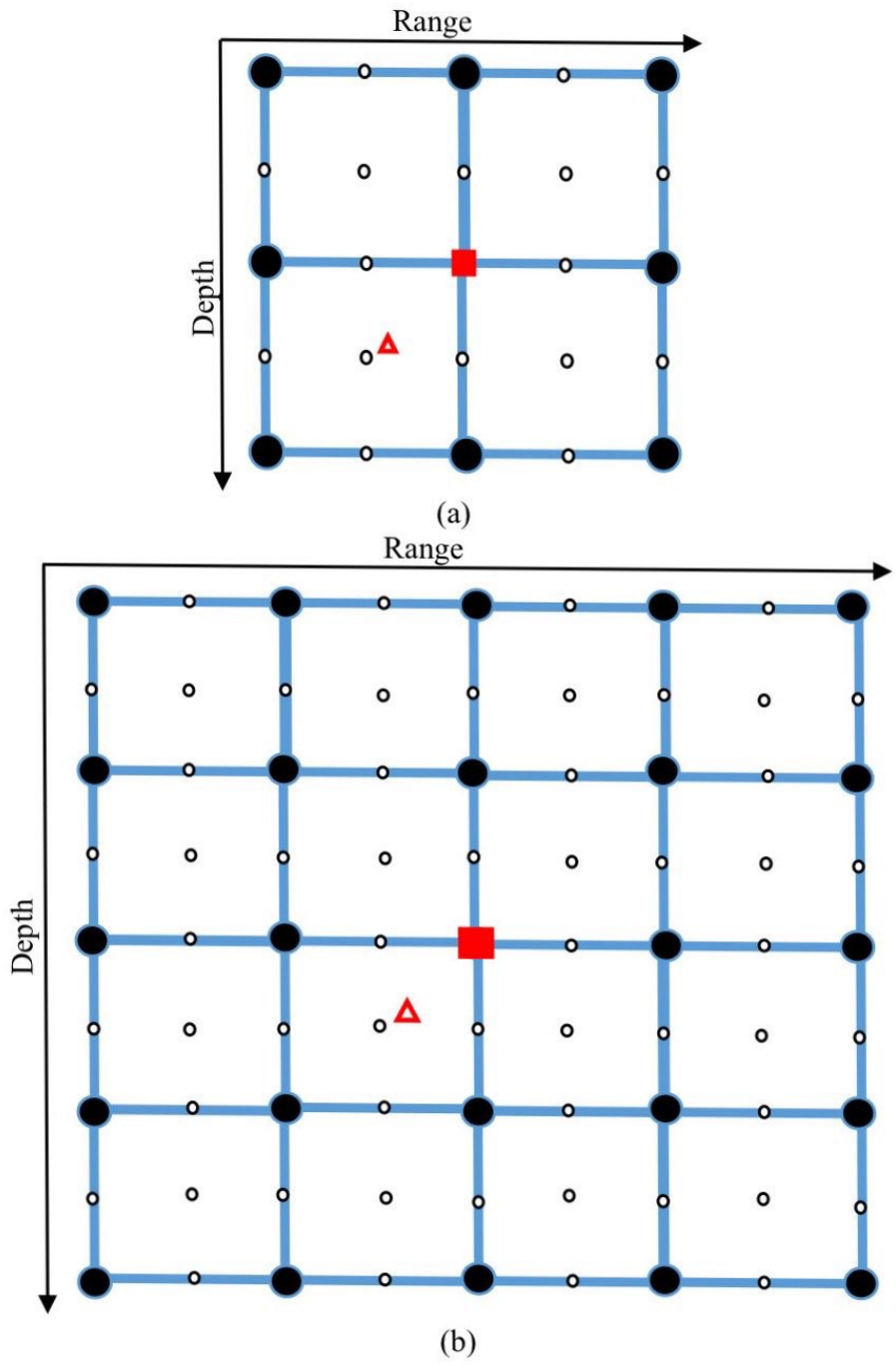

Fig. 3.1 The structure of refined areas in two cases: (a) the size of the refined area is $2C_{\mathrm{r}} \times 2C_{\mathrm{d}}$; (b) the size of refined area is $4C_{\mathrm{r}} \times 4C_{\mathrm{d}}$, where C_{r} and C_{d} are coarse grid steps in range and depth, respectively. The refined grid step in depth is $F_{\mathrm{d}} = C_{\mathrm{d}}/2$, the refined grid step in range is $F_{\mathrm{r}} = C_{\mathrm{r}}/2$. Notation: $\triangle$ is the true receiver position, $\blacksquare$ is the coarse location estimate, $\bullet$ are coarse grid points, $\circ$ are refined grid points.

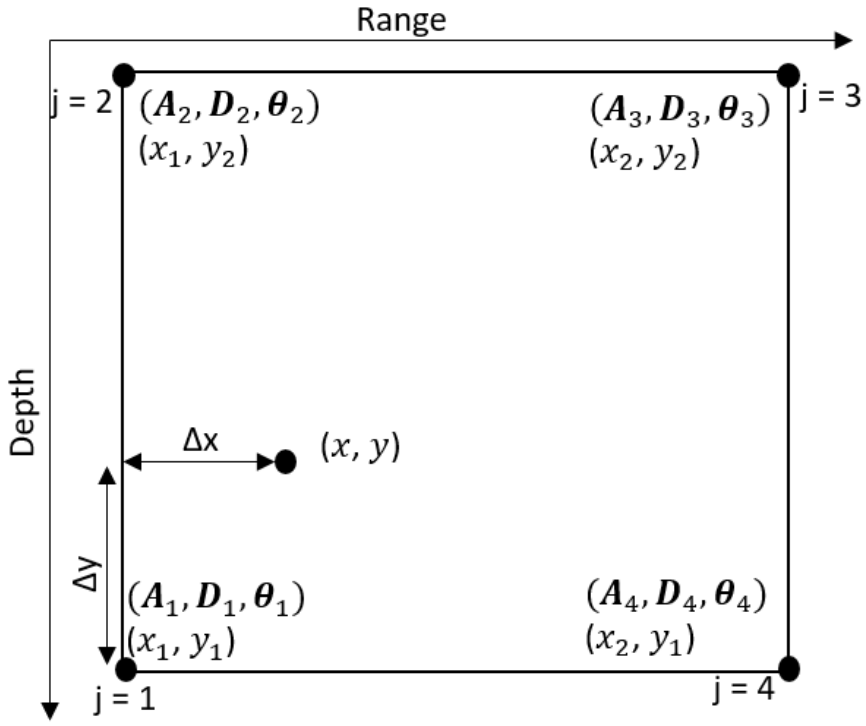

Fig. 3.2 An illustration of bilinear interpolation. Points (x_1,y_1), (x_1,y_2), (x_2,y_2), (x_2,y_1) are grid points on the coarse grid map. The point (x,y) is the refined grid point. The vectors $\mathbf{a}_j$, $\mathbf{d}_j$, $\boldsymbol{\theta}_j$, $j = 1,\ldots,4$, are vectors of the ray amplitudes, delays and angles of arrivals for the jth coarse grid point in this figure.

Consider an example of the bilinear interpolation of the acoustic field at the refined grid point (x,y) using the acoustic fields computed at the four neighbouring coarse grid points, as illustrated in Fig. 3.2. To compute amplitudes and delays for rays arriving at the point (x,y), we use the approach in [95].

The bilinear interpolation of the acoustic field at the refined grid point (x,y) can be computed using the following steps.

(1) Identify the four nearest coarse grid points to the refined grid point (x,y), denoted as (x_1, y_1), (x_2, y_2), (x_3, y_3), and (x_4, y_4), respectively. These four points form a rectangular region surrounding the refined grid point, as shown in Fig. 3.2.

(2) Compute the weights for the four nearest coarse grid points based on their relative distances to the refined grid point.

(3) Compute the bilinear interpolation of the acoustic field at the refined grid point as a weighted average of the acoustic fields at the four nearest coarse grid points, using the computed weights.

(4) Repeat the interpolation process for all the refined grid points in the refined area.

Furthermore, the approach in [95] is illustrated in Fig. 3.2. The vector of amplitudes is given by

$$\mathbf{a} = \begin{bmatrix} (1-w_1)(1-w_2)\mathbf{a}_1 \\ (1-w_1)w_2\mathbf{a}_2 \\ w_1 w_2 \mathbf{a}_3 \\ w_1(1-w_2)\mathbf{a}_4 \end{bmatrix},$$

where $\mathbf{a}_j$ is the $\ell_j \times 1$ vector of arrival amplitudes at the jth coarse grid point, $j = 1,\ldots,4$. $\ell_j \leqslant \ell_{\max}$, $\ell_{\max}$ defines the maximum number of arrivals. The weights are given by

$$\begin{aligned} w_1 &= (x-x_1)/(x_2-x_1), \\ w_2 &= (y-y_1)/(y_2-y_1), \end{aligned} \tag{3.1}$$

where w_1 and w_2 represent proportional distance in the x direction and y direction, respectively. The vector of delays is given by

$$\mathbf{d} = \begin{bmatrix} \mathbf{d}_1 + \Delta\mathbf{d}_1 \\ \mathbf{d}_2 + \Delta\mathbf{d}_2 \\ \mathbf{d}_3 + \Delta\mathbf{d}_3 \\ \mathbf{d}_4 + \Delta\mathbf{d}_4 \end{bmatrix}, \tag{3.2}$$

where $\mathbf{d}_j$ is the $\ell_j \times 1$ vector of arrival delays at the jth coarse grid point. The adjusted delays from position (x_j, y_j) to position (x, y) are computed as

$$\Delta\mathbf{d}_j = (\Delta x_j \cos\boldsymbol{\theta}_j + \Delta y_j \sin\boldsymbol{\theta}_j)/c_j, \tag{3.3}$$

where

$$\begin{aligned} \Delta x_j &= x - x_j, \\ \Delta y_j &= y - y_j, \end{aligned} \tag{3.4}$$

$\boldsymbol{\theta}_j$ is the $\ell_j \times 1$ vector of arrival angles at the jth coarse grid point, $j = 1,\ldots,4$, and c_j is the sound speed at the depth of the jth coarse grid point.

Elements of the frequency response for the nth refined grid point, the point (x, y) as shown in Fig. 3.2, are given by

$$g_n^{m_0}(f_k) = \sum_{i=0}^{\ell_1+\ell_2+\ell_3+\ell_4-1} a_i e^{-j2\pi f_k d_i}, \tag{3.5}$$

where $k = 0, \ldots, K-1$, a_i and d_i are elements of vectors $\mathbf{a}$ and $\mathbf{d}$, respectively. The vector $\mathbf{g}_n^{m_\mathrm{o}}$ with elements from (3.5) is used to compute the AF $c_n^{m_\mathrm{o}}$.

With such a refinement, an improved position estimate is found from the maximum AF within the refinement area:

$$n_\mathrm{o} = \arg \max_{n=1,\ldots,M_R} c_n^{m_\mathrm{o}}, \tag{3.6}$$

where M_R is the number of refined grid points in the vicinity of the coarse receiver location estimate m_o and the set of values $c_n^{m_\mathrm{o}}$ over n from 1 to M_R is the AF computed on the refined grid map. As examples, for the refined area in Fig. 3.1a, $M_R = 25$; for the refined area in Fig. 3.1b, $M_R = 81$. As will be shown in Section 3.4.1, the refinement can greatly reduce the error between the estimated and true receiver positions.

3.2.1 Multiple refinement areas

The receiver position is found as the position of the global AF maximum. The AF, as a continuous function of range and depth, apart from the global maximum, has multiple local maxima. With a finite spatial sampling rate, i.e. finite grid steps in range and depth, the AF maximum on the grid map might correspond to a local maxima. In this situation, the location estimate is an outlier, i.e. the location error can be arbitrary high. The refinement does not overcome this problem since it is possible that the refinement is performed in the vicinity of the outlier.

In order to solve this problem, we can choose several AF maxima, the number of which is defined as N_max, from the coarse grid map, perform refinement in the vicinity of each of them and find the AF maximum jointly on all the N_max refinement areas.

This can be implemented as illustrated in Fig. 3.3. Firstly, the AF maximum is found on the coarse grid map, the maximum position is $m_\mathrm{o}^{(1)}$. Then, coarse grid points in the corresponding refinement area, around the coarse grid point $m_\mathrm{o}^{(1)}$, are removed from the coarse grid map. We will consider two cases of removing the coarse grid points. In the first case, only the maximum point is removed (one point). In the second case, 9 points are removed including the maximum and 8 neighbouring coarse points. Then the AF maximum at the grid position $m_\mathrm{o}^{(2)}$ is found on the updated coarse grid map. The same procedure can be repeated to find the third AF maximum at the position $m_\mathrm{o}^{(3)}$, etc. For each new grid position with AF maximum, the refinement is now performed in the vicinity of the possible candidate for receiver location. The position of a joint AF maximum over N_max multiple refinement areas is the final location estimate. As will be shown in subsection 3.4.1, the multiple refinement process can remove outliers in the localization process.

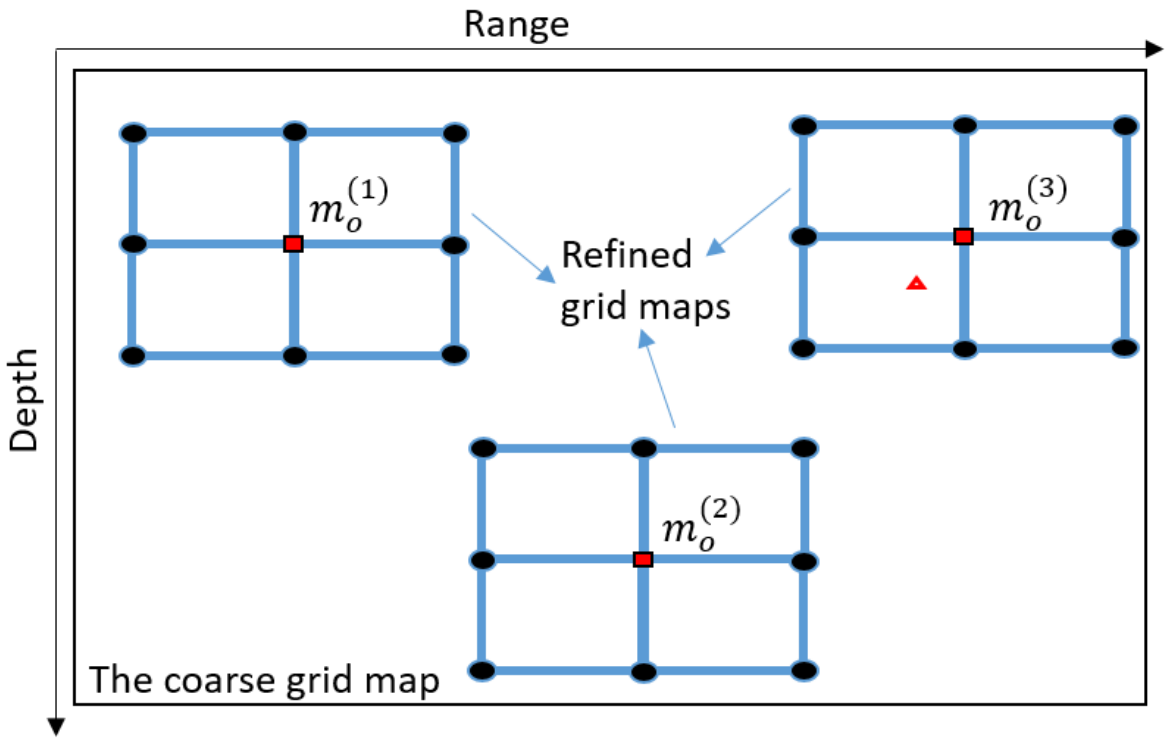

Fig. 3.3 An illustration of multiple refinement areas ($N_{\max} = 3$ as an example) in the area of interest.

3.3 Complexity of the two-step localization

In this subsection, we present an analysis of the complexity of the proposed localization technique.

For the localization, the following steps should be carried out:

1. Coarse step, including the AF computation in (2.7) processed by an efficient algorithm in (2.5), and finding the AF maximum.

2. Refinement step, including the computation of $N_{\max}$ refined grid maps with the bilinear interpolation described by (3.2) to (3.5), computation of the refined AFs and their maxima using (2.7), (2.5) and (3.6).

Specifically, for the coarse step, in (2.7), the vector $\tilde{\mathbf{g}}_{t,m}$, related to the channel frequency response on the mth grid point corresponding to the tth coarse grid map can be pre-computed and stored into memory. Here, we consider the computation of the vector $\tilde{\mathbf{h}}_t$, related to the estimated channel frequency response. $\tilde{\mathbf{h}}_t = \tilde{\mathbf{F}}\text{abs}(\tilde{\mathbf{F}}^H\mathbf{h}_t)$ which requires two FFT operations of size K; when using the split-radix FFT algorithm in [96], the complexity of computing each FFT requires $K\log_2 K$ multiply and accumulate operations (MACs). The complexity of computing $\text{abs}(\tilde{\mathbf{F}}^H\mathbf{h}_t)$, requires $6K$ MACs. In (2.5), the computation is considered for every grid point in each grid map. The complexity of computing $\tilde{\mathbf{q}}$ requires the FFT operation of size pK, which requires $pK\log_2 pK$ MACs; the complexity of computing $\tilde{\mathbf{g}}_m^H \odot \tilde{\mathbf{h}}$ is K MACs; the complexity of computing square of elements in $\tilde{\mathbf{q}}$, $|\tilde{\mathbf{q}}|^2$, requires $2pK$ MACs; the complexity of computing the maximum requires pK MACs; for the $\|\tilde{\mathbf{h}}\|_2^2$, the complexity of this computation is about K MACs. Therefore, the complexity of computing the coarse receiver localization is

$$C_{\text{coarse}} \approx N_T[2K\log_2 K + 6K + M(pK\log_2 pK + 3pK + 2K)]. \tag{3.7}$$

For the refined step, based on the tth coarse grid map, the complexity of computing (3.5) requires $4K\ell_{\max}$ for every refined point corresponding to each local maxima. The complexity of computing the refined AFs using (2.7) and (2.5) is the same as the coarse step for each point, it requires $2K\log_2 K + 6K + pK\log_2 pK + 3pK + 2K$ MACs. Therefore, the complexity of computing the fine receiver localization for each trial is given as,

$$C_{\text{fine}} \approx N_T N_{\max} M_{\text{R}}(4K\ell_{\max} + 8K + 2K\log_2 K + pK\log_2 pK + 3pK). \tag{3.8}$$

The total complexity of computing the coarse-to-fine receiver localization is

$$C_{\text{total}} = C_{\text{coarse}} + C_{\text{fine}}. \tag{3.9}$$

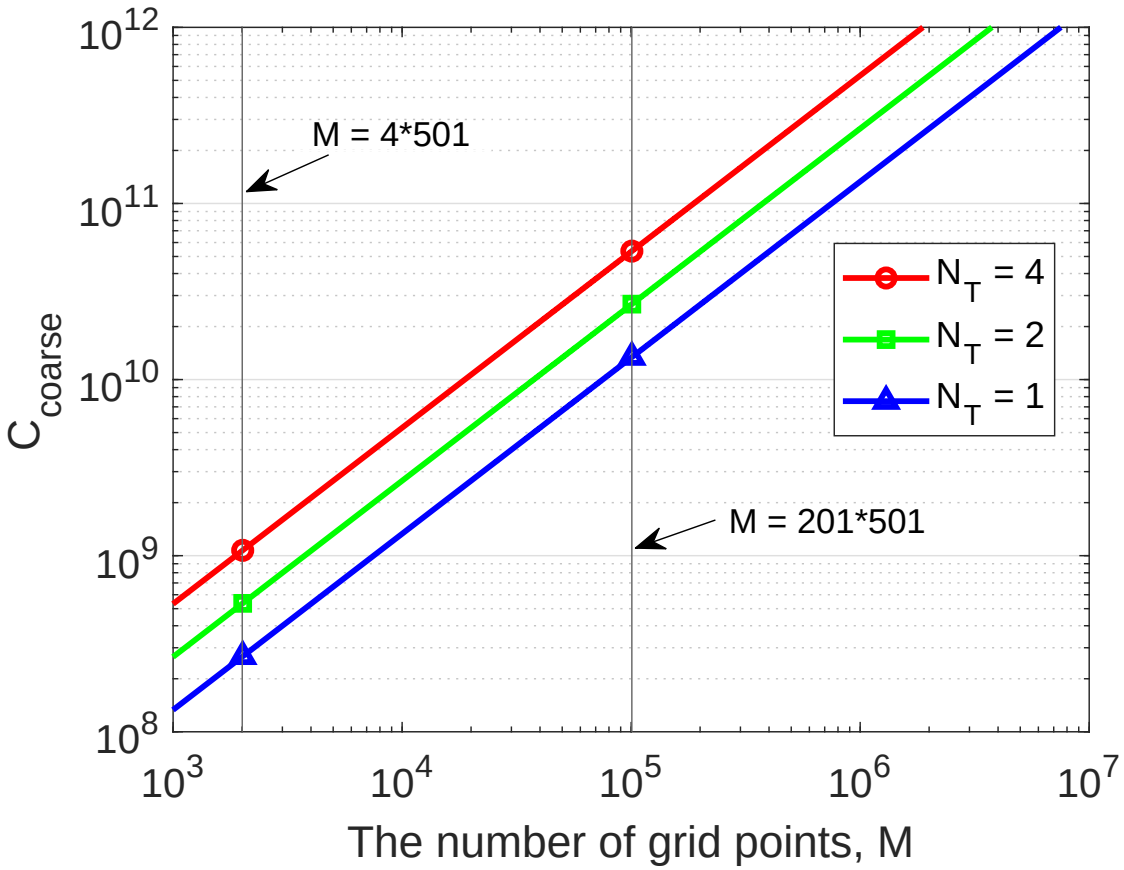

Fig. 3.4 The coarse-search complexity of the proposed localization algorithm against the number of transmit antennas N_T when the number of the coarse grid points is M.

The complexity for coarse-search computation and fine-search computation is shown in Fig. 3.4 and Fig. 3.5. Fig. 3.4 shows the complexity of the coarse localization algorithm with different number of transmit antennas N_T. For the whole area of interest with $M = 201 \times 501 \approx 10^5$ coarse grid points, the complexity of the coarse search for $N_T = 4$ transmit antennas, C_{coarse}, $\approx 5.7 \times 10^{10}$ MACs. This complexity may be excessive for a general-purpose processor, especially the ones that can be practically used on low-power communication nodes. However, most of the computation is based on the FFT and vector multiplication, i.e., operations well suited to implementation as hardware accelerators [97, 98]; moreover, since the coarse search involves multiple parallel computations, its hardware implementation, e.g., on Field Programmable Gate Array (FPGA) design platforms can be very efficient, making this stage of the proposed localization algorithm feasible. As for the coherent AF, as was mentioned in [69], the number of the grid points M needs to be

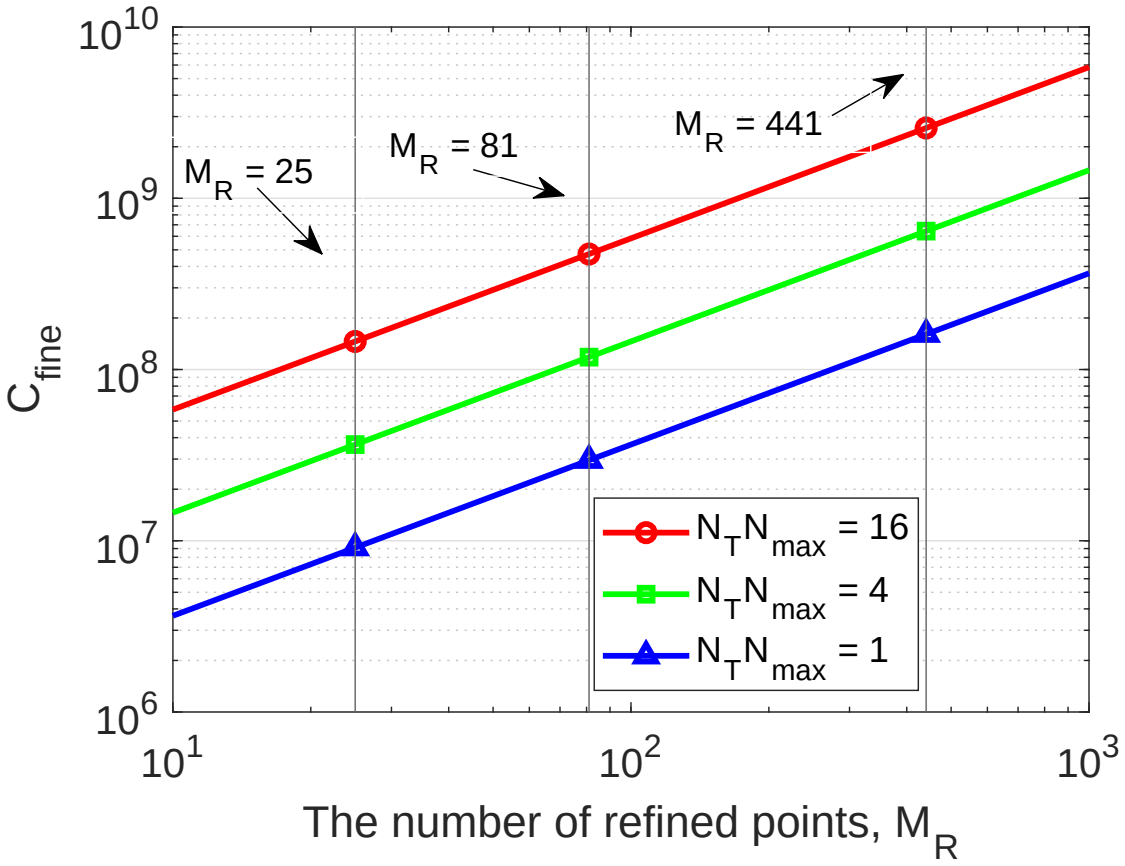

Fig. 3.5 The fine-search complexity of the proposed localization algorithm against the number of transmit antennas N_T when the number of the refined points is M_R.

significantly higher even for such a low carrier frequency as $f_c = 3072$ Hz, thus making the coarse search less suitable for practical implementation than that with the non-coherent AF.

A reduction in the coarse-search computation can be achieved by using a pre-localization of the receiver by any known methods. E.g., the knowledge of the receiver depth can significantly reduce the grid size M and, as will be shown in subsection 3.4.3, also results in a higher localization accuracy. As an example, from Fig. 3.4, it is seen that with 4 coarse grid points in depth, the total number of grid points is reduced to $M = 4 \times 501 \approx 2000$; in this case, $C_{\text{coarse}} \approx 1.1 \times 10^9$ MACs, which is more affordable at the receiver node.

Fig. 3.5 shows the complexity of the fine localization algorithm with different combinations of the product $N_T N_{\max}$. For the highest accuracy, when the refined steps are set to $F_r = F_d = 0.1$ m, we have $M_R = 441$ points in a refined area, and with $N_T = 4$ and $N_{\max} = 4$, the fine-search complexity, $C_{\text{fine}} \approx 1 \times 10^9$ MACs, which is high, but still lower than the complexity of the coarse search. For the lower localization accuracy, when the refined steps are set to $F_r = F_d = 0.5$ m ($M_R = 25$), the fine-search complexity, $C_{\text{fine}} \approx 9 \times 10^6$ MACs for $N_T = 1$ and $N_{\max} = 1$, which is significantly lower than the coarse-search complexity. Thus, the refinement stage does not result in significant increase in the total algorithm complexity compared to the coarse-search complexity.

3.4 Numerical results

In this section, we present results of numerical experiments for coarse-to-fine localization techniques by using two SSPs including the uniform SSP and the SWellEx-96 SSP. Firstly, we use the simple acoustic environment with the uniform SSP to validate refinement techniques, which is to prove its feasibility (in subsection 3.4.1 and subsection 3.4.2). Then, we do numerical experiments in a more complex acoustic environment with the SWellEx-96 SSP, which is to prove its robustness (in subsection 3.4.2, subsection 3.4.3 and subsection 3.4.4). In addition, scenarios with CSI imperfections are considered in subsection 3.4.3 and subsection 3.4.4. In these numerical experiments, the static sea surface is assumed, and we mainly consider the flat surface, but the sinusoidal surface with the SWellEx-96 SSP is considered in subsection 3.4.3.

The CSI imperfections, such as mismatched environments and inaccurate channel estimation, are critical factors that influence the performance of UWA localization systems in real-world scenarios. For mismatched environments, the SSP can be influenced by the environment change, then SSP errors happen, finally resulting in the extra localization errors; varying sea surfaces are also a factor to cause the imperfect CSI, leading to the localiza-

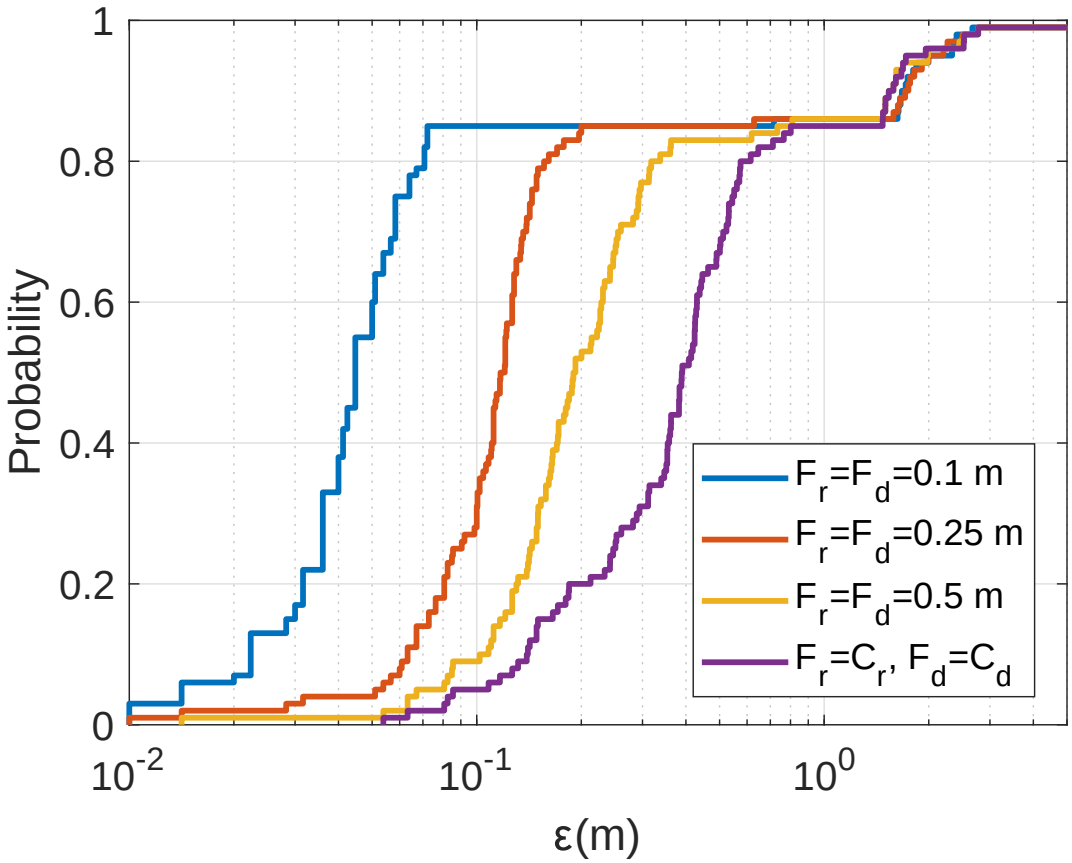

Fig. 3.6 CDF of the localization error ε for the coarse-to-fine localization using the non-coherent AF against different refined steps in range F_{r} and depth F_{d} with a refinement area of size 2 m $\times$ 2 m as shown in Fig. 3.1(a); the SSP is uniform as shown in Fig. 2.3; the number of transmit antenna is $N_T = 1$.

tion errors. For the inaccurate channel estimation, with the noisy underwater situation, the estimated CSI can be obtained imperfectly, finally resulting in inaccurate results.

Therefore, it is necessary to apply the proposed localization algorithms to validate the robustness in both perfect CSI and imperfect CSI.

3.4.1 Coarse-to-fine localization

We now demonstrate the benefit of the refinement for improving the localization performance. Fig. 3.6, Fig. 3.7 and Fig. 3.8 show the localization accuracy against the refinement steps in both depth and range with two sizes of refinement areas. It can be seen that the localization accuracy proportionally improves with a reduction in the refinement step, as long as there are no outliers.

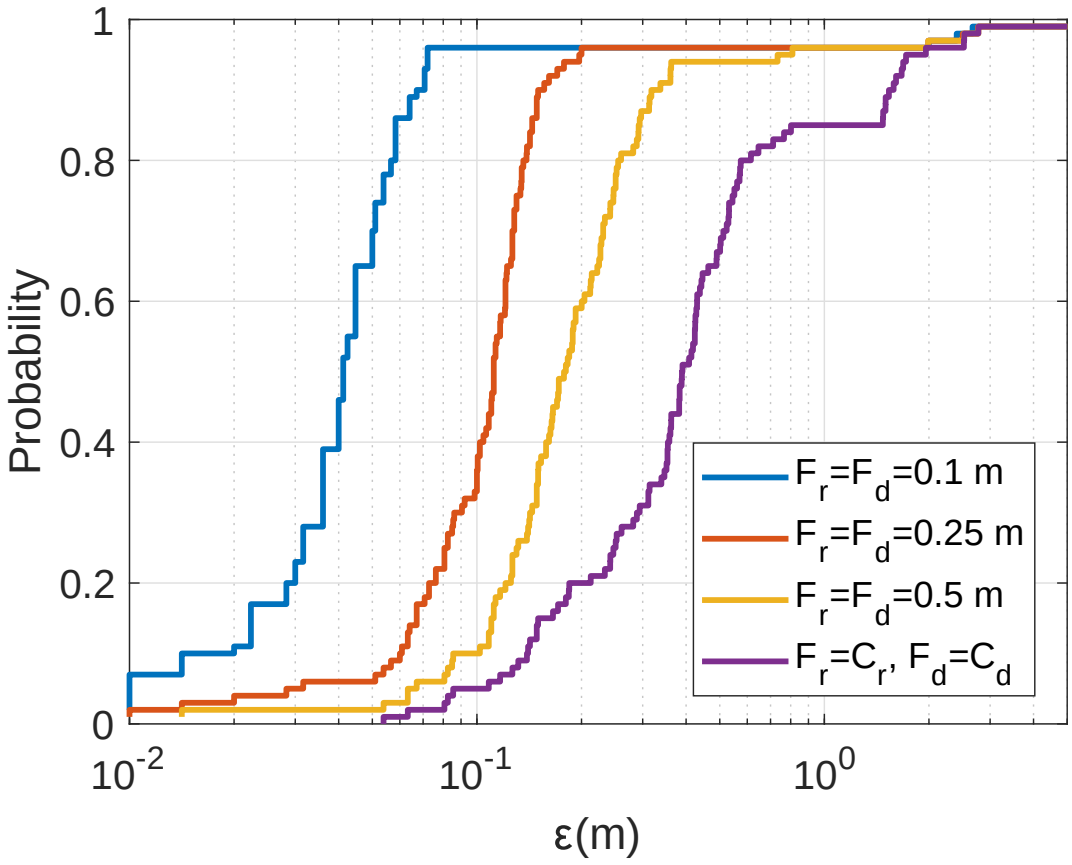

Fig. 3.7 CDF of the localization error ε for the coarse-to-fine localization using the non-coherent AF against different refined steps in range F_{r} and depth F_{d} with a refinement area of size 4 m $\times$ 4 m as shown in Fig. 3.1(b); the SSP is uniform as shown in Fig. 2.3; the number of transmit antenna is $N_T = 1$.

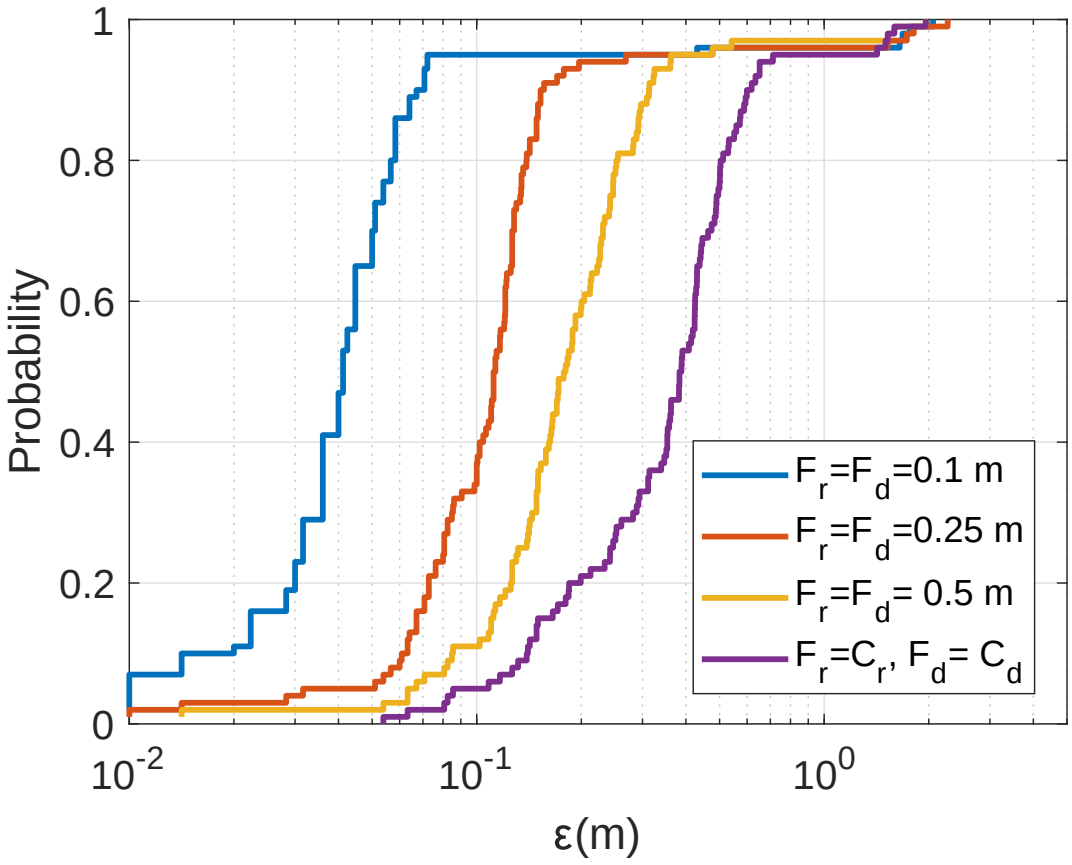

Fig. 3.8 CDF of the localization error ε for the coarse-to-fine localization using the non-coherent AF against different refined steps in range F_{r} and depth F_{d} with a refinement area of size 2 m $\times$ 2 m as shown in Fig. 3.1(a); the SSP is uniform as shown in Fig. 2.3; the number of transmit antenna is $N_T = 4$.

Fig. 3.6 presents results for one transmit antenna, and the refinement area in Fig. 3.1a. It is seen that if the non-coherent AF maximum on the coarse grid map is found in one of four coarse grid points surrounding the grid cell where the receiver is positioned, i.e., $\varepsilon < 1.4$ m, then the localization accuracy improves proportionally to the reduction in the refined step. It is also seen that there is a "step" in the CDF at $\varepsilon \approx 1.4$ m. This error corresponds to the maximum distance within the grid cell, and this means that, in a significant number of the trials, the non-coherent AF maximum is found in neighbouring grid cells.

Compared to Fig. 3.6, Fig. 3.7 is also for one transmit antenna, but the refinement area is increased by four times as shown in Fig. 3.1b. Apart from the same observations found in Fig. 3.6, with the same refined steps, the number of outliers significantly reduces when using a lager size of refinement area.

Compared to Fig. 3.6, Fig. 3.8 maintains the refinement area from Fig. 3.1a while increasing the number of transmit antennas to four. It can be seen that the localization accuracy significantly improves for all the grid steps, which shows similar localization accuracy to the results in Fig. 3.7. It indicates that, with a correct choice of the refinement area, the same improvement can be achieved as with the increase in the number of transmit antennas. Obviously, in practice, the increase in the refinement area would be much easier to implement. However, simultaneous increase in the refinement area and in the number of transmit antennas brings extra benefits.

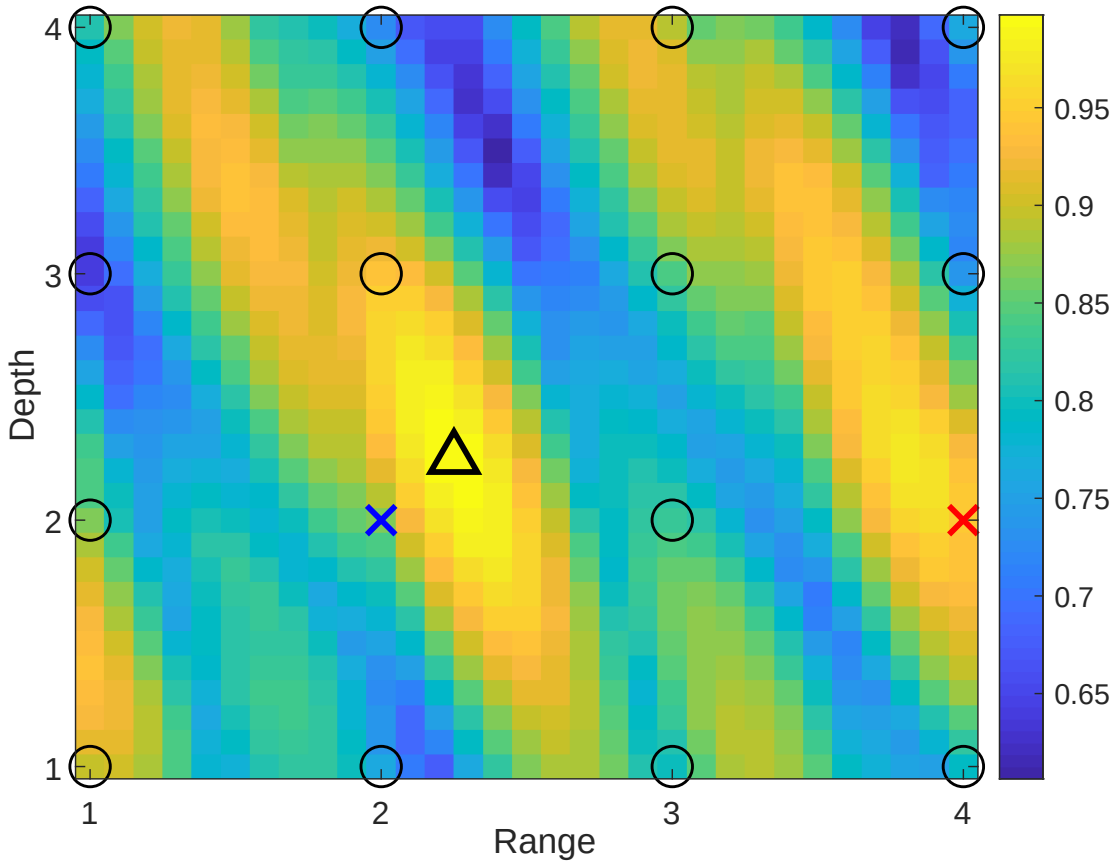

Fig. 3.9 An example of the "continuous-range continuous-depth" non-coherent AF in an area of 3 m $\times$ 3 m. The circles are positions of coarse grid points; the triangle is the position of the receiver; the blue cross is the coarse grid point closest to the true position of the receiver; the red cross is the coarse grid point with the AF maximum on the coarse grid map; $N_{\mathrm{T}} = 1$.

Fig. 3.9 illustrates one such case. The increase in the refinement area from 2 m $\times$ 2 m to 4 m $\times$ 4 m (as shown in Fig. 3.1b), improves the localization accuracy as can be seen from the comparison of Fig. 3.6 and Fig. 3.7. The increase in the refinement area allows somewhat reduction in "small" outliers. The number of outliers can also be reduced by increasing the number of transmit antennas, as demonstrated in Fig. 3.8. In this case, not only "small", but also "large" outliers are also eliminated. It will be shown in subsection 3.4.2 that the probability of outliers can be significantly reduced when using multiple refinement areas.

3.4.2 Multiple refinement areas

We now demonstrate the benefit of using multiple refinement areas for improving the localization performance, primarily by reducing the probability of outliers. Fig. 3.10 shows

the localization accuracy against the number of refinement areas $N_{\max}$. In this experiment, after finding an AF maximum on the coarse grid map, the maximum point is removed before the search for the next maximum. It can be seen that even with such large range and depth refined steps ($F_{\mathrm{r}} = F_{\mathrm{d}} = 0.5$ m), the search in two refinement areas significantly reduces the probability of outliers. Further increase in the number of refinement areas to $N_{\max} = 4$ provides further significant improvement; the probability of localization error $\varepsilon < 1$ m is as high as 96%. Note that this performance is achieved with only one transmit antenna. With two transmit antennas, as can be seen in Fig. 3.11, there are no outliers and the localization error is lower than 0.5 m in all simulation trials.

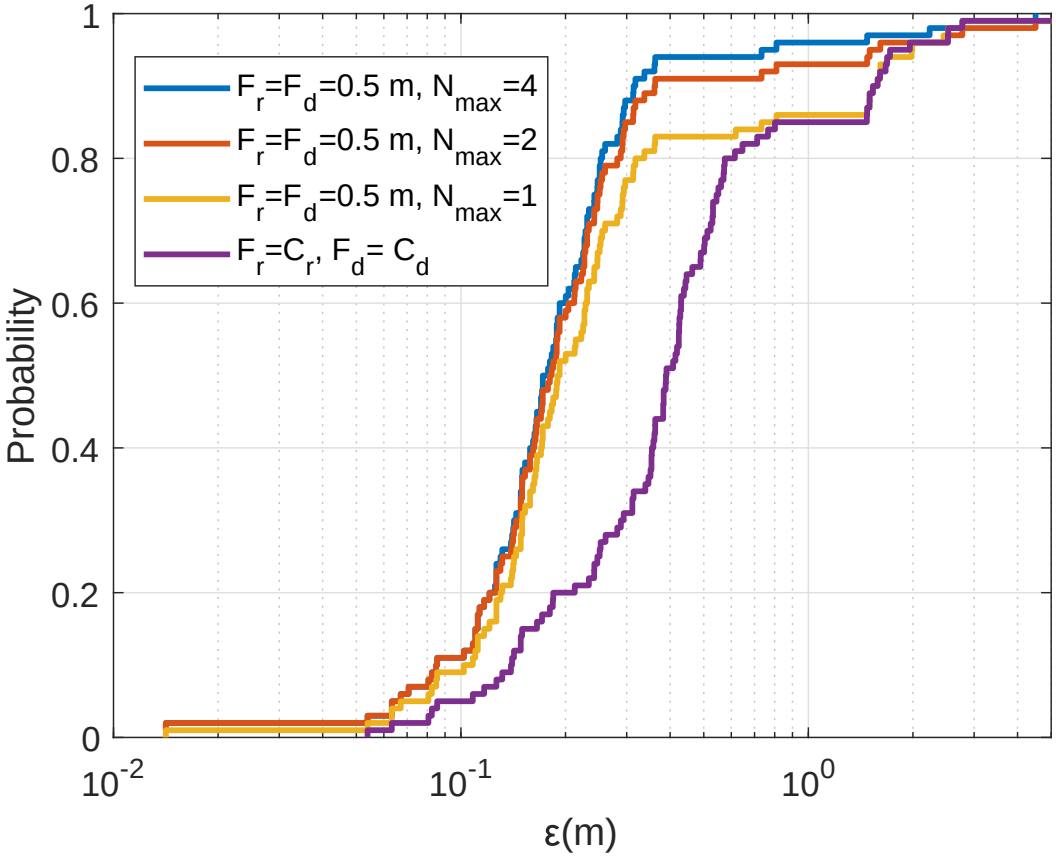

Fig. 3.10 CDF for the localization error ε in the acoustic environment with the uniform SSP against the number $N_{\max}$ of refinement areas; $N_{\mathrm{T}} = 1$, the size of a refinement area is 2 m $\times$ 2 m as shown in Fig. 3.1a.

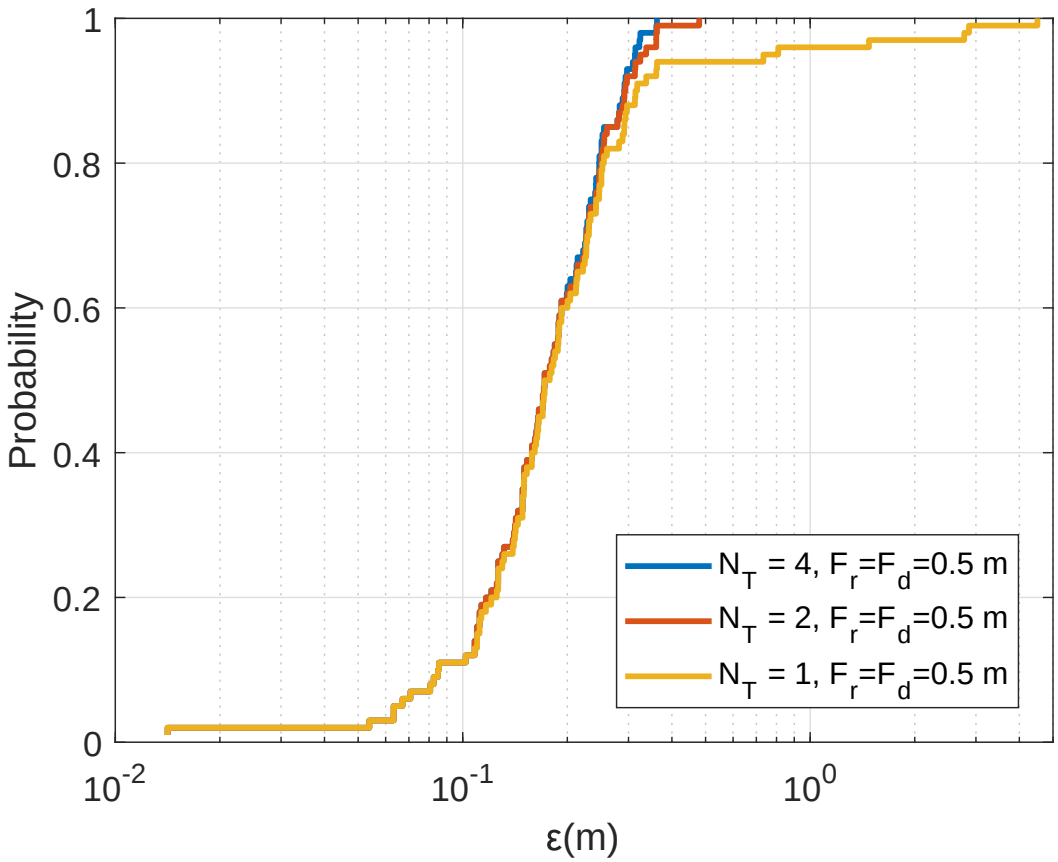

Fig. 3.11 CDF for the localization error ε in the acoustic environment with the uniform SSP against the number of transmit antennas N_{T}; $F_{\mathrm{r}} = F_{\mathrm{d}} = 0.5$ m, the number of refinement areas is $N_{\max} = 4$, where only one point is removed after finding the next maximum and the refinement area is 2 m $\times$ 2 m as shown in Fig. 3.1a.

In Fig. 3.12, we compare the localization performance with multiple refinement areas at different refined steps using four transmit antennas. With $N_{\mathrm{T}} = 4$ and $N_{\max} = 4$, the localization accuracy depends only on the refined step size, the smaller the refined step, the higher accuracy can be achieved.

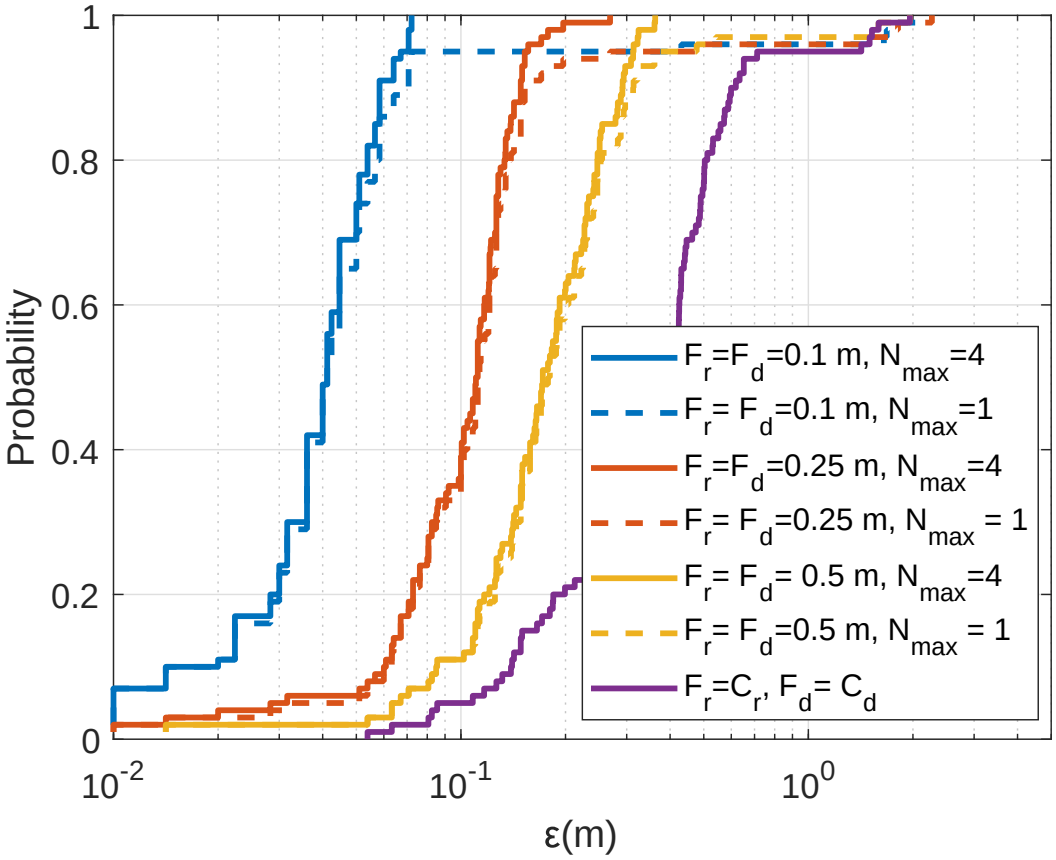

Fig. 3.12 CDF for the localization error ε in the acoustic environment with the uniform SSP against the refinement step and multiple refinement areas, where only one point is removed after finding the next coarse AF maximum; $N_{\mathrm{T}} = 4$, the refinement area is 2 m $\times$ 2 m as shown in Fig. 3.1a.

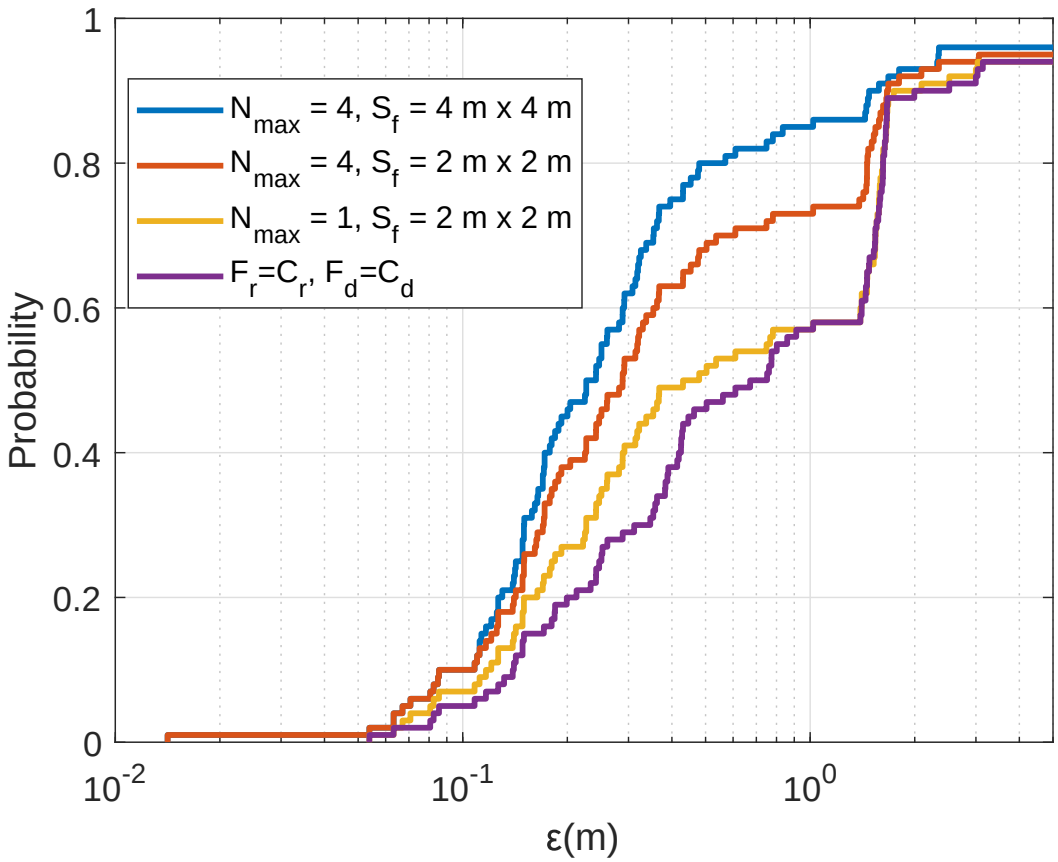

Fig. 3.13 CDF for the localization error ε in the acoustic environment with the SWellEx-96 SSP against the size of the refinement area S_f and number of refinement areas N_max, where one point is removed after finding the next coarse AF maximum; $N_\mathrm{T} = 1$; $F_\mathrm{r} = F_\mathrm{d} = 0.5$ m.

We now present results for another acoustic environment, with the SSP from the SWellEx-96 experiment [64] shown in Fig. 2.3.

Recall that in Fig. 3.10, we showed the localization performance with different number and size of refinement areas for the uniform SSP. The refined step used is 0.5 m. Fig. 3.13 shows the localization performance for the SWellEx-96 SSP. As can be seen from comparison of results in Fig. 3.10 and Fig. 3.13, the coarse localization performance with one transmit antenna with the SSP from the SWellEx-96 experiment provides significantly more outliers than that with the uniform SSP environment. For the uniform SSP, 85% of cases have the error $\varepsilon < 1.4$ m, whereas, for the SWellEx-96 SSP, only 58% of cases have such localization accuracy. By adopting four refinement areas of size 2 m $\times$ 2 m, the probability of outliers in the SWellEx-96 SSP environment is reduced from 42% to 26%, while in the uniform SSP environment, it is reduced from 15% to 4%. Even with a larger refinement area of 4 m $\times$ 4 m, in the SWellEx-96 SSP environment, the probability of outliers is still as high as 14%.

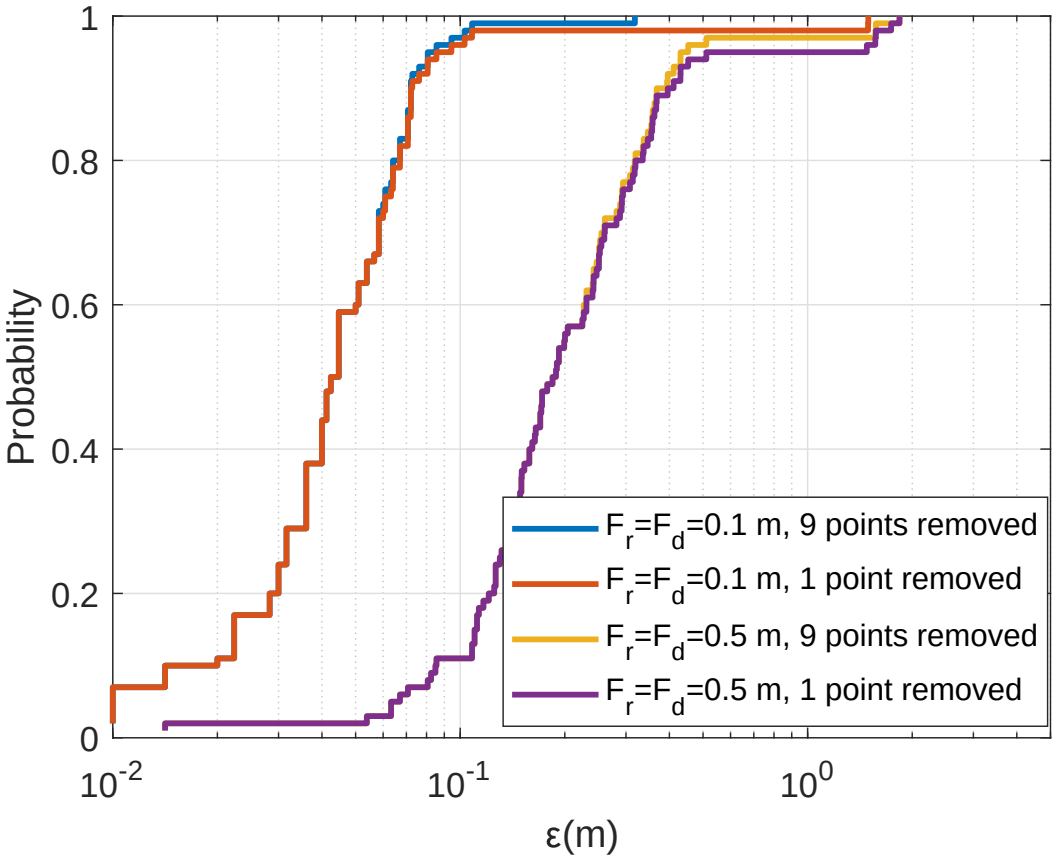

Fig. 3.14 CDF for the localization error ε in the acoustic environment with the SWellEx-96 SSP against refined steps $F_\mathrm{r} = F_\mathrm{d}$; $N_\mathrm{T} = 4$; $N_\mathrm{max} = 4$, after finding the AF maximum, two cases are considered, 1 point and 9 points are removed from the coarse grid map as described in subsection 3.2.1; the refinement area is $S_\mathrm{f} = 4$ m $\times$ 4 m (as shown in Fig. 3.1b).

In Fig. 3.14, we show the localization performance with the SWellEx SSP using four transmit antennas. Two cases are considered as described in subsection 3.2.1. For the first case, only one point is removed from the coarse grid map after finding the AF maximum; in the second case, nine points are removed. It can be seen that the use of four transmit antennas allows a significant reduction in the number of outliers. The localization accuracy can be further improved by using a smaller refined step. It can also be seen that when a smaller refined step is used, the localization performance can be further improved by removing more (nine) points from the coarse grid map before finding the next maximum. This can be explained by the fact that positions of several maxima are close to each other resulting in overlapping refinement areas, thus reducing the probability of finding the global maximum. For the rest of the section, we adopt the case of removing nine points from the coarse grid map when a smaller refined step (0.1m) is used.

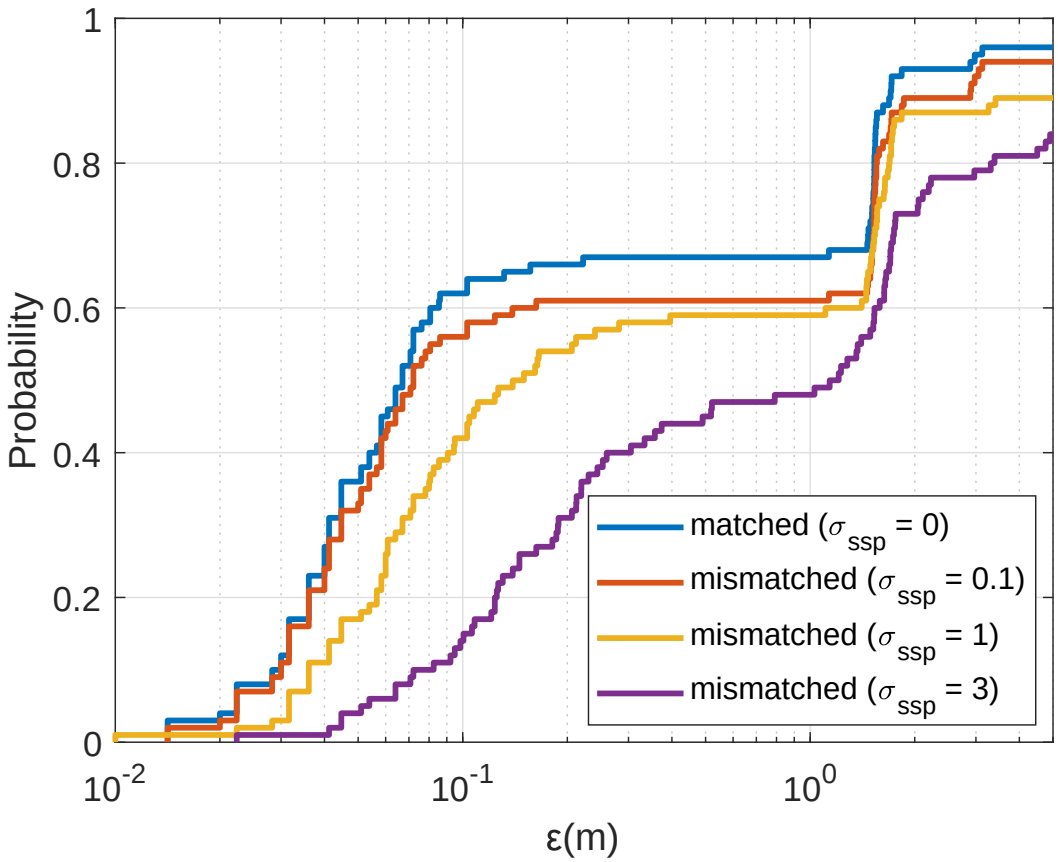

Fig. 3.15 CDF for the localization error ε in mismatched acoustic environments against the variance of sound speed σ^2_{ssp}; $N_{\text{T}} = 1$; $N_{\text{max}} = 4$, nine points are removed after finding the next coarse AF maximum; the refinement steps, $F_{\text{r}} = F_{\text{d}} = 0.1$ m; the size of a refinement area is 2 m $\times$ 2 m (as shown in Fig. 3.1a).

3.4.3 Mismatched environments

In this subsection, we consider scenarios with mismatched environments when acoustic parameters used for computation of the dictionary differ from real acoustic parameters.

In the first experiment, the dictionary is computed using the SWellEx-96 SSP, while the true SSP used in the experiment is given by

$$\text{SSP}(i) = \text{SSP}(i) + n(i), i = 1, ..., N_{\text{d}}, \tag{3.10}$$

where N_{d} is the number of depth points with SSP values, i is the index of the corresponding depth, $n(i)$ are independent Gaussian random numbers with a variance of σ^2_{ssp}.

The SWellEx-96 SSP and a realization of the mismatched SSP used in the experiment in the case $\sigma_{\text{ssp}} = 1$ m/s is shown in Fig. 2.3. Fig. 3.15 shows the localization performance for different levels of SSP mismatch. It can be seen that the localization performance is close to the matched performance for $\sigma_{\text{ssp}} \leq 1$ m/s. The performance degrades for a higher level of mismatch of the SSP ($\sigma_{\text{ssp}} = 3$ m/s). It can be concluded that the localization performance is robust against a small mismatch in the SSP.

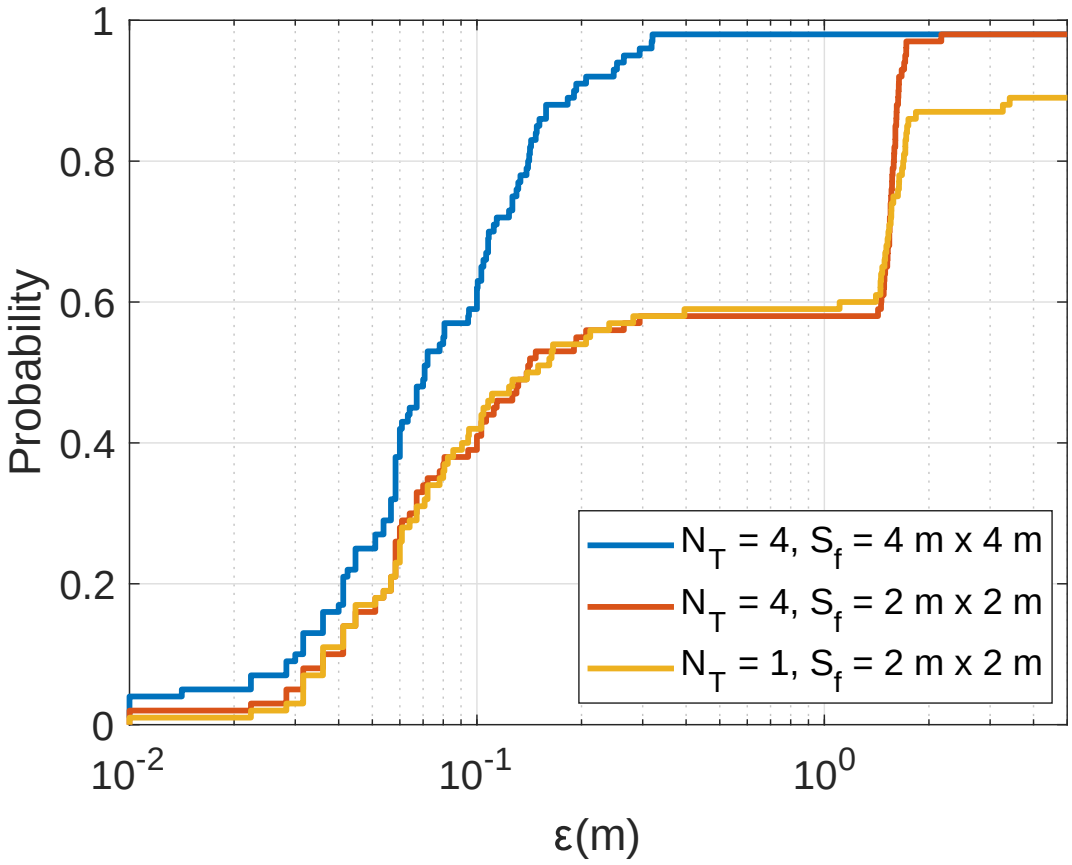

Fig. 3.16 CDF for the localization error ε in a mismatched acoustic environment when $\sigma_{\text{ssp}} = 1$ m/s as shown in Fig. 2.3 when depth of the sensor is unknown. $N_{\text{T}} = 4$; $N_{\text{max}} = 4$, nine points are removed after finding the next coarse AF maximum; the refinement steps, $F_{\text{r}} = F_{\text{d}} = 0.1$ m; the size of two refinement areas are 2 m $\times$ 2 m and 4 m $\times$ 4 m (as shown in Fig. 3.1).

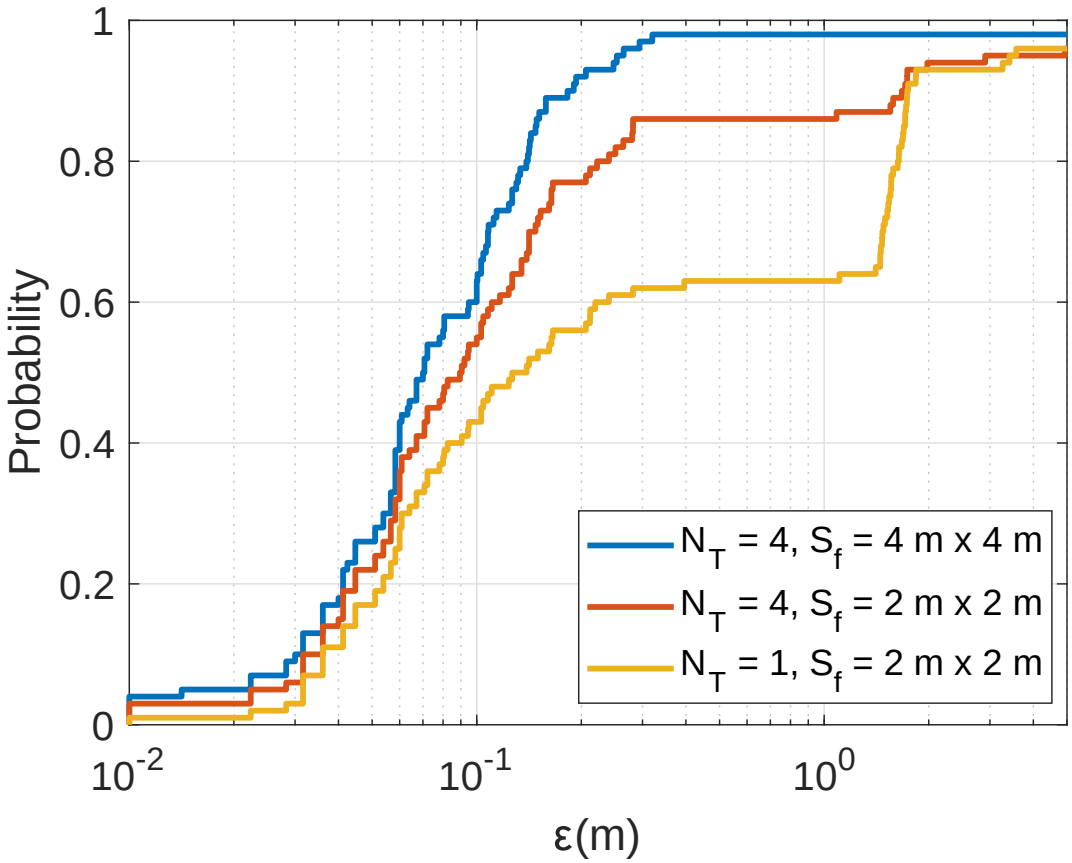

Fig. 3.17 CDF for the localization error ε in a mismatched acoustic environment when $\sigma_{\text{ssp}} = 1$ m/s as shown in Fig. 2.3 when the depth of the sensor is known. $N_{\text{T}} = 4$; $N_{\text{max}} = 4$, nine points are removed after finding the next coarse AF maximum; the refinement steps, $F_{\text{r}} = F_{\text{d}} = 0.1$ m; the size of two refinement areas are 2 m $\times$ 2 m and 4 m $\times$ 4 m (as shown in Fig. 3.1).

To reduce the sensitivity of a mismatched model, we consider a scenario when the depth of the receiver is known. This can be easily achieved in practice by using a receiver equipped with a depth sensor. Fig. 3.16 and Fig. 3.17 illustrate the localization performance of a mismatched acoustic environment with a SSP uncertainty of $\sigma_{\text{ssp}} = 1$ m/s, comparing the cases where the depth of the receiver is unknown and known, respectively.

In Fig. 3.16, it is observed that the localization performance can be improved by increasing the number of transmit antennas to $N_{\text{T}} = 4$. Additionally, further improvement in performance can be achieved by increasing the size of refinement areas to 4 m $\times$ 4 m, resulting in a localization error ε smaller than 0.3 m in 99% of the trials. It suggests that increasing the number of transmit antennas and refining the localization area can lead to improved

localization accuracy in a mismatched acoustic environment, where the receiver depth is unknown.

In Fig. 3.17, assuming the depth of the receiver is known, it can be seen that the localization performance improves. The most significant improvement is observed when using $N_{\mathrm{T}} = 4$ and a small refinement area of $2\mathrm{m} \times 2$ m. It indicates that accurate knowledge of the receiver depth allows for better compensation of SSP uncertainties, resulting in improved localization accuracy.

Therefore, the results suggest that both increasing the number of transmit antennas and refining the localization area can be effective strategies to mitigate the effects of the SSP uncertainties in UWA localization. Additionally, accurate knowledge of the receiver depth can significantly improve localization performance, highlighting the importance of incorporating depth information in UWA localization systems.

The use of a depth sensor at the receiver provides valuable information that can be used to mitigate the effects of the SSP uncertainty in UWA localization. By knowing the depth of the receiver, the model can better account for the variation in the SSP with depth, leading to improved localization performance even in the presence of mismatched acoustic environments. This highlights the importance of incorporating accurate depth information in UWA localization systems to reduce the sensitivity to SSP uncertainties and improve overall performance.

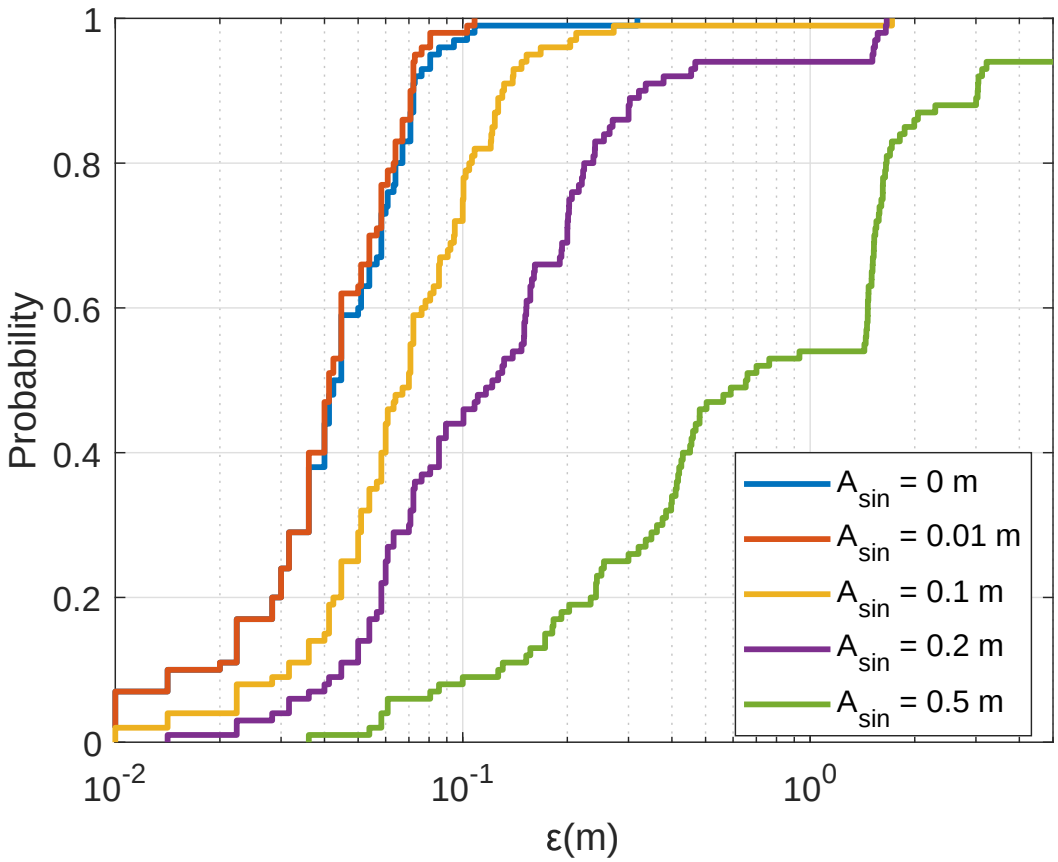

Fig. 3.18 CDF for the localization error ε in the acoustic environment of the sinusoidal surface with the SWellEx-96 SSP against different amplitudes A_{sin} ($A_{\text{sin}} = 0$ indicates a flat surface); $N_{\text{T}} = 4$; $N_{\text{max}} = 4$, nine points are removed after finding the next coarse AF maximum; the refinement steps, $F_{\text{r}} = F_{\text{d}} = 0.1$ m; the size of the refinement area is 4 m $\times$ 4 m (as shown in Fig. 3.1b).

In Fig. 3.18, we consider the scenario where the dictionary is computed assuming a flat sea surface, whereas the "real" sea surface is a sinusoid of amplitude A_{sin} and a period of 8 m. We consider a range of sea surface amplitudes from 0.01 m to 0.5 m. It can be observed that as the sea surface amplitude increases, the localization error also increases.

Obviously, the presence of a sinusoidal sea surface introduces additional uncertainties in the sound propagation environment, because the sea surface acts as a reflective boundary that can cause scattering, diffraction, and refraction of sound waves. These effects can increase the multipath effect and phase distortion, finally, leading to localization errors in the underwater communication system.

As seen in Fig.3.18, for the sea surface amplitude $A_{\text{sin}} < 0.2$ m, the localization error remains below 2 m in all simulation trials. This level of error may be acceptable for

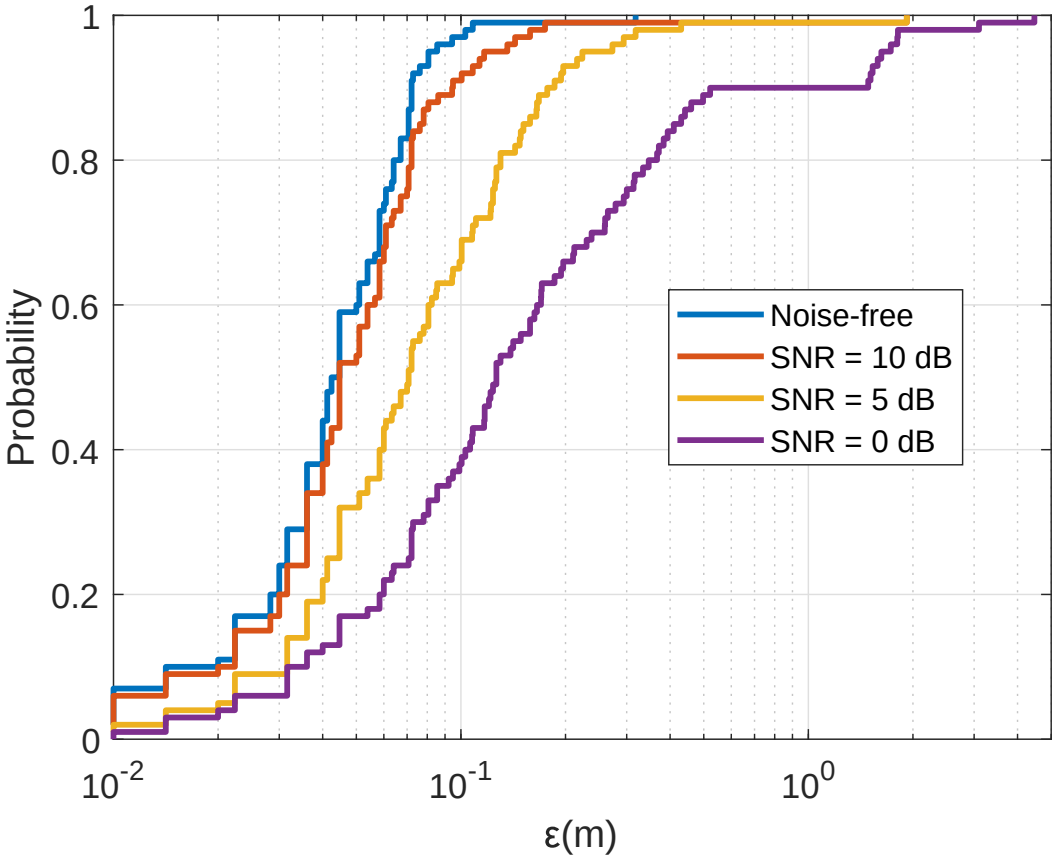

Fig. 3.19 CDF for the localization error ε in the acoustic environment with the SWellEx-96 SSP against the SNR of channel response estimation; $N_{\mathrm{T}} = 4$; $N_{\max} = 4$, nine points are removed after finding the next coarse AF maximum; the refinement steps, $F_{\mathrm{r}} = F_{\mathrm{d}} = 0.1$ m; the size of the refinement area is 4 m $\times$ 4 m (as shown in Fig. 3.1b).

many underwater communication applications. However, as the sea surface amplitude increases beyond this threshold, the localization error becomes larger, indicating the increased challenges in accurately estimating the positions of underwater nodes in the presence of significant sea surface deformations.

3.4.4 Inaccurate channel estimation

In this experiment, the channel frequency response $\widetilde{h}(f)$ between a transmit antenna and the receiver at a frequency f is given by

$$\widetilde{h}(f) = \hat{h}(f) + n(f). \tag{3.11}$$

The estimated channel frequency vector $\widetilde{\mathbf{h}}$ is now represented as $\widetilde{\mathbf{h}} = [\widetilde{h}(f_0), ..., \widetilde{h}(f_{K-1})]^T$. The noise samples $n(f_k)$ are independent complex-valued random Gaussian numbers with zero mean and variance σ^2. The signal-to-noise ratio (SNR) of the channel response estimate is defined as

$$\text{SNR} = \frac{1}{\sigma^2}\frac{1}{K}\sum_{k=0}^{K-1}|\hat{h}(f_k)|^2. \tag{3.12}$$

Fig. 3.19 shows the localization results against the SNR of the channel response estimate. It can be seen that for SNR = 10 dB, the localization results are close to that of the perfect channel response estimation. It also indicates that even at an SNR as low as 5 dB, the localization error is smaller than 2 meters in all trials, demonstrating the robustness of the localization performance against the estimation error of the channel response. It suggests that the proposed localization algorithm can perform well even in low SNR conditions, where the channel response estimate may be noisy or inaccurate. The fact that the localization error remains below a certain threshold (2 meters in this case) despite the low SNR levels indicates that the algorithm can mitigate the effects of estimation errors and still provide accurate localization results.

The results suggest that the proposed localization algorithm is robust against estimation errors in the channel response, which is a positive indication of its performance in real-world UWA sensor network applications.

3.5 Conclusions

In this chapter, localization accuracy has been further investigated, and a two-step technique for receiver localization has been proposed to reduce computation and enhance accuracy. This technique is based on pre-computation of a grid map using channel state information obtained from the acoustic environment. The source location found at the coarse search step is improved using a finer grid through AF interpolation to find a more accurate estimate of the source location. To further enhance the accuracy of localization, a joint refinement of the AF in the vicinities of several maxima is proposed to reduce outliers. Therefore, these proposed techniques potentially improve the accuracy of the estimated position by allowing for a more precise representation of the underwater environment. The proposed approach brings about a significant reduction in complexity and memory storage requirements for UWA communication receivers and has potential applications in various underwater communication and navigation systems. Numerical examples and simulations in different UWA environments, varying the number of transmit antennas, and considering different accuracy levels for the

estimation of the acoustic channel response, have demonstrated that the proposed techniques can achieve high localization accuracy.

Based on the localization technique described in this chapter, transmit beamforming techniques with different linear precoders is considered and investigated in Chapter 4.

Chapter 4

Transmit beamforming using coarse-to-fine localization methods

4.1 Introduction

Beamforming methods are commonly used in underwater acoustic (UWA) communication systems, especially for target localization in underwater sensor networks [69, 99–104].

The traditional beamforming techniques (such as transmit beamforming and receiver beamforming) have been used in the UWA communication systems to improve the capacity. Transmit beamforming is a technique where the transmitter has knowledge of the channel state information (CSI) between the transmitter and the receiver, and the CSI is usually obtained through feedback from the receiver [105, 106]. With this channel knowledge, the transmitter can shape the transmitted signals in a way that optimally utilizes the channel characteristics to improve capacity. Receiver beamforming [107], is a technique used at the receiver side to combine or process the signals received from multiple antennas. It can be implemented independently at each receiver without affecting the performance of other links in the system. However, a receiver beamforming technique that relies on large antenna arrays at the receiver end maybe impractical in certain UWA communication scenarios due to the size and weight constraint of the receiver equipment [108]. Therefore, we will focus on transmit beamforming in UWA communication.

In transmit beamforming, accurate CSI is needed at the transmitter to adapt the transmitted signals based on the channel characteristics. Typically, channel estimation is performed at the receiver, and the estimated CSI is then fed back to the transmitter using a feedback channel. The feedback channel is used to transmit the estimated CSI, which includes information about the channel conditions, such as channel gains, phases, and directions from the receiver

to the transmitter. This allows the transmitter to adjust the beamforming weights or phases of the transmitted signals to optimize the signal quality and mitigate interference at the receiver. However, in most UWA communication systems, especially with narrowband channels, the amount of data required for feedback can be large and constrain data throughput capacity. It may incur overheads and delay associated with feedback containing the entire CSI.

To reduce the amount of data required for the CSI feedback, all possible CSIs at both the transmitter and receiver are based on grid maps, which can be pre-computed into a dictionary. In this case, the receiver only needs to send back the index of the CSI from the pre-computed dictionary, which indicates the best match to the CSI estimate [69]. This approach can significantly reduce the amount of data needed for CSI feedback and especially mitigate the challenges associated with limited bandwidth and low data rates in the narrowband feedback UWA channels.

The accuracy of the estimated CSI is crucial for designing transmit beamforming, because any errors in the estimated CSI can degrade the detection performance in UWA communication systems. This problem can be resolved by the coarse-to-fine localization algorithms proposed in Chapter 3. This chapter considers a two-step localization technique that aims to improve the detection performance in UWA communication networks with multiple transmit antennas or an array of transducers at the base station and single-antenna receivers.

In the first step, the ambiguity function (AF) maximum is found by comparing the estimated channel frequency response with the precomputed frequency responses in a grid map. This step provides a coarse estimation of the spatial location of the receiver in terms of range and depth; in the second step, a refined spatial sampling of the AF is performed in the vicinity of the maximum found in the coarse grid. This allows for a more accurate localization of the receiver within the area of interest. This refined sampling helps to further improve the localization accuracy, reducing the potential errors introduced by the coarse estimation in the first step. By using the two-step technique, high localization accuracy can be achieved while reducing complexity and memory storage compared to a single-step localization approach.

In addition, in UWA communication systems with multiple transmit antennas and receivers, transmit beamforming requires coordination among multiple transmit antennas to adapt the weights or phases of the transmitted signals. This is because transmit beamforming from each transmit antenna can affect the interference to all other users, and optimizing the beamforming weights or phases for one user may impact the signals received by other users in the system.

To reduce the interference between users, transmit beamforming has to be done jointly in the entire network [109], for example with spatial division multiple access (SDMA). SDMA,

as a spacial diversity technique, exploits the spatial separation between multiple transmit antennas at the transmitter and receive antennas at the receiver. In this way, multiple users can receive signals simultaneously over the same frequency band with less interference, which improves system capacity and spectral efficiency.

To make a further reduction of interference, including the co-channel interference and intersymbol interference (ISI), precoding can be used, as a key technique for the SDMA in multiuser systems. With the knowledge of CSI, precoding involves the linear or non-linear transformation of the transmitted signals before being sent through multiple transmit antennas at the transmitter. Precoding can minimize interference between users and make a further improvement in system capacity and spectral efficiency. In this thesis, we mainly focus on the linear precoding techniques.

Linear precoding schemes [110–113] are commonly used in UWA communication for designing transmit beamformers in multiuser channels. Linear precoding schemes include zero forcing (ZF) [56], regularized channel inversion [114], minimum mean square error (MMSE) [115] and constant envelope [116], which are relatively simple to implement compared to non-linear techniques. These linear precodings exhibit a favourable tradeoff between performance and complexity, and can achieve significant performance gains in terms of interference suppression. In this thesis, we mainly focus on ZF precoding and an approximate MMSE precoding scheme to design transmit beamforming.

ZF precoding aims to decouple the multiuser channel into multiple independent subchannels [56, 117–120], where the transmitted signals are precoded to minimize the interference caused by other users' signals at the intended receiver. ZF precoding is designed to eliminate interference between multiple users in multi-user systems. The other relative merits of this precoding are its computational efficiency and relatively simple implementation. However, it is limited by its sensitivity to channel estimation errors and potential amplification of noise at the receiver, which may degrade the performance in practical underwater environments with uncertain and time-varying channels. Despite its limitations, ZF can be an effective linear precoding scheme for transmit beamforming in UWA communication systems.

While the ZF beamforming method can provide good detection performance in some underwater scenarios, it is not as effective in more complex and time-varying environments. Other linear precoding schemes, such as MMSE precoding, can be considered. MMSE precoding can minimize the mean squared error between the transmitted signals and the desired received signals, taking into account the interference caused by other users' signals and the noise at the receiver. One of the merits of the MMSE precoding is its noise mitigation. It can provide a tradeoff between interference suppression and noise amplification, which can be more suitable in certain scenarios. In addition, MMSE precoding is more robust to

channel estimation errors compared to the ZF precoding, it can provide better performance in scenarios with imperfect channel knowledge.

Although a MMSE precoder is computationally more complex than the ZF precoder, it can be an effective linear precoding scheme in UWA communication systems when accurate channel estimation is feasible and the system requirements demand a better tradeoff between interference suppression and noise amplification.

In this chapter, we investigate transmit beamforming precoders, including a ZF precoder and approximate MMSE precoder, based on the two-step localization technique proposed in Chapter 3 for transmit beamforming with multiple transmit antennas and multiple receivers, each receiver equipped with a single antenna in scenarios similar to that in [69]. Specifically, the system works in the following way: in a UWA communication system with SDMA, the two-step localization technique is applied to obtain an accurate estimated CSI, which is compared to all possible CSIs from a pre-computed dictionary at the receiver for the best match; the receiver sends the index of the best match to the transmitter through the feedback link. The estimated CSI can be found by matching the index to the precomputed dictionary at the transmitter. The linear precoder, such as ZF and MMSE precoders, can be built based on the matched CSI. It is worth mentioning that in designing the MMSE precoder, generally, the SNR has to be known at the receiver, and the SNR should be sent back to the transmitter, in our case, the SNR is assumed to be known at the transmitter (it is treated as a constant design parameter) to reduce the complexity. Note that the perfect knowledge of SNR at the transmit beamformer generally can improve the detection performance compared to the approach we are using here. However, this would require a feedback channel of high capacity, which is not practical. As will be seen below, even without such knowledge, the approximate MMSE beamformer significantly improves the detection performance compared with the ZF beamformer.

To validate the performance of transmit beamforming algorithms, we use the channel simulator based on the BELLHOP ray/beam tracing model [86, 121, 122] and the passband Waymark simulator [33, 123, 124] to investigate UWA signal transmission for accurate localization and high detection performance.

The following notation is used. Boldface upper case letters denote matrices, boldface lower case letters denote column vectors and standard lower case letters denote scalars. The superscript $(\cdot)^T$, $(\cdot)^H$, $(\cdot)^{-1}$, $(\cdot)^\dagger$ denote the transpose, the conjugate transpose, matrix inverse and the pseudo-inverse, respectively. $\mathbb{R}$ is the set of real numbers and $\mathbb{C}$ is the set of complex numbers. $Re\{z\}$ denotes the real part x of a complex number $z = x + iy$.

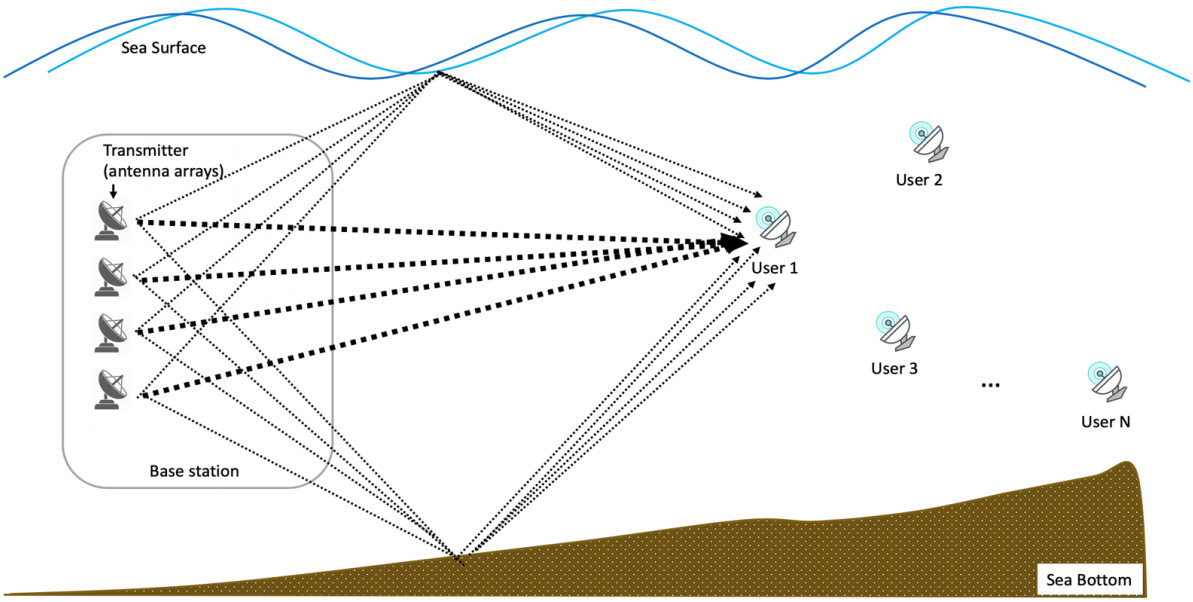

Fig. 4.1 The UWA communication network system.

4.2 Problem to solve

Fig 4.1 shows the structure of an UWA communication network system. We focus on the downlink data transmission. It can be seen that under the sea, there is a base station with multiple transmit antennas and multiple users, each user equipped with one antenna. The base station tries to transmit signals to the multiple users. For the simplicity, the base station just transmits signals to User 1, in fact, the base station needs to transmit signals to all the users at the same time. However, it cannot work simultaneously, because in that case, there are plenty of interference among these users and these users cannot receive the information reliably.

To mitigate or avoid interference from other users, transmit beamforming is adopted, and we apply the estimated CSI to design the transmit beamforming. However, the main problem of designing the transmit beamforming is the channel estimation, which can only be done at receivers. This should exist a feedback channel (from the receiver to the transmitter) to pass the CSI to the transmit beamforming. However, the amount of this CSI is very high with respect to the typical UWA channel capacity, which makes such feedback transmission not practical. To solve this problem, the receiver localization technique based on the grid computations were introduced and further investigated in Chapter 2 and Chapter 3. With such localization, the feedback channel is only used to transmit the grid index, which requires a feedback channel of much lower capacity than for transmission of the CSI.

4.3 System model

In this section, we present a communication scenario, including channel, transmit beamformers, transmitter and receiver in a view of the frequency domain. Unless otherwise stated, variables in the following equations are at subcarrier frequency $f \in \{f_0, ..., f_{K-1}\}$ and K is the number of subcarrier frequencies.

In such a multi-user (N_R users) system with a broadcast channel, the received signal at a frequency $f \in \{f_0, ..., f_{K-1}\}$ is given by

$$y_r(f) = \mathbf{h}_r^T(f)\mathbf{x}(f) + n_r(f),\ r = 1, ..., N_R, \tag{4.1}$$

where $y_r(f)$ is the signal received by the r-th user, $\mathbf{h}_r(f) = [h_{r,1}(f), ..., h_{r,N_T}(f)]^T$ represents the channel frequency response between transmit antennas and the r-th user, $\mathbf{x}(f)$ is the $N_T \times 1$ transmitted signal vector and $n_r(f)$ is the Gaussian noise with zero mean and variance $\sigma_r^2(f)$.

With N_T transmit antennas and N_R users ($N_R \leq N_T$), the model in (4.1) can be rewritten as

$$\mathbf{y}(f) = \mathbf{H}(f)\mathbf{x}(f) + \mathbf{n}(f), \tag{4.2}$$

where $\mathbf{y}(f) = [y_1(f), ..., y_{N_R}(f)]^T \in \mathbb{C}^{N_R \times 1}$ is the signal vector received by N_R users, $\mathbf{n}(f) = [n_1(f), ..., n_{N_R}(f)]^T \in \mathbb{C}^{N_R \times 1}$ is the noise vector and the channel can be described by the channel matrix

$$\mathbf{H}(f) = \begin{bmatrix} h_{1,1}(f) & h_{1,2}(f) & \cdots & h_{1,N_T}(f) \\ h_{2,1}(f) & h_{2,2}(f) & \cdots & h_{2,N_T}(f) \\ \vdots & \vdots & \ddots & \vdots \\ h_{N_R,1}(f) & h_{N_R,2}(f) & \cdots & h_{N_R,N_T}(f) \end{bmatrix} \tag{4.3}$$

of size $N_R \times N_T$.

4.3.1 Transmit beamforming

In a multi-user system with multiple transmit antennas, the transmitted signal vector $\mathbf{x}(f) = [x_1(f), ..., x_{N_T}(f)]^T \in \mathbb{C}^{N_T \times 1}$ can be represented as a linear transformation of the information symbols when the linear precoding (transmit beamforming) methods applied [69, 117],

$$\mathbf{x}(f) = \mathbf{T}(f)\mathbf{s}(f), \tag{4.4}$$

where $\mathbf{T}(f) \in \mathbb{C}^{N_T \times N_R}$ is the precoding matrix (beamformer) at the frequency f, $\mathbf{s}(f) = [s_1(f), ..., s_{N_R}(f)]^T \in \mathbb{C}^{N_R \times 1}$ is the information symbol vector.

Zero-forcing beamforming

The transmit precoding offers interference elimination benefits, leading to improved performance in multi-users systems. However, its high computational and hardware complexity can make it challenging to implement in real-time and resource-constrained systems. The ZF precoder provides a tradeoff between complexity and performance. In particular, such a precoder does not require the knowledge of SNR at subcarriers, thus simplifying the implementation.

In ZF beamforming [117, 125], interference between users can be reduced to zero, and the precoding matrix $\mathbf{T}(f)$ satisfies

$$[\mathbf{H}(f)\mathbf{T}(f)]_{k,j} = 0, \quad \text{if} \quad k \neq j. \tag{4.5}$$

Therefore, the product $\mathbf{H}(f)\mathbf{T}(f) \in \mathbb{C}^{N_R \times N_R}$ represents a diagonal matrix, which is given by

$$\mathbf{H}(f)\mathbf{T}(f) = \mathbf{I}_{N_R}. \tag{4.6}$$

ZF precoding matrix $\mathbf{T}(f)$ is the pseudo-inverse of $\mathbf{H}(f)$,

$$\mathbf{T}(f) = \mathbf{H}(f)^{\dagger} = \mathbf{H}(f)^{H} \left[\mathbf{H}(f)\mathbf{H}^{H}(f)\right]^{-1}. \tag{4.7}$$

The beamformer $\mathbf{T}(f)$ can be rewritten as

$$\begin{aligned} \mathbf{T}(f) &= \left[\mathbf{T}^{(1)}(f) \quad \mathbf{T}^{(2)}(f), ..., \mathbf{T}^{(N_R)}(f)\right] \\ &= \begin{bmatrix} T_{1,1}(f) & T_{1,2}(f) & \cdots & T_{1,N_R}(f) \\ T_{2,1}(f) & T_{2,2}(f) & \cdots & T_{2,N_R}(f) \\ \vdots & \vdots & \ddots & \vdots \\ T_{N_T,1}(f) & T_{N_T,1}(f) & \cdots & T_{N_T,N_R}(f) \end{bmatrix}, \end{aligned} \tag{4.8}$$

where its column, which can be represented as $\mathbf{T}^{(n)}(f) = [T_{1,n}(f), ..., T_{N_T,n}(f)]^T \in \mathbb{C}^{N_T \times 1}$, is a beamformer weight for the n-th user. After beamforming, the transmitted signal for the n-th user is given by

$$\mathbf{x}_n(f) = \mathbf{T}^{(n)}(f)\mathbf{s}(f). \tag{4.9}$$

In Eq. (4.7), the ZF precoding matrix is designed to eliminate the interference by inverting the channel matrix. In this way, the receiving signal for each user can be aligned with the intended direction, effectively mitigating interference from other users. In fact, ZF beamforming can achieve optimal interference suppression in ideal conditions when the

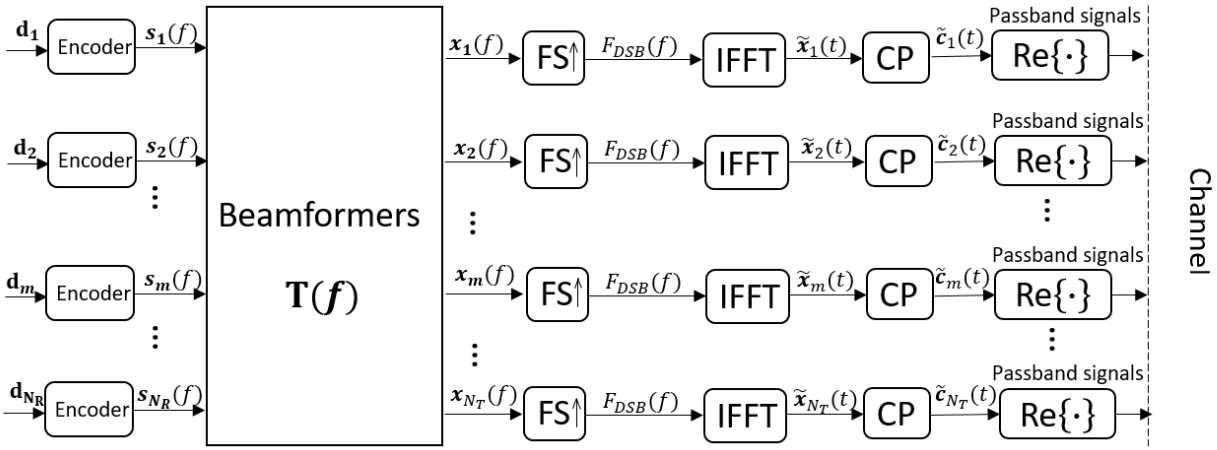

Fig. 4.2 The diagram of the transmitter process when applying transmit beamforming with N_T transmit antennas and N_R users.

channel matrix is perfectly known and invertible. However, ZF beamforming, as a suboptimal method, is generally power inefficient and the detection performance drops rapidly under imperfect channel knowledge.

Approximate MMSE precoder

MMSE beamforming, as a solution to balance the transmission energy and interference level, is another suboptimal strategy for the minimum detection error [126]. Compared to ZF beamforming, MMSE beamforming provides a tradeoff between interference suppression and noise amplification. It considers the noise covariance matrix when designing the MMSE precoder matrix.

Generally, the SNR at the receiver needs to be obtained. However, it is not feasible to obtain the SNR at the receiver at all the subcarriers and send this information back to the transmitter in real-time. Therefore, an assumed SNR is used, and Eq. (4.6) and Eq. (4.7) are modified by using the diagonal loading, thus the approximate MMSE precoding matrix is given as,

$$\mathbf{T}(f) = \mathbf{H}(f)^H \left[\mathbf{H}(f)\mathbf{H}^H(f) + \gamma \mathbf{I}_{N_R}\right]^{-1}, \tag{4.10}$$

where $1/\gamma$ is the assumed SNR.

The MMSE beamforming can provide better performance than the ZF beamforming in scenarios with imperfect channel knowledge and noisy channels.

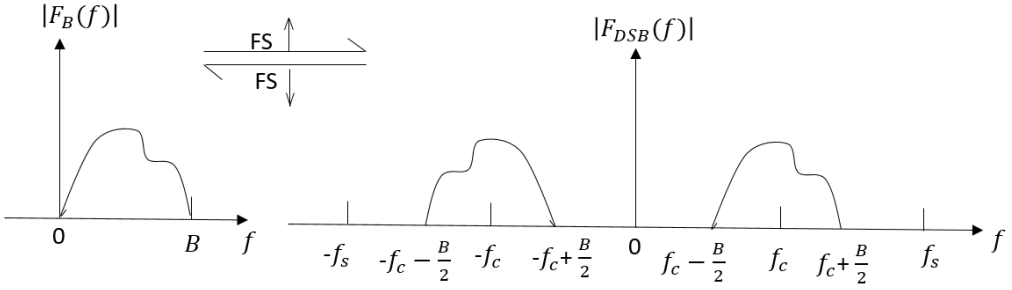

Fig. 4.3 The mutual conversion between a baseband signal and a passband signal in the frequency domain by using complex modulation and demodulation techniques. $F_B(f)$ is the frequency spectrum of a baseband signal and $F_{DSB}(f)$ represents the frequency spectrum with double side bands of a passband signal, the carrier frequency is f_c and the bandwidth is B. (Note, FS indicates frequency shift).

4.3.2 Transmitter

The structure of the transmitter process is described in Fig. 4.2. The original data is encoded into BPSK symbols, creating blocks of these symbols, and applying precoding with a designed transmit beamformer in the frequency domain, which is described in subsection 4.3.1. After the beamforming process, each block of precoded BPSK symbols is up-shifted in frequency to the desired frequency range with the carrier frequency f_c, which is illustrated in Fig. 4.3. The modulated symbol's spectrum can be transformed into a time-domain OFDM symbol by applying the inverse *fast Fourier transform* (IFFT) to the set of modulated symbols.

As an example of the m-th transmit antenna transmission, the consecutive OFDM symbol can be represented as

$$\tilde{x}_m(n) = \frac{1}{\sqrt{K}} \sum_{f=0}^{K-1} x_m(f) e^{j2\pi nf/K},\ n = 0, ..., K-1, \tag{4.11}$$

where $\tilde{x}_m(n)$ is a transmitted signal vector for the m-th transmit antenna $m \in \{1, ..., N_T\}$.

To mitigate the effect of multipath fading and intersymbol interference (ISI), a cyclic prefix (CP) is added to the beginning of each OFDM symbol. The CP is a copy of the last portion of the OFDM symbol and the length of the CP in our case is set to $N_{cp} = K$; such a long CP is required due to high delay spreads of UWA channels. After insertion of the CP, the OFDM symbol is given as

$$\tilde{\mathbf{c}}_m = [\tilde{x}_m(K - N_{cp} + 1),\ ...\ , \tilde{x}_m(K)\ \tilde{x}_m(1),\ ...\ , \tilde{x}_m(K)], \tag{4.12}$$

where the vector $\tilde{\mathbf{c}}_m$ is a size of $1 \times (K + N_{cp})$ for one OFDM symbol, as shown in Fig. 4.4.

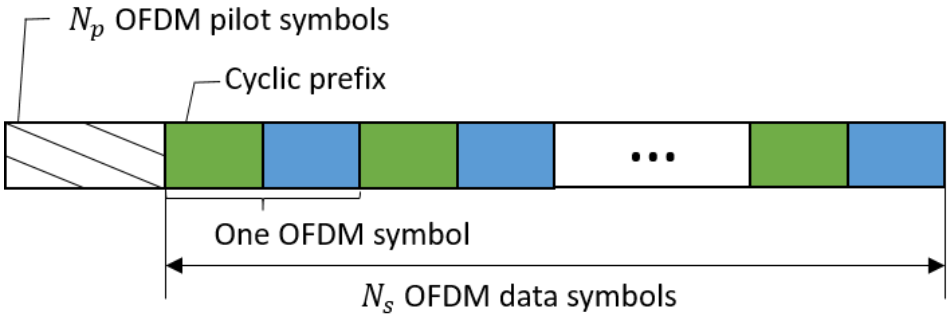

Fig. 4.4 The diagram of a sequence of transmitted OFDM symbols.

Finally, the real parts of OFDM signals from N_T transmit antennas are transmitted simultaneously to N_R users through the channel modelled using the Waymark simulator and the Bellhop.

4.3.3 Receiver

The received signal is given as

$$y_r(k) = \sum_{m=1}^{N_T} y_{rm}(k) + n_r(k),\ r = 1,...,N_R, \tag{4.13}$$

where $y_r(k)$ represents the passband signal received at the r-th receiver and $y_{mr}(k)$ represents the received signal between the r-the user and the m-th transmit antenna. $n_r(k)$ is the Gaussian noise with zero mean and variance σ_r^2 to the r-th user; the noise includes the ambient noise and interference from other user signals.

The passband received signal is demodulated into frequency-domain OFDM symbols by applying the *fast Fourier transform* (FFT). In this way, a passband signal $y_r(k)$ is converted into a baseband signal $\tilde{y}_r(k)$ in the frequency domain.

The time synchronization is assumed to be perfect so that the CP can be removed. Therefore, the best position to remove can be found through calculation, the process of removing the CP of a baseband signal for the r-th receiver can be given as

$$\begin{aligned} w_r(k) =& [\tilde{y}_r((N_{cp}+\tau) : (N_{cp}+\tau+K-1)),\ \dots, \\ & \tilde{y}_r(iL_s) + (N_{cp}+\tau) : iL_s + (N_{cp}+\tau+K-1)), \\ & , \dots, \\ & \tilde{y}_r(N_sL_s + (N_{cp}+\tau) : N_sL_s + \\ & (N_{cp}+\tau+K-1))], \end{aligned} \tag{4.14}$$

where the vector $\mathbf{w}_r$ represents the receiving signal without the CP, size of $1 \times N_s K$ and τ is the suitable starting position to remove the CP, N_s represents the whole length of the OFDM symbol, $L_s = N_{cp} + K$.

For channel estimation, pilot symbols are applied and we use the least square (LS) channel estimation, assuming that the number of pilot symbols is N_p ($N_p << N_s$). Based on one pilot OFDM symbol as an example, the LS estimate of the channel frequency response $h(f)$ at a subcarrier f can be specified as

$$\hat{h}(f) = \frac{w(f)}{s(f)},\ f = 0, ..., K-1, \tag{4.15}$$

where $w(f)$ represents the receiving signal and $s(f)$ represents the pilot symbol transmitted from the m-th transmit antenna at the frequency f.

4.4 Numerical results

In this section, we consider a multi-antenna MISO-OFDM system with N_T transmit antennas and N_R users (in the following parts, these will also called receivers), and each user equipped with single receive antenna. The multi-antenna system is aimed at transmitting N_R data packets simultaneously to N_R users. In this section, numerical experiments are presented, and the objectives of the numerical experiments are as follows.

- Comparison of transmit beamforming performance using uncoded and encoded transmission.
- Analysis of the performance of combining the coarse-to-fine localization with transmit beamforming with different precoders applied.
- Analysis of transmit beamforming performance in the case of random positions of receivers within an area of interest and for different localization algorithms.
- Analysis of performance of transmit beamforming for different numbers of users and transmit antennas.

In the experiments, to evaluate the detection performance of transmit beamforming, two metrics, the bit error rate (BER) and frame error rate (FER) are used. The BER is defined as

$$\text{BER} = \frac{\text{Number of bits with errors}}{\text{Total number of bits}}, \tag{4.16}$$

i.e., BER is the ratio of the number of received bits with errors to the total number of the original bits. A lower BER indicates better detection performance of transmit beamforming.

The FER is defined as

$$\text{FER} = \frac{\text{Number of frames with errors}}{\text{Total number of frames}}, \tag{4.17}$$

where FER represents the probability of the number of frames (OFDM symbols in our case) received with errors to the total number of original frames transmitted. A frame is a group of bits structured in a specific way for transmission. An error may occur when at least one received bit in a frame is incorrect. A lower FER also indicates better detection performance of transmit beamforming.

The main simulation parameters are given in Table 4.1.

Table 4.1 Parameters for transmit beamforming based on the receiver localization.

Variable name	**Value**	**Description**
N_T	$1,2,3,4$	Number of transmit antennas
N_R	$2,3$	Number of receivers
N_p	$1,10$	Number of OFDM pilot symbols
N_s	$100,1000$	Number of OFDM symbols
r_c	$1/2,1/3,1/4,1/8$	Coding rate
C_d	1 m	Coarse grid step in depth
C_r	1 m	Coarse grid step in range
D_T	$50,60,70,80$ m	Depth of transmit antennas
D_l	200 m	Depth for area of interest
K	1024	Number of subcarriers
R_l	500 m	Range for area of interest
S_c	201×501	Size of the coarse grid map

In an example simulation scenario, a code rate of 1/2 is considered, $N_R = 2$ data packets (vector $\mathbf{d}_1 \in \mathbb{R}^{1\times(K/2)}$ and vector $\mathbf{d}_2 \in \mathbb{R}^{1\times(K/2)}$), each data packet contains one OFDM symbol (correspondingly, this is repeated for every OFDM symbol), each data packet comprising $K/2$ data bits, which are encoded using convolutional encoding, interleaving and BPSK modulation to generate BPSK symbols, $\mathbf{s}_1 \in \mathbb{R}^{1\times K}$ and $\mathbf{s}_1 \in \mathbb{R}^{1\times K}$, respectively. Specifically, a convolution encoder of rate $r_c = 1/2$ with a generator polynomial [23 35] in octal is applied to encode the user data symbols. Therefore, every $K/2$ bits of each data packet are encoded into a K-bit message. Then the message bits are interleaved and transformed into BPSK symbols.

These symbols are divided into N_s consecutive blocks of BPSK symbols corresponding to each data packet. Each block of BPSK symbols for the two data packets is separately represented as $\mathbf{b}_1 \in \mathbb{R}^{1\times K}$ and $\mathbf{b}_2 \in \mathbb{R}^{1\times K}$, both $b_1(f)$ and $b_2(f)$ are scalars at subcarrier frequencies $f = f_0, ..., f_{K-1}$ covering the frequency range of the communication system. Then the N_s consecutive blocks of the BPSK symbols corresponding to each data packet are processed to precode BPSK symbols corresponding to each transmit antenna by the jointly designed beamformers $\mathbf{T}(f) \in \mathbb{C}^{2\times 2}$.

4.4.1 Perfect knowledge of CSI

In this subsection, the transmitter has perfect knowledge of CSI and receiver localization is assumed to be perfect. The receivers are located between grid points. The performance of the ZF transmit beamforming with the uncoded and encoded signal transmission in different acoustic environments with uniform and SWellEx-96 SSPs is investigated by using the BER and FER. Furthermore, in a more general case for users, we investigate the detection performance of transmit beamforming with the ZF precoder and approximate MMSE precoder with different assumed SNRs.

Scenario 1: Uncoded transmission and encoded transmission

In this scenario, $N_T = 2$ transmit antennas and $N_R = 2$ users are considered, where User 1 is located at the depth of 162.94 m and range of 181.09 m from the transmitter, while User 2 is located at the depth of 181.16 m and range of 497.14 m. These two users are located between grid points in the area of interest. $N_s = 1000$ OFDM symbols are transmitted.

Fig. 4.5 and Fig. 4.6 show BER performance of the ZF transmit beamforming for User 1 and User 2, respectively. In the acoustic environment with the uniform SSP, both users have good detection performance either uncoded or coded transmission. BER performance of the coded transmission for both User 1 and User 2 improves significantly, compared to the uncoded signal transmission when the SNR is greater than about 4 dB. Compared to the uniform SSP, the BER performance in the acoustic environment with the SWellEx-96 SSP is similar for User 1, and is significantly better for User 2. Coded signal transmission will be applied in the following simulations scenarios.

Fig. 4.7 shows the FER detection performance of the ZF transmit beamforming with coded signal transmission for User 1 and User 2, respectively. It can be seen that the FER performance has a behaviour similar to that of the BER. To obtain more accurate detection performance in a frame level, FER is chosen to measure the detection performance of transmit beamforming, focusing on User 1 (due to User 1 and User 2 having a similar result), for the

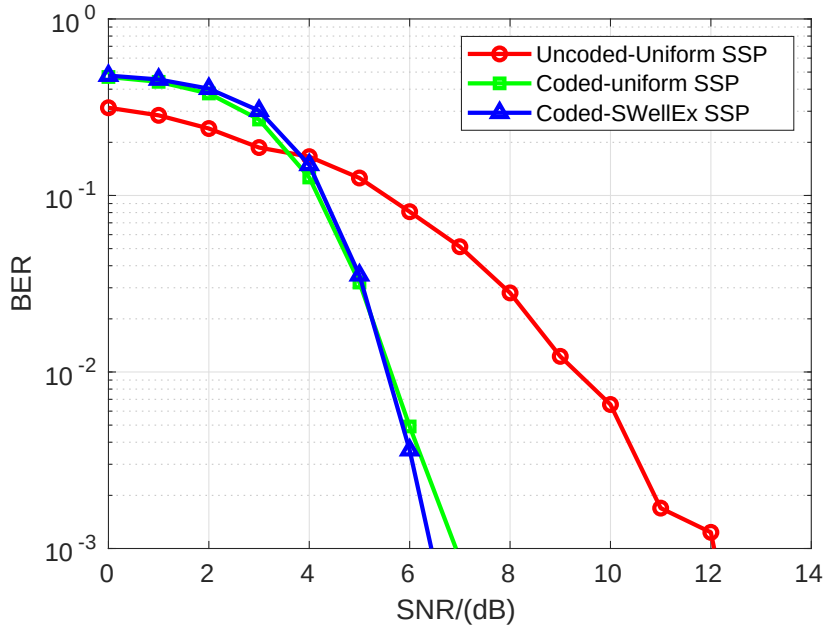

Fig. 4.5 BER performance for User 1 of transmit beamforming with the ZF precoder against SNR for uncoded and coded transmission; $N_s = 1000$ OFDM symbols are transmitted in the acoustic environments with the uniform SSP and SWellEx-96 SSP, shown in Fig. 2.3.

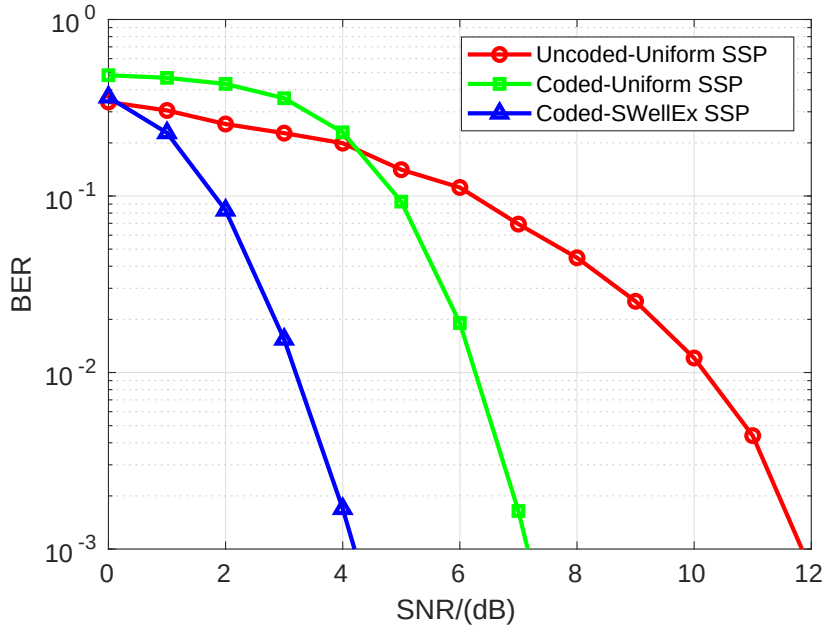

Fig. 4.6 BER performance for User 2 of transmit beamforming with the ZF precoder against SNR for uncoded and coded transmission; $N_s = 1000$ OFDM symbols are transmitted in the acoustic environments with the uniform SSP and SWellEx-96 SSP, shown in Fig. 2.3.

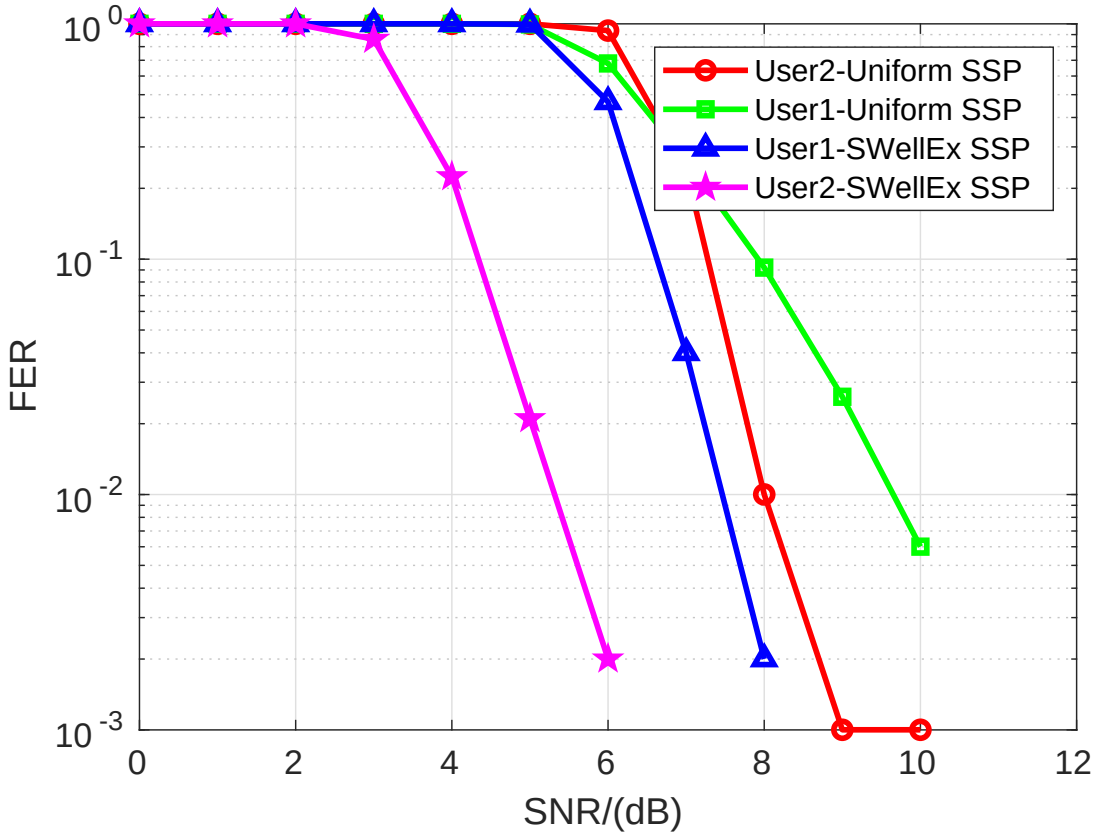

Fig. 4.7 FER performance of transmit beamforming with the ZF precoder against SNR for User 1 and User 2 with coded transmission; $N_s = 1000$ OFDM symbols are transmitted in the acoustic environments with the uniform SSP and SWellEx-96 SSP, shown in Fig. 2.3.

following scenarios. All the following scenarios are in the acoustic environment with the SWellEx-96 SSP.

Scenario 2: ZF and MMSE precoders

In this scenario, $N_T = 2$ transmit antennas and $N_R = 2$ users are considered, where positions of these two users are randomly chosen from 100 locations in the area of interest. 100 trials are conducted and $N_s = 100$ OFDM symbols are transmitted. We investigate the detection performance of transmit beamforming with the ZF precoder and MMSE precoder with different assumed SNRs.

Fig. 4.8 shows the detection performance of the ZF precoder and approximate MMSE precoder with different assumed SNRs: $\text{SNR}_{\text{est}} = 5, 10, 20, 30$ dB. It can be seen that with the perfect CSI knowledge and receiver localization accuracy, the ZF precoder has the best detection performance among other cases; for the approximate MMSE with different

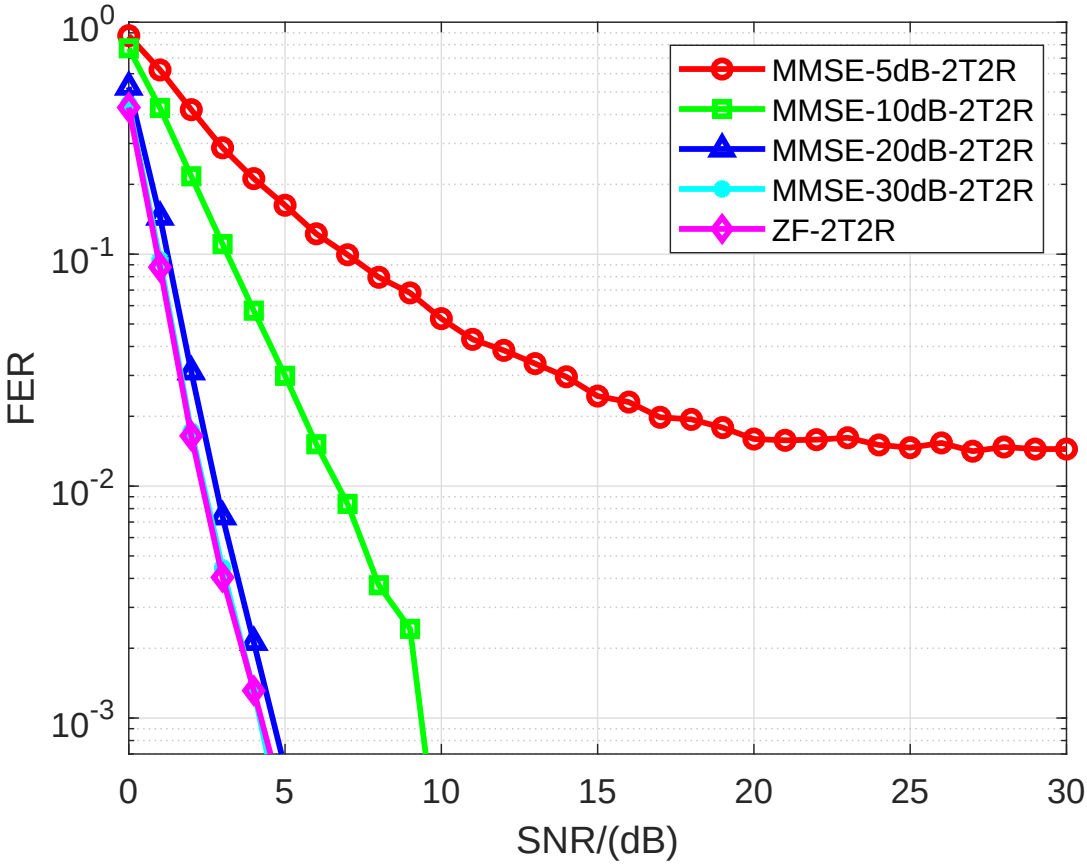

Fig. 4.8 FER performance for User 1 of transmit beamforming with the ZF precoder and the approximate MMSE precoder with $\text{SNR}_{\text{est}} = 5$, 10, 20, 30 dB against SNR; $N_s = 100$ OFDM symbols are transmitted in the acoustic environment with the SWellEx-96 SSP, shown in Fig. 2.3.

SNR_{est}, the detection performance can be improved by increasing the assumed SNR to $\text{SNR}_{\text{est}} = 30$ dB, which achieves similar detection performance with the ZF precoder. For the case of the approximate MMSE precoder with the assumed SNR, $\text{SNR}_{\text{est}} = 5$ dB, the detection performance of the receiver degrades; more specifically, there is a floor level due to the noise interference induced. However, even in the presence of lower assumed SNR, the receiver can still operate with a reasonable FER of approximately 10^{-2} (or 1%).

4.4.2 Imperfect knowledge of CSI

Compared to the perfect knowledge of the CSI and perfect receiver localization, it is necessary and more practical to investigate the imperfect knowledge of the CSI and receiver localization. The receivers are located between grid points for a practical situation. Combined with the receiver localization proposed in Chapter 3, we investigate the detection performance of transmit beamforming with different precoders, with different numbers of transmit antennas and multiple receiver positions. In addition, the case of different coding rates has also been explored and investigated.

Scenario 3: Coarse-to-fine localization for multiple receiver positions with transmit beamforming

In this scenario, we demonstrate the benefit of the approximate MMSE precoder for improving the detection performance of transmit beamforming when imperfect knowledge of CSI provided.

Fig. 4.9 shows the detection performance of different precoders against SNR for User 1 in a multi-user system with $N_T = 2$ transmit antennas and $N_R = 2$ users. By comparing results in Fig. 4.8 and Fig. 4.9, it is apparent that the detection performance of the receiver degrades with such the receiver localization accuracy; more specifically, with the ZF precoder, the detection performance drops significantly. Obviously, the ZF beamformer is very sensitive to the imperfect CSI. It can be seen that the approximate MMSE precoder improves performance significantly compared to the ZF precoder. It can also be seen that the detection performance for the approximate MMSE precoder with different assumed SNRs, $\text{SNR}_{\text{est}} = 5, 10, 20, 30$ dB improves in varying proportions. The detection performance improves greatly when the approximate MMSE precoder is applied with the assumed SNR, $\text{SNR}_{\text{est}} = 10$ dB. In addition, there is a floor level due to the multiuser interference, which cannot be completely cancelled by the designed transmit beamforming based on the CSI.

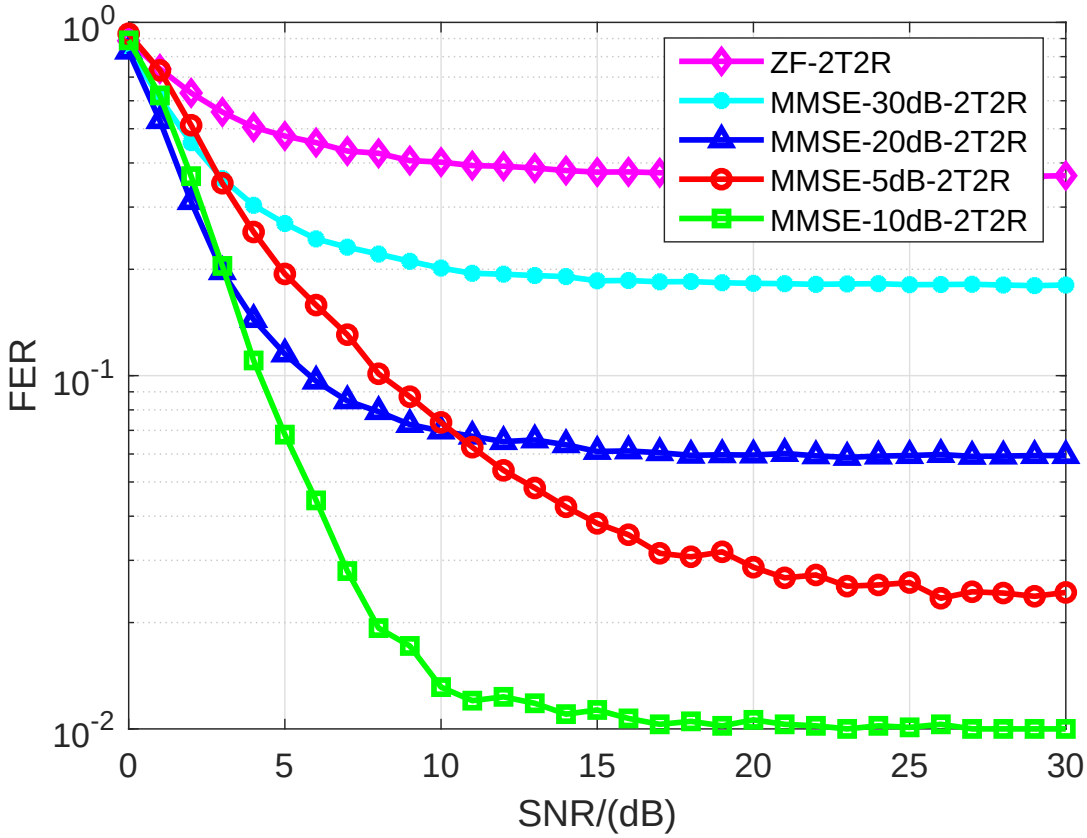

Fig. 4.9 FER performance for User 1 of transmit beamforming with the ZF precoder and the approximate MMSE precoder with $\mathrm{SNR}_{\mathrm{est}} = 5, 10, 20, 30$ dB against SNR; the simulation parameters are $N_T = 2$ transmit antennas; $N_R = 2$ receivers; $N_s = 100$ OFDM symbols transmitted in the acoustic environment with the SWellEx-96 SSP, shown in Fig. 2.3. Coarse-to-fine localization, localization parameter setting: $N_{\mathrm{T}} = 4$; $N_{\max} = 4$, nine points are removed after finding the next coarse AF maximum; in the refinement steps, $F_{\mathrm{r}} = F_{\mathrm{d}} = 0.1$ m; the size of the refinement area is 4 m $\times$ 4 m, shown in Fig. 3.1b.

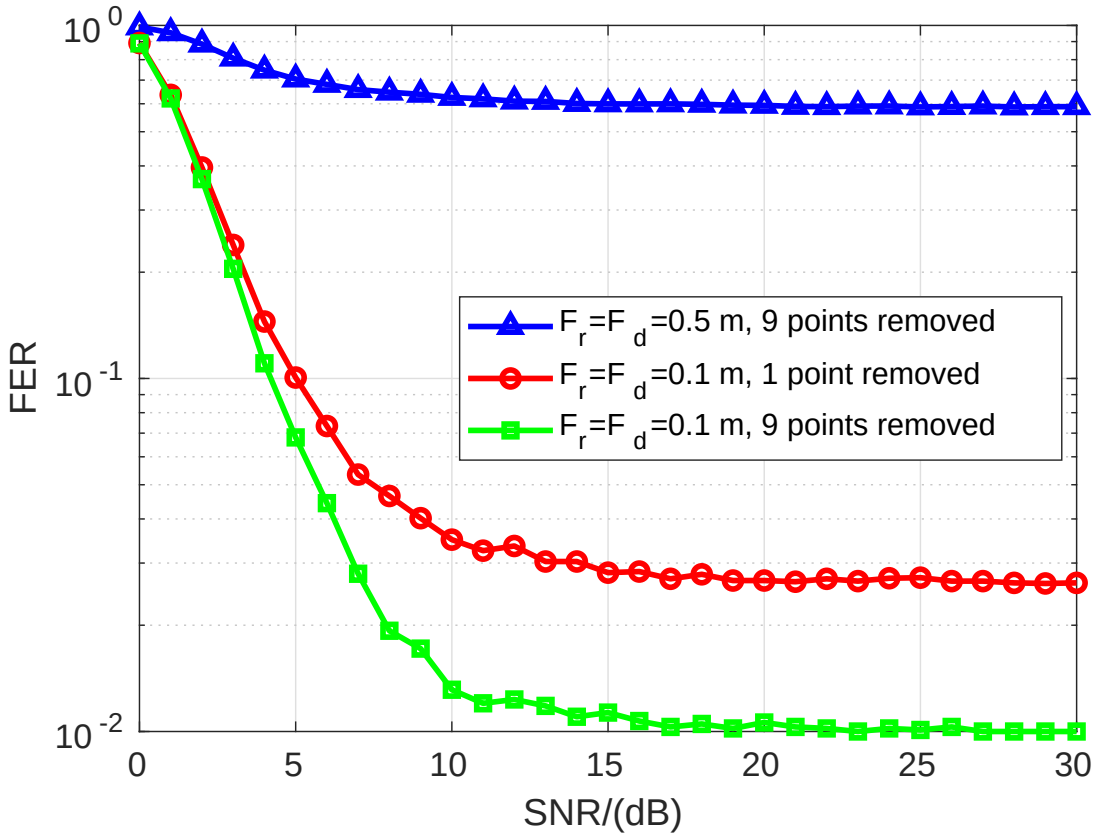

Fig. 4.10 FER performance for User 1 of transmit beamforming with the approximate MMSE precoder with the assumed $\mathrm{SNR}_{\mathrm{est}}$, $\mathrm{SNR}_{\mathrm{est}} = 10$ dB against SNR for different localization accuracies, as illustrated in Fig 3.14; the simulation parameters are $N_T = 2$ transmit antennas; $N_R = 2$ receivers; $N_s = 100$ OFDM symbols transmitted in the acoustic environment with the SWellEx-96 SSP, shown in Fig. 2.3. Coarse-to-fine localization, localization parameter setting: $N_{\mathrm{T}} = 4$; $N_{\max} = 4$, after finding the AF maximum, two cases considered, 1 point and 9 points are removed from the coarse grid map as described in subsection 3.2.1; the refinement area is $S_{\mathrm{f}} = 4$ m $\times$ 4 m, shown in Fig. 3.1b.

Scenario 4: Different imperfect CSIs

In this scenario, three different coarse-to-fine localization accuracies are chosen from Fig. 3.14. Based on the 1-m resolution coarse grid map, with two different refined steps in different refinement algorithms are investigated.

Fig. 4.10 shows the FER performance for User 1 in a transmit beamforming system with an approximate MMSE precoder, assuming a specific estimated $\mathrm{SNR}_{\mathrm{est}}$, $\mathrm{SNR}_{\mathrm{est}} = 10$ dB; the FER performance is evaluated against SNR for three different cases of localization accuracies.

In the case of coarse-to-fine localization algorithm with the refinement steps, $F_{\mathrm{r}} = F_{\mathrm{d}} = 0.1$ m; nine points are removed from the coarse grid map after finding the AF maximum. The localization error is smaller than 0.1 m in 97% of the trials, as shown in Fig 3.14, as can be seen in Fig. 4.10, good detection performance can be achieved with such localization, with the FER reaching 10^{-2}. This suggests that the beamformer performs well in the case that the accurate localization is available.

In the case of coarse-to-fine localization algorithm with the refinement steps, $F_{\mathrm{r}} = F_{\mathrm{d}} = 0.1$ m when one point is removed from the coarse grid map after finding the AF maximum, as shown in Fig 3.14, the localization error increases slightly, the localization error for one trial is over 1 m and in 97% of the trials, the localization error is below 0.1 m, the detection performance slightly drops, resulting in an FER of 0.084, as shown in Fig. 4.10. In this case, the beamformer can still achieve relatively good detection performance, although not as good as in the case above.

Furthermore, in the case of the coarse-to-fine localization algorithm with the refinement steps, $F_{\mathrm{r}} = F_{\mathrm{d}} = 0.5$ m and nine points removed from the coarse grid map after finding the AF maximum, the localization error increases to 0.5 m in 97% of the trails, as shown in Fig 3.14. In this case, the detection performance experiences a significant degradation, with a floor-level FER of 0.6, as shown in Fig. 4.10. It indicates that transmit beamforming becomes less effective when using the receiver localization with a relatively low localization accuracy.

These observations highlight the sensitivity of transmit beamforming to the accuracy of the receiver localization. When a high accuracy in receiver localization is guaranteed, transmit beamforming can significantly enhance the detection performance. However, any degradation in localization accuracy can lead to a decline in the detection performance. Therefore, more accurate and reliable localization information are crucial for designing an effective transmit beamforming system to improve the detection performance in underwater acoustic communication scenarios.

Therefore, the coarse-to-fine algorithm with the refinement steps, $F_{\mathrm{r}} = F_{\mathrm{d}} = 0.1$ m; and a refinement area size of 4 m $\times$ 4 m (as shown in Fig. 3.1b) provides better localization

accuracy, which is applied in the following scenarios to further investigate the transmit beamforming.

Scenario 5: Multiple transmit antennas and receiver positions

In this scenario, multiple transmit antennas and multiple receivers to design transmit beamforming have been investigated. Specifically, two scenarios are considered, with $N_T = 4$ and $N_R = 2$, and with $N_T = 4$ and $N_R = 3$.

To achieve better detection, we can increase the number of transmit antennas when designing transmit beamforming. Fig. 4.11 shows the FER performance of transmit beamforming with different precoders against SNR in a multiuser system with $N_T = 4$ and $N_R = 2$. By comparing results in Fig. 4.9 and Fig. 4.11, an increase in the number of transmit antennas from $N_T = 2$ to $N_T = 4$ greatly improves the detection performance. Specifically, the detection performance of transmit beamforming with all precoders can be achieved, with the FER reaching 10^{-2} when SNR $= 10$ dB.

Fig. 4.12 shows the FER performance for User 1 of transmit beamforming with different precoders against SNR in a multiuser system with $N_T = 4$ transmit antennas and $N_R = 3$ receivers. By comparing results in Fig. 4.11 and Fig. 4.12, it is apparent that the detection performance of the receiver improves significantly when increasing the number of receivers; more specifically, with the ZF precoder and approximate MMSE precoder with an assumed SNR, $\text{SNR}_{\text{est}} = 30$ dB, the detection performance improves by approximately one order of magnitude 10^{-1}. It can be seen that when applied the approximate MMSE precoder with an assumed SNR, $\text{SNR}_{\text{est}} = 5,\ 10,\ 20$ dB, the improvement of the detection performance is even more significant, around one order of magnitude greater 10^{-2}; especially for the approximate MMSE precoder with an assumed SNR, $\text{SNR}_{\text{est}} = 10$ dB, exceptional performance is demonstrated, with the FER reaching as low as 10^{-4} when the SNR is close to 10 dB.

Scenario 6: Various coding rates

Table 4.2 Maximum free distance (d_f) for convolutional codes with various coding rates (adapted from [2–4]).

Code rate (r_c)	**Constraint length (k)**	**Generator in octal**	d_f
$1/2$	5	$[23,35]$	7
$1/2$	7	$[133,171]$	10
$1/3$	7	$[133,145,175]$	15
$1/4$	7	$[133,135,147,163]$	20
$1/8$	7	$\begin{bmatrix} 153 & 111 & 165 & 173 \\ 135 & 135 & 147 & 137 \end{bmatrix}$	40

The coding rate is an essential factor in designing transmit beamforming since it directly influences the data throughput and the robustness of a multi-user UWA system. The main parameters of coding rates used in our simulation are given in Table 4.2.

In this scenario, a multiuser system with various coding rates and transmit beamforming with $N_T = 4$ and $N_R = 2$ is investigated. The two receivers (users) are chosen from 100 receivers randomly in area of interest, 4950 trials are conducted and $N_s = 100$ OFDM symbols are transmitted. Fig. 4.13 shows the FER performance of transmit beamforming for various coding rates $r_c = 1/2, 1/3, 1/4, 1/8$ and constraint lengths $k = 5, 7$. For the case of the code rate $1/2$, the result with a constraint length $k = 7$ has a slightly better performance than one with a constraint length $k = 5$. When the constraint length $k = 7$ and various coding rates $r_c = 1/2, 1/4, 1/8$ are applied, the higher the coding rate, the more error correction capability has the code, thus, the better detection performance. However, this results in more redundant information and more complexity. Therefore, a proper coding rate should be considered for taking a trade-off between error correction, data rate and complexity.

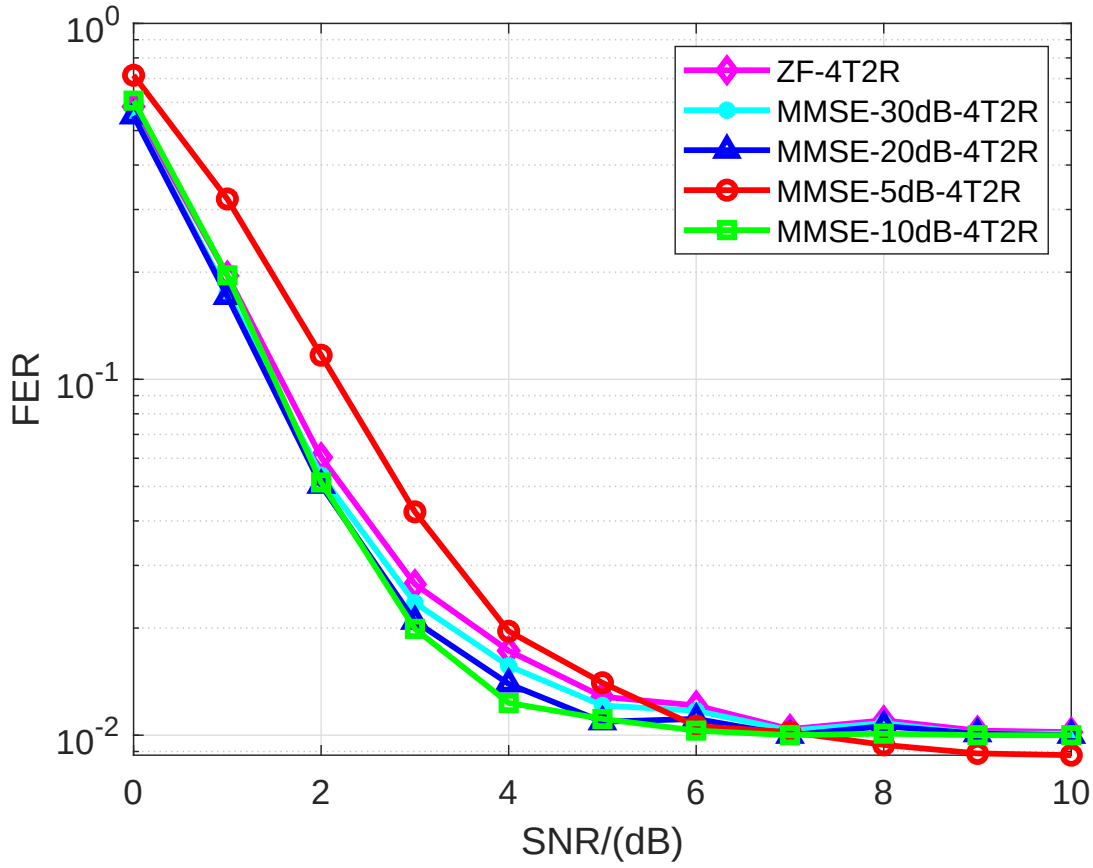

Fig. 4.11 FER performance for User 1 of transmit beamforming with the ZF precoder and the approximate MMSE precoder with $\mathrm{SNR}_{\mathrm{est}} = 5, 10, 20, 30$ dB against SNR; the simulation parameters are $N_T = 4$ transmit antennas; $N_R = 2$ receivers; $N_s = 100$ OFDM symbols transmitted in the acoustic environment with the SWellEx-96 SSP, shown in Fig. 2.3. Coarse-to-fine localization, localization parameter setting: $N_{\mathrm{T}} = 4$; $N_{\mathrm{max}} = 4$, nine points are removed after finding the next coarse AF maximum; in the refinement steps, $F_{\mathrm{r}} = F_{\mathrm{d}} = 0.1$ m; the size of the refinement area is 4 m $\times$ 4 m (shown in Fig. 3.1b).

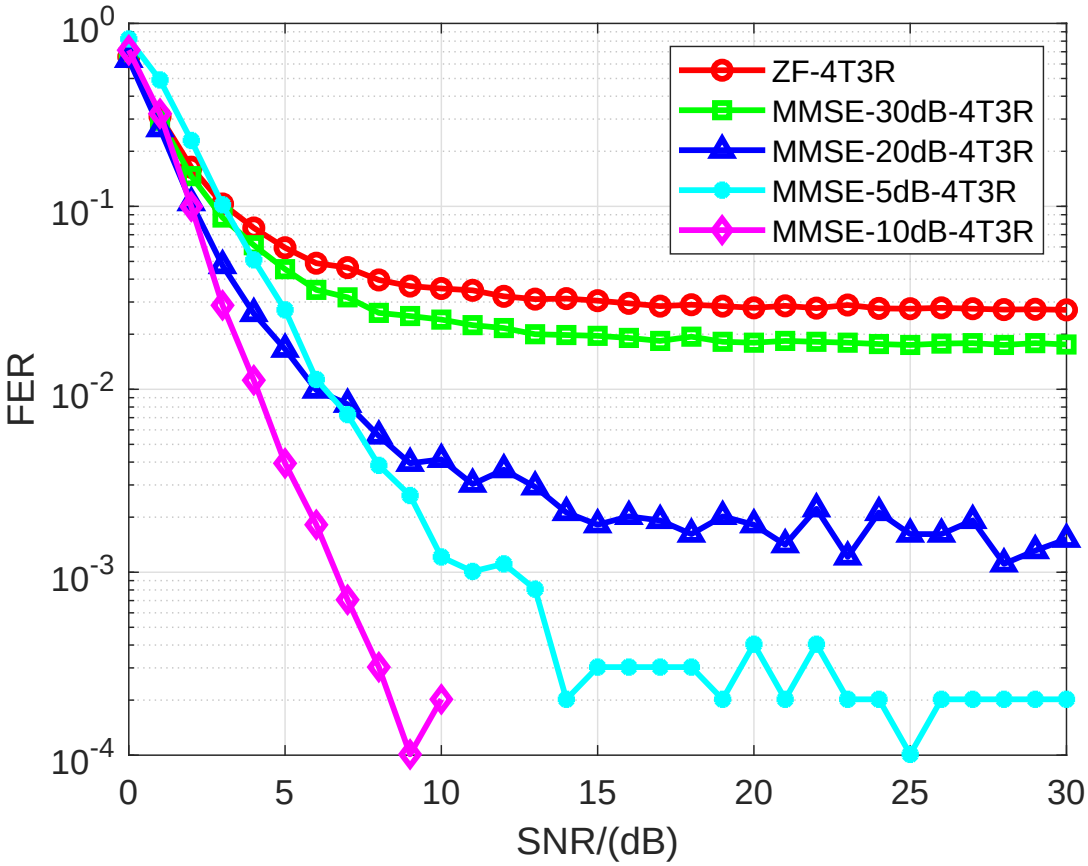

Fig. 4.12 FER performance for User 1 of transmit beamforming with the ZF precoder and the approximate MMSE precoder with $\mathrm{SNR}_{\mathrm{est}} = 5, 10, 20, 30$ dB against SNR; the simulation parameters are $N_T = 4$ transmit antennas; $N_R = 3$ receivers; $N_s = 100$ OFDM symbols transmitted in the acoustic environment with the SWellEx-96 SSP, shown in Fig. 2.3. Coarse-to-fine localization, localization parameter setting: $N_{\mathrm{T}} = 4$; $N_{\mathrm{max}} = 4$, nine points are removed after finding the next coarse AF maximum; in the refinement steps, $F_{\mathrm{r}} = F_{\mathrm{d}} = 0.1$ m; the size of the refinement area is 4 m $\times$ 4 m (shown in Fig. 3.1b).

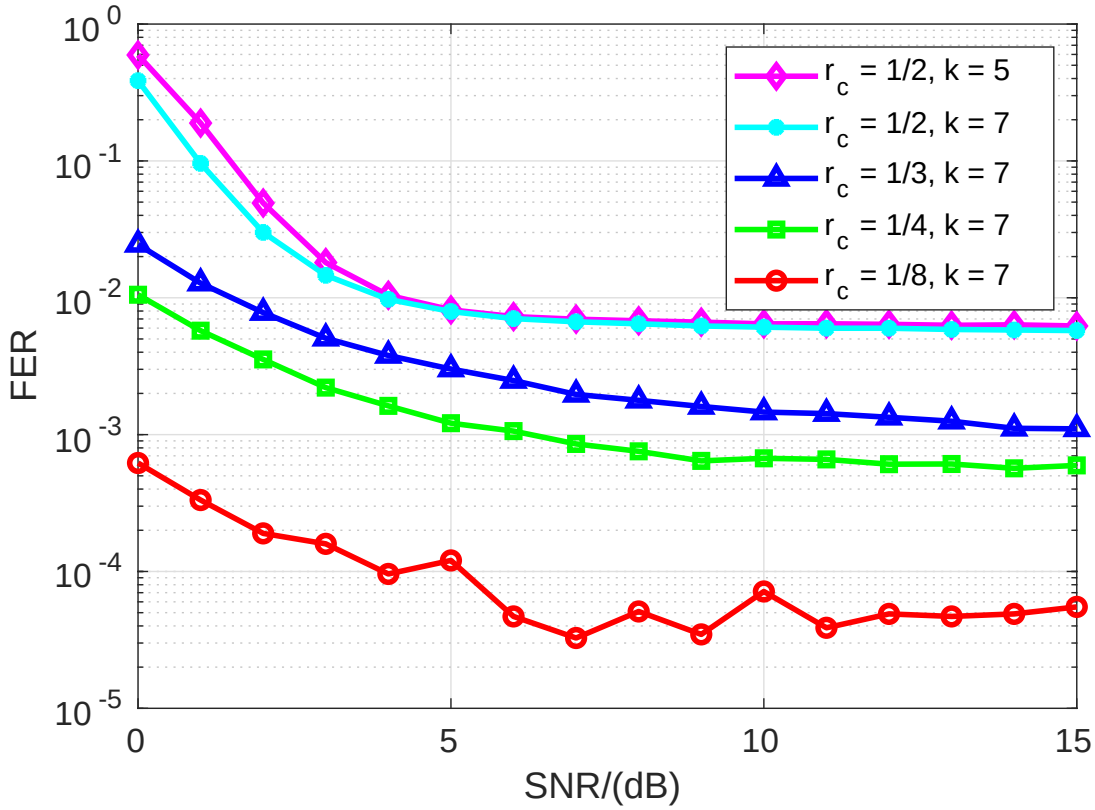

Fig. 4.13 FER performance for User 1 of transmit beamforming with the approximate MMSE precoder with $\mathrm{SNR}_{\mathrm{est}} = 10$ dB against SNR for different coding rates; $N_s = 100$ OFDM symbols are transmitted in the acoustic environment with the SWellEx-96 SSP, shown in Fig. 2.3.

4.5 Conclusions

In this chapter, different beamforming techniques with multiple receivers are investigated, which is based on the proposed coarse-to-fine localization algorithms in Chapter 3. With the perfect CSI and accurate receiver locations, ZF beamformer has better performance than approximate MMSE beamformers with different assumed SNRs. The robustness of the detection performance has also been investigated when the knowledge of the CSI and receiver localization are imperfect. In this situation, the approximate MMSE beamformer with an appropriately assumed SNR can improve the detection performance. High detection performance is shown in numerical results when multiple transmit antennas are applied to multiuser UWA communication systems. Accurate localization information can significantly improve the detection performance of transmit beamforming.

Chapter 5

Conclusions and further work

5.1 Summary of the work

The goal of this thesis is to design multiple transmit antenna techniques to communicate through the UWA channel with multiple receivers equipped with single antennas using improved localization of the receivers with respect to the transmit antennas. The contribution from this work is summarized as follows.

- A non-coherent AF based on MFP techniques is proposed, which significantly improves the localization performance, compared to the coherent AF previously used for this propose, especially at high frequencies.
- A two-step (coarse-to-fine) localization technique is proposed, which allows high localization accuracy and a reduction in complexity and memory storage, compared to single step localization.
- A joint refinement scheme with multiple refinement areas is proposed, which reduces the number of outliers and achieves highly accurate position estimates by comparing the vicinities of several maxima.
- Transmit beamforming techniques based on the proposed localization techniques are proposed and investigated with the purpose of improving the detection performance.

Chapter 2 presents a new localization method based on matching the CSI estimated at the receiver to the CSI pre-computed at the grid points in an area of interest. The proposed method can not only mitigate the distortion of phase information in the received signals, but can also work well at high frequencies, thus, allowing more accurate location estimates. The proposed

non-coherent AF method has a significant advantage for receiver localization compared to the coherent AF method. The results show there is a reduction for false localization estimate and outliers, and the accuracy of the MFP localization has been improved. The results suggest that even in the case of a single transmit antenna, when using the non-coherent AF, it is possible to achieve useful results for localization of the single-antenna receiver. For the non-coherent AF method, the number of grid points covering an area of interest is significantly reduced and consequently the amount of computation required for the localization is also significantly reduced, thus making the use of the non-coherent AF more practical. Moreover, the non-coherent AF method also results in a smaller memory requirement for saving the information on the grid.

Chapter 3 proposed several maxima search, multiple refinement and coarse-to-fine localization techniques. The several maxima search efficiently mitigates outliers due to a finite spatial sampling rate, thus, improving the localization accuracy. A joint refinement technique with multiple refinement areas brings about a further reduction in outliers and improves the localization accuracy. These techniques can achieve a very high localization accuracy, thus compensating for possibly low space resolution at the coarse grid when using the non-coherent AF method. Since the refinement areas are typically much smaller than the whole localization area, this improvement is achieved with relatively small computational load. The joint search over multiple refinement areas allows one to avoid localization outliers than can appear due to errors at the coarse stage in finding the AF area global maximum.

Chapter 4 investigates different beamforming techniques combined with the proposed coarse-to-fine localization. The investigation is used to develop beamforming techniques with different linear precoders. The beamforming techniques are used with multiple transmit antennas and single-antenna receivers. The results show that the approximate MMSE precoder with an assumed SNR has better detection performance than other precoders used for comparison.

5.2 Future work

In this section, some suggestions for future work are given based on this thesis. The suggestions for future work are as follows.

1. In Chapter 2 and Chapter 3, both coarse localization and coarse-to-fine localization are proposed based on the grid computation. As illustrated in Chapter 2, grid maps cover the area of interest, the CSI for every grid point needs to be pre-computed and stored in both the transmitter and the receiver, which requires a high computation complexity. Although the non-coherent AF can reduce the number of grid points, this number still

can be too high for real-time implementation in a communication receiver limited in computation resources. Therefore, it is necessary to investigate techniques to address how the number of grid points can be further reduced to decrease the computation complexity. For example, for this purpose, the basis expansion model (BEM) approach for representation of the channel response can be used.

2. In Chapter 3 and Chapter 4, the localization techniques and beamforming techniques are investigated. The investigation is based on the least square (LS) channel estimation. However, LS channel estimation is not very efficient. Therefore, designing a more efficient channel estimator might be beneficial to the performance improvement and complexity reduction for both the localization and beamforming. The basis expansion model (BEM) channel estimation is certainly a topic of further exploration.

References

[1] L. Liao, "Underwater acoustic localization with applications to multiuser communications," PhD thesis, University of York, August 2018, available at https://etheses.whiterose.ac.uk/22119/1/thesis.pdf.

[2] K. Larsen, "Short convolutional codes with maximal free distance for rates 1/2, 1/3, and 1/4 (corresp.)," *IEEE Transactions on Information Theory*, vol. 19, no. 3, pp. 371–372, 1973.

[3] J. P. Odenwalder, *Optimal decoding of convolutional codes*. University of California, Los Angeles, 1970.

[4] D. Daut, J. Modestino, and L. Wismer, "New short constraint length convolutional code constructions for selected rational rates (corresp.)," *IEEE Transactions on Information Theory*, vol. 28, no. 5, pp. 794–800, 1982.

[5] M. Stojanovic, "Underwater acoustic communications: Design considerations on the physical layer," in *IEEE Fifth Annual Conference on Wireless on Demand Network Systems and Services (WONS), Garmisch-Partenkirchen, Germany*, 23-25 January 2008, pp. 1–10.

[6] J. Murray and D. Ensberg, "The SwellEx-96 experiment," https://asa.scitation.org/doi/abs/10.1121/1.420796, Accessed: 2022-01-05.

[7] P. He, L. Shen, B. Henson, and Y. V. Zakharov, "Coarse-to-fine localization of underwater acoustic communication receivers," *Sensors*, vol. 22, no. 18, p. 6968, 2022.

[8] S. Al-Dharrab, M. Uysal, and T. Duman, "Cooperative underwater acoustic communications," *IEEE Communications Magazine*, vol. 51, no. 7, pp. 146–153, 2013.

[9] J. Blandin and P. Léon, "Network architectures for underwater systems: two applications of the CAN bus," in *IEEE Oceanic Engineering Society. Conference Proceedings (Cat. No.98CH36259), Nice, France*, vol. 1, 28 September - 01 October 1998, pp. 503–507.

[10] K. Chen, M. Ma, E. Cheng, F. Yuan, and W. Su, "A survey on MAC protocols for underwater wireless sensor networks," *IEEE Communications Surveys & Tutorials*, vol. 16, no. 3, pp. 1433–1447, 2014.

[11] H. Kaushal and G. Kaddoum, "Underwater optical wireless communication," *IEEE Access*, vol. 4, pp. 1518–1547, 2016.

[12] J. Preisig, "Acoustic propagation considerations for underwater acoustic communications network development," *ACM SIGMOBILE Mobile Computing and Communications Review*, vol. 11, no. 4, pp. 2–10, 2007.

[13] M. Erol-Kantarci, H. T. Mouftah, and S. Oktug, "A survey of architectures and localization techniques for underwater acoustic sensor networks," *IEEE Communications Surveys & Tutorials*, vol. 13, no. 3, pp. 487–502, 2011.

[14] L. Lanbo, Z. Shengli, and C. Jun-Hong, "Prospects and problems of wireless communication for underwater sensor networks," *Wireless Communications and Mobile Computing*, vol. 8, no. 8, pp. 977–994, 2008.

[15] M. Stojanovic, "Recent advances in high-speed underwater acoustic communications," *IEEE Journal of Oceanic Engineering*, vol. 21, no. 2, pp. 125–136, 1996.

[16] M. Chitre, S. Shahabudeen, and M. Stojanovic, "Underwater acoustic communications and networking: Recent advances and future challenges," *Marine Technology Society Journal*, vol. 42, no. 1, pp. 103–116, 2008.

[17] A. O. Bicen, A. B. Sahin, and O. B. Akan, "Spectrum-aware underwater networks: Cognitive acoustic communications," *IEEE Vehicular Technology Magazine*, vol. 7, no. 2, pp. 34–40, 2012.

[18] J. Partan, J. Kurose, and B. N. Levine, "A survey of practical issues in underwater networks," *ACM SIGMOBILE Mobile Computing and Communications Review*, vol. 11, no. 4, pp. 23–33, 2007.

[19] V. M. Janik, "Underwater acoustic communication," *Animal communication networks*, p. 390, 2005.

[20] A. C. Singer, J. K. Nelson, and S. S. Kozat, "Signal processing for underwater acoustic communications," *IEEE Communications Magazine*, vol. 47, no. 1, pp. 90–96, 2009.

[21] A. Song, A. Abdi, M. Badiey, and P. Hursky, "Experimental demonstration of underwater acoustic communication by vector sensors," *IEEE Journal of Oceanic Engineering*, vol. 36, no. 3, pp. 454–461, 2011.

[22] H. Song and W. Hodgkiss, "Efficient use of bandwidth for underwater acoustic communication," *The Journal of the Acoustical Society of America*, vol. 134, no. 2, pp. 905–908, 2013.

[23] J.-g. Huang, H. Wang, C.-b. He, Q.-f. Zhang, and L.-y. Jing, "Underwater acoustic communication and the general performance evaluation criteria," *Frontiers of Information Technology & Electronic Engineering*, vol. 19, no. 8, pp. 951–971, 2018.

[24] A. Song, M. Stojanovic, and M. Chitre, "Editorial underwater acoustic communications: Where we stand and what is next?" *IEEE Journal of Oceanic Engineering*, vol. 44, no. 1, 2019.

[25] A. Matos, A. Martins, A. Dias, B. Ferreira, J. M. Almeida, H. Ferreira, G. Amaral, A. Figueiredo, R. Almeida, and F. Silva, "Multiple robot operations for maritime search and rescue in euRathlon 2015 competition," in *IEEE OCEANS, Shanghai, China*, 10-13 April 2016, pp. 1–7.

[26] F. Louza, J. Osowsky, F. Xavier, E. Vale, L. Maia, R. Vio, M. Simoes, V. Barroso, and S. Jesus, "Communications and biological monitoring experiment in an upwelling environment at Cabo Frio island bay," in *IEEE OCEANS, Marseille, France*, 17-20 June 2019, pp. 1–7.

[27] K. Zwolak, B. Simpson, B. Anderson, E. Bazhenova, R. Falconer, T. Kearns, H. Minami, J. Roperez, A. Rosedee, H. Sade, and N. Tinmouth, "An unmanned seafloor mapping system: The concept of an AUV integrated with the newly designed USV SEA-KIT," in *IEEE OCEANS, Aberdeen, UK*, 19-22 June 2017, pp. 1–6.

[28] G. Tabella, N. Paltrinieri, V. Cozzani, and P. S. Rossi, "Wireless sensor networks for detection and localization of subsea oil leakages," *IEEE Sensors Journal*, vol. 21, no. 9, pp. 10 890–10 904, 2021.

[29] Y. V. Zakharov and V. Kodanev, "Experimental study of an underwater acoustic communication system with pseudonoise signals," *Acoustical Physics*, vol. 40, no. 5, pp. 707–715, 1994.

[30] Y. V. Zakharov and V. Kodanev, "Doppler scattering adapted reception in a hydroacoustic cornmunication channel," *Acoust. Phys*, vol. 41, pp. 219–223, 1995.

[31] M. Stojanovic, "Underwater acoustic communications," in *IEEE Proceedings of Electro/International, Boston, MA, USA*, 21-23 June 1995, pp. 435–440.

[32] Y. V. Zakharov and V. Kodanev, "Multipath-Doppler diversity of OFDM signals in an underwater acoustic channel," in *IEEE International Conference on Acoustics, Speech, and Signal Processing. Proceedings (Cat. No. 00CH37100), Istanbul, Turkey*, vol. 5, 05-09 June 2000, pp. 2941–2944.

[33] C. Liu, Y. V. Zakharov, and T. Chen, "Doubly selective underwater acoustic channel model for a moving transmitter/receiver," *IEEE Transactions on Vehicular Technology*, vol. 61, no. 3, pp. 938–950, 2012.

[34] Y. V. Zakharov and A. K. Morozov, "OFDM transmission without guard interval in fast-varying underwater acoustic channels," *IEEE Journal of Oceanic Engineering*, vol. 40, no. 1, pp. 144–158, 2014.

[35] J. Li, Y. V. Zakharov, and B. Henson, "Multibranch autocorrelation method for doppler estimation in underwater acoustic channels," *IEEE Journal of oceanic engineering*, vol. 43, no. 4, pp. 1099–1113, 2017.

[36] D. B. Kilfoyle, J. C. Preisig, and A. B. Baggeroer, "Spatial modulation experiments in the underwater acoustic channel," *IEEE Journal of Oceanic Engineering*, vol. 30, no. 2, pp. 406–415, 2005.

[37] M. Stojanovic and J. Preisig, "Underwater acoustic communication channels: Propagation models and statistical characterization," *IEEE Communications Magazine*, vol. 47, no. 1, pp. 84–89, 2009.

[38] W. H. Tranter, T. S. Rappaport, K. L. Kosbar, and K. S. Shanmugan, *Principles of communication systems simulation with wireless applications*. Prentice Hall New Jersey, 2004, vol. 1.

[39] P. C. Etter, *Underwater acoustic modeling and simulation*. CRC Press, 2018.

[40] M. Stojanovic, "On the relationship between capacity and distance in an underwater acoustic communication channel," *ACM SIGMOBILE Mobile Computing and Communications Review*, vol. 11, no. 4, pp. 34–43, 2007.

[41] J. A. Catipovic, "Performance limitations in underwater acoustic telemetry," *IEEE Journal of Oceanic Engineering*, vol. 15, no. 3, pp. 205–216, 1990.

[42] Y. M. Tsang and R. S. Cheng, "Optimal resource allocation in SDMA/multiinput-single-output/OFDM systems under QoS and power constraints," in *IEEE Wireless Communications and Networking Conference, Atlanta, GA, USA*, vol. 3, 21-25 March 2004, pp. 1595–1600.

[43] P. A. Van Walree, "Propagation and scattering effects in underwater acoustic communication channels," *IEEE Journal of Oceanic Engineering*, vol. 38, no. 4, pp. 614–631, 2013.

[44] J. Tao, Y. R. Zheng, C. Xiao, and T. Yang, "Robust MIMO underwater acoustic communications using turbo block decision-feedback equalization," *IEEE Journal of Oceanic Engineering*, vol. 35, no. 4, pp. 948–960, 2010.

[45] J. Tao, Y. R. Zheng, C. Xiao, T. Yang, and W.-B. Yang, "Channel equalization for single carrier MIMO underwater acoustic communications," *EURASIP Journal on Advances in Signal Processing*, vol. 2010, no. 1, p. 281769, 2010.

[46] M. Chitre, S. Shahabudeen, L. Freitag, and M. Stojanovic, "Recent advances in underwater acoustic communications & networking," in *IEEE OCEANS, Quebec City, QC, Canada*, 15-18 September 2008, pp. 1–10.

[47] C. He, J. Huang, Q. Zhang, and X. Shen, "Single carrier frequency domain equalizer for underwater wireless communication," in *IEEE WRI International Conference on Communications and Mobile Computing, Kunming, China*, vol. 1, 06-08 January 2009, pp. 186–190.

[48] H. Yan, S. Zhou, Z. Shi, J.-H. Cui, L. Wan, J. Huang, and H. Zhou, "DSP implementation of SISO and MIMO OFDM acoustic modems," in *IEEE OCEANS, Sydney, NSW, Australia*, 24-27 May 2010, pp. 1–6.

[49] X. Huang, "Capacity criterion-based power loading for underwater acoustic OFDM system with limited feedback," in *IEEE International Conference on Wireless Communications, Networking and Information Security, Beijing, China*, 25-27 June 2010, pp. 54–58.

[50] M. Stojanovic, "Low complexity OFDM detector for underwater acoustic channels," in *IEEE OCEANS, Boston, MA, USA*, 18-21 September 2006.

[51] B. Li, S. Zhou, M. Stojanovic, and L. Freitag, "Pilot-tone based ZP-OFDM demodulation for an underwater acoustic channel," in *IEEE OCEANS, Boston, MA, USA*, 18-21 September 2006.

[52] Z. Liu and T. Yang, "On overhead reduction in time-reversed OFDM underwater acoustic communications," *IEEE Journal of Oceanic Engineering*, vol. 39, no. 4, pp. 788–800, 2013.

[53] S. Roy, T. M. Duman, V. McDonald, and J. G. Proakis, "High-rate communication for underwater acoustic channels using multiple transmitters and space–time coding: Receiver structures and experimental results," *IEEE Journal of Oceanic Engineering*, vol. 32, no. 3, pp. 663–688, 2007.

[54] H. Song, P. Roux, W. Hodgkiss, W. Kuperman, T. Akal, and M. Stevenson, "Multiple-input-multiple-output coherent time reversal communications in a shallow-water acoustic channel," *IEEE Journal of Oceanic Engineering*, vol. 31, no. 1, pp. 170–178, 2006.

[55] B. Li, J. Huang, S. Zhou, K. Ball, M. Stojanovic, L. Freitag, and P. Willett, "MIMO-OFDM for high-rate underwater acoustic communications," *IEEE Journal of Oceanic Engineering*, vol. 34, no. 4, pp. 634–644, 2009.

[56] Q. H. Spencer, A. L. Swindlehurst, and M. Haardt, "Zero-forcing methods for downlink spatial multiplexing in multiuser MIMO channels," *IEEE transactions on signal processing*, vol. 52, no. 2, pp. 461–471, 2004.

[57] X. Ge, J. Hu, C.-X. Wang, C.-H. Youn, J. Zhang, and X. Yang, "Energy efficiency analysis of MISO-OFDM communication systems considering power and capacity constraints," *Mobile Networks and Applications*, vol. 17, no. 1, pp. 29–35, 2012.

[58] G. Johnston, "Long term underwater positioning technologies for the offshore oil and gas industry," in *IEEE OCEANS, Aberdeen, UK*, 18-21 June 2007, pp. 1–4.

[59] S. Zhou and Z. Wang, *OFDM for underwater acoustic communications*. John Wiley & Sons, 2014.

[60] R. Hartman, W. Hawkinson, and K. Sweeney, "Tactical underwater navigation system (TUNS)," in *IEEE ION Position, Location and Navigation Symposium, Monterey, CA, USA*, 05-08 May 2008, pp. 898–911.

[61] C.-M. Lee, P.-M. Lee, S.-W. Hong, S.-M. Kim, W. Seong *et al.*, "Underwater navigation system based on inertial sensor and Doppler velocity log using indirect feedback Kalman filter," *International Journal of Offshore and Polar Engineering*, vol. 15, no. 02, 2005.

[62] V. Chandrasekhar, W. K. Seah, Y. S. Choo, and H. V. Ee, "Localization in underwater sensor networks: survey and challenges," in *Proceedings of the 1st International Workshop on Underwater Networks, Los Angeles, CA, USA*, 25 September 2006, pp. 33–40.

[63] K.-C. Lee, J.-S. Ou, and M.-C. Huang, "Underwater acoustic localization by principal components analyses based probabilistic approach," *Applied acoustics*, vol. 70, no. 9, pp. 1168–1174, 2009.

[64] H.-P. Tan, R. Diamant, W. K. Seah, and M. Waldmeyer, "A survey of techniques and challenges in underwater localization," *Ocean Engineering*, vol. 38, no. 14-15, pp. 1663–1676, 2011.

[65] R. Stuart, "Acoustic digital spread spectrum: AN ENABLING TECHNOLOGY-Ross-Stuart (Nautronix) examines how to use new acoustic spread spectrum technology to enhance current subsea positioning and communication," *Sea Technology*, vol. 46, no. 10, pp. 15–20, 2005.

[66] A. Tomczak, G. Stępień, T. Abramowski, and A. Bejger, "Subsea wellhead spud-in marking and as-built position estimation method based on ultra-short baseline acoustic positioning," *Measurement*, vol. 195, p. 111155, 2022.

[67] J. Almeida, B. Matias, A. Ferreira, C. Almeida, A. Martins, and E. Silva, "Underwater localization system combining iUSBL with dynamic SBL in ¡VAMOS! trials," *Sensors*, vol. 20, no. 17, p. 4710, 2020.

[68] P. Hursky, M. B. Porter, M. Siderius, and V. K. McDonald, "High-frequency (8–16 kHz) model-based source localization," *The Journal of the Acoustical Society of America*, vol. 115, no. 6, pp. 3021–3032, 2004.

[69] L. Liao, Y. V. Zakharov, and P. D. Mitchell, "Underwater localization based on grid computation and its application to transmit beamforming in multiuser UWA communications," *IEEE Access*, vol. 6, pp. 4297–4307, 2018.

[70] I. F. Akyildiz, D. Pompili, and T. Melodia, "Underwater acoustic sensor networks: research challenges," *Ad Hoc Networks*, vol. 3, no. 3, pp. 257–279, 2005.

[71] J. Heidemann, W. Ye, J. Wills, A. Syed, and Y. Li, "Research challenges and applications for underwater sensor networking," in *IEEE Wireless Communications and Networking Conference (WCNC), Las Vegas, NV, USA*, vol. 1, 03-06 April 2006, pp. 228–235.

[72] M. Beniwal and R. Singh, "Localization techniques and their challenges in underwater wireless sensor networks," *Internton Journal of Computer Science and Information Technologies*, vol. 5, no. 3, pp. 4706–4710, 2014.

[73] G. Tuna and V. C. Gungor, "A survey on deployment techniques, localization algorithms, and research challenges for underwater acoustic sensor networks," *International Journal of Communication Systems*, vol. 30, no. 17, pp. 1–21, 2017.

[74] J. Yan, X. Zhang, X. Luo, Y. Wang, C. Chen, and X. Guan, "Asynchronous localization with mobility prediction for underwater acoustic sensor networks," *IEEE Transactions on Vehicular Technology*, vol. 67, no. 3, pp. 2543–2556, 2017.

[75] M. Y. I. Zia, J. Poncela, and P. Otero, "State-of-the-art underwater acoustic communication modems: Classifications, analyses and design challenges," *Wireless Personal Communications*, vol. 116, no. 2, pp. 1325–1360, 2021.

[76] X. Su, I. Ullah, X. Liu, and D. Choi, "A review of underwater localization techniques, algorithms, and challenges," *Journal of Sensors*, vol. 2020, 2020.

[77] M. Moradi, J. Rezazadeh, and A. S. Ismail, "A reverse localization scheme for underwater acoustic sensor networks," *Sensors*, vol. 12, no. 4, pp. 4352–4380, 2012.

[78] J. Luo, L. Fan, S. Wu, and X. Yan, "Research on localization algorithms based on acoustic communication for underwater sensor networks," *Sensors*, vol. 18, no. 1, p. 67, 2017.

[79] I. Ullah, J. Chen, X. Su, C. Esposito, and C. Choi, "Localization and detection of targets in underwater wireless sensor using distance and angle based algorithms," *IEEE Access*, vol. 7, pp. 45 693–45 704, 2019.

[80] E. K. Westwood, "Broadband matched-field source localization," *The Journal of the Acoustical Society of America*, vol. 91, no. 5, pp. 2777–2789, 1992.

[81] B. M. Worthmann, H. Song, and D. R. Dowling, "High frequency source localization in a shallow ocean sound channel using frequency difference matched field processing," *The Journal of the Acoustical Society of America*, vol. 138, no. 6, pp. 3549–3562, 2015.

[82] B. M. Worthmann, H. Song, and D. Dowling, "Adaptive frequency-difference matched field processing for high frequency source localization in a noisy shallow ocean," *The Journal of the Acoustical Society of America*, vol. 141, no. 1, pp. 543–556, 2017.

[83] G. Byun, H. C. Song, and J. S. Kim, "Performance comparisons of array invariant and matched field processing using broadband ship noise and a tilted vertical array," *The Journal of the Acoustical Society of America*, vol. 144, no. 6, pp. 3067–3074, 2018.

[84] F. A. Hunter and W. A. Kuperman, "Range-coherent matched field processing for low signal-to-noise ratio localization," *The Journal of the Acoustical Society of America*, vol. 150, no. 1, pp. 270–280, 2021.

[85] A. B. Baggeroer, W. A. Kuperman, and P. N. Mikhalevsky, "An overview of matched field methods in ocean acoustics," *IEEE Journal of Oceanic Engineering*, vol. 18, no. 4, pp. 401–424, 1993.

[86] M. B. Porter, "BELLHOP3D User Guide," [Online].Available:https://usermanual.wiki/Document/Bellhop3D20User20Guide202016725.915656596/html, 2016, Accessed: December 20, 2021.

[87] R. Su, D. Zhang, C. Li, Z. Gong, R. Venkatesan, and F. Jiang, "Localization and data collection in AUV-aided underwater sensor networks: Challenges and opportunities," *IEEE Network*, vol. 33, no. 6, pp. 86–93, 2019.

[88] A. Toky, R. P. Singh, and S. Das, "Localization schemes for underwater acoustic sensor networks-a review," *Computer Science Review*, vol. 37, p. 100241, 2020.

[89] Y. Song, J. Qian, R. Miao, W. Xue, R. Ying, and P. Liu, "HAUD: A high-accuracy underwater dataset for visual-inertial odometry," in *IEEE Sensors, Sydney, Australia*, 31 October - 03 November 2021, pp. 1–4.

[90] Z. Zhou, J.-H. Cui, and S. Zhou, "Localization for large-scale underwater sensor networks," in *Springer NETWORKING Ad Hoc and Sensor Networks, Wireless Networks, Next Generation Internet: 6th International IFIP-TC6 Networking Conference, Atlanta, GA, USA*, 14-18 May 2007, pp. 108–119.

[91] M. T. Isik and O. B. Akan, "A three dimensional localization algorithm for underwater acoustic sensor networks," *IEEE Transactions on Wireless Communications*, vol. 8, no. 9, pp. 4457–4463, 2009.

[92] N. Javaid, H. Maqsood, A. Wadood, I. A. Niaz, A. Almogren, A. Alamri, and M. Ilahi, "A localization based cooperative routing protocol for underwater wireless sensor networks," *Mobile Information Systems*, vol. 2017, 2017.

[93] K. Hao, H. Shen, Y. Liu, B. Wang, and X. Du, "Integrating localization and energy-awareness: A novel geographic routing protocol for underwater wireless sensor networks," *Mobile Networks and Applications*, vol. 23, pp. 1427–1435, 2018.

[94] J. V. Gómez, F. E. Sandnes, and B. Fernández, "Sunlight intensity based global positioning system for near-surface underwater sensors," *Sensors*, vol. 12, no. 2, pp. 1930–1949, 2012.

[95] M. Siderius and M. B. Porter, "Modeling broadband ocean acoustic transmissions with time-varying sea surfaces," *The Journal of the Acoustical Society of America*, vol. 124, no. 1, pp. 137–150, 2008.

[96] P. Duhamel and H. Hollmann, "Split radix FFT algorithm," *Electronics Letters*, vol. 20, no. 1, pp. 14–16, 1984.

[97] X. Chen, Y. Lei, Z. Lu, and S. Chen, "A variable-size FFT hardware accelerator based on matrix transposition," *IEEE Transactions on Very Large Scale Integration (VLSI) Systems*, vol. 26, no. 10, pp. 1953–1966, 2018.

[98] J. Heo, Y. Jung, S. Lee, and Y. Jung, "FPGA implementation of an efficient FFT processor for FMCW radar signal processing," *Sensors*, vol. 21, no. 19, p. 6443, 2021.

[99] K. T. Wong, "Adaptive source localisation and blind beamforming for underwater acoustic wideband fast frequency-hop signals of unknown hop sequences and unknown arrival angles using a vector-hydrophone," in *IEEE Wireless Communications and Networking Conference (WCNC) (Cat. No. 99TH8466), New Orleans, LA, USA*, vol. 2, 21-24 September 1999, pp. 664–668.

[100] T. Yang, "A study of spatial processing gain in underwater acoustic communications," *IEEE Journal of Oceanic Engineering*, vol. 32, no. 3, pp. 689–709, 2007.

[101] K. T. Wong and M. D. Zoltowski, "Self-initiating music-based direction finding in underwater acoustic particle velocity-field beamspace," *IEEE Journal of Oceanic Engineering*, vol. 25, no. 2, pp. 262–273, 2000.

[102] J. Li, Q.-H. Lin, K. Wang, and C.-Y. Kang, "Performance analysis for focused beamformers in passive underwater acoustic localization," *IEEE Access*, vol. 6, pp. 18 200–18 208, 2018.

[103] D. F. Nsalo Kong, C. Shen, C. Tian, and K. Zhang, "A new low-cost acoustic beamforming architecture for real-time marine sensing: Evaluation and design," *Journal of Marine Science and Engineering*, vol. 9, no. 8, p. 868, 2021.

[104] F. A. Bozzi and S. M. Jesus, "Joint vector sensor beam steering and passive time reversal for underwater acoustic communications," *IEEE Access*, vol. 10, pp. 66 952–66 960, 2022.

[105] F. Rashid-Farrokhi, K. R. Liu, and L. Tassiulas, "Transmit beamforming and power control for cellular wireless systems," *IEEE Journal on selected areas in communications*, vol. 16, no. 8, pp. 1437–1450, 1998.

[106] E. Visotsky and U. Madhow, "Optimum beamforming using transmit antenna arrays," in *IEEE 49th Vehicular Technology Conference (Cat. No. 99CH36363), Houston, TX, USA*, vol. 1, 16-20 May 1999, pp. 851–856.

[107] E. L. Holzman and A. K. Agrawal, "A comparison of active phased array, corporate beamforming architectures," in *IEEE Proceedings of International Symposium on Phased Array Systems and Technology, Boston, MA, USA*, 15-18 October 1996, pp. 429–434.

[108] F. Rashid-Farrokhi, K. R. Liu, and L. Tassiulas, "Transmit diversity and equalization for power controlled wireless networks," in *IEEE Conference Record of the Thirty-First Asilomar Conference on Signals, Systems and Computers (Cat. No. 97CB36136), Pacific Grove, CA, USA*, vol. 1, 02-05 November 1997, pp. 620–624.

[109] D. Gerlach and A. Paulraj, "Adaptive transmitting antenna arrays with feedback," *IEEE Signal Processing Letters*, vol. 1, no. 10, pp. 150–152, 1994.

[110] A. Wiesel, Y. C. Eldar, and S. Shamai, "Linear precoding via conic optimization for fixed MIMO receivers," *IEEE transactions on signal processing*, vol. 54, no. 1, pp. 161–176, 2005.

[111] M. Stojnic, H. Vikalo, and B. Hassibi, "Rate maximization in multi-antenna broadcast channels with linear preprocessing," *IEEE Transactions on Wireless Communications*, vol. 5, no. 9, pp. 2338–2342, 2006.

[112] M. Joham, W. Utschick, and J. A. Nossek, "Linear transmit processing in MIMO communications systems," *IEEE Transactions on signal Processing*, vol. 53, no. 8, pp. 2700–2712, 2005.

[113] S. Shi, M. Schubert, and H. Boche, "Downlink MMSE transceiver optimization for multiuser MIMO systems: Duality and sum-MSE minimization," *IEEE Transactions on Signal Processing*, vol. 55, no. 11, pp. 5436–5446, 2007.

[114] C. B. Peel, B. M. Hochwald, and A. L. Swindlehurst, "A vector-perturbation technique for near-capacity multiantenna multiuser communication-part I: Channel inversion and regularization," *IEEE Transactions on Communications*, vol. 53, no. 1, pp. 195–202, 2005.

[115] F. Rusek, D. Persson, B. K. Lau, E. G. Larsson, T. L. Marzetta, O. Edfors, and F. Tufvesson, "Scaling up MIMO: Opportunities and challenges with very large arrays," *arXiv preprint arXiv:1201.3210*, 2012.

[116] S. Zhang, R. Zhang, and T. J. Lim, "MISO multicasting with constant envelope precoding," *IEEE Wireless Communications Letters*, vol. 5, no. 6, pp. 588–591, 2016.

[117] A. Wiesel, Y. C. Eldar, and S. Shamai, "Zero-forcing precoding and generalized inverses," *IEEE Transactions on Signal Processing*, vol. 56, no. 9, pp. 4409–4418, 2008.

[118] K. Karakayali, R. Yates, G. Foschini, and R. Valenzuela, "Optimum zero-forcing beamforming with per-antenna power constraints," in *IEEE International Symposium on Information Theory, Nice, France*, 24-29 June 2007, pp. 101–105.

[119] P. Zetterberg, "Experimental investigation of TDD reciprocity-based zero-forcing transmit precoding," *EURASIP Journal on Advances in Signal Processing*, vol. 2011, pp. 1–10, 2011.

[120] Q. Shi, C. Peng, W. Xu, M. Hong, and Y. Cai, "Energy efficiency optimization for MISO SWIPT systems with zero-forcing beamforming," *IEEE Transactions on Signal Processing*, vol. 64, no. 4, pp. 842–854, 2015.

[121] M. B. Porter, "The BELLHOP manual and user's guide: Preliminary draft," *Heat, Light, and Sound Research, Inc., La Jolla, CA, USA, Tech. Rep*, vol. 260, 2011.

[122] L. Dong, H. Dong, and J. Hovem, "Bellhop–A modeling approach to sound propagation in the ocean," in *Proceedings of the 36th Scandinavian Symposium on Physical Acoustics, Geilo, Norway*, 2-6 February 2014, pp. 1–4.

[123] B. Henson, J. Li, Y. V. Zakharov, and C. Liu, "Waymark baseband underwater acoustic propagation model," in *IEEE Underwater Communications and Networking (UComms), Sestri Levante, Italy*, 03-05 September 2014, pp. 1–5.

[124] L. Liao, B. Henson, and Y. Zakharov, "Grid waymark baseband underwater acoustic transmission model," in *Underwater Acoustics Conference and Exhibition, Skiathos, Greece*, 3-8 September 2017, pp. 343–350.

[125] T. Yoo and A. Goldsmith, "Optimality of zero-forcing beamforming with multiuser diversity," in *IEEE International Conference on Communications (ICC), Seoul, South Korea*, vol. 1, 16-20 May 2005, pp. 542–546.

[126] B. M. Hochwald, C. B. Peel, and A. L. Swindlehurst, "A vector-perturbation technique for near-capacity multiantenna multiuser communication-Part II: Perturbation," *IEEE Transactions on Communications*, vol. 53, no. 3, pp. 537–544, 2005.